uOttawa

L'Université canadienne
Canada's university

FACULTÉ DES ÉTUDES SUPÉRIEURES ET POSTOCTORALES

uOttawa

L'Université canadienne
Canada's university

FACULTY OF GRADUATE AND POSDOCTORAL STUDIES

Sean Bradley Farrell
AUTEUR DE LA THÈSE / AUTHOR OF THESIS

M.Sc. (Earth Sciences)
GRADE / DEGREE

Department of Earth Sciences
FACULTÉ, ÉCOLE, DÉPARTEMENT / FACULTY, SCHOOL, DEPARTMENT

The Sulphur Isotope Geochemistry of Carbonatites and Associated Silicate Rocks from the Superior Province of the Canadian Shield

TITRE DE LA THÈSE / TITLE OF THESIS

I. Clark
DIRECTEUR (DIRECTRICE) DE LA THÈSE / THESIS SUPERVISOR

K. Bell
CO-DIRECTEUR (CO-DIRECTRICE) DE LA THÈSE / THESIS CO-SUPERVISOR

EXAMINATEURS (EXAMINATRICES) DE LA THÈSE / THESIS EXAMINERS

J. Blenkinsop

K. Nattori

Gary W. Slater
LE DOYEN DE LA FACULTÉ DES ÉTUDES SUPÉRIEURES ET POSTDOCTORALES /
DEAN OF THE FACULTY OF GRADUATE AND POSTDOCORAL STUDIES

The Sulphur Isotope Geochemistry of Carbonatites and Associated Silicate Rocks from the Superior Province of the Canadian Shield

By
Sean Bradley Farrell, B.Sc.(Hons)

Thesis submitted to the Faculty of Graduate and Postdoctoral Studies in partial fulfillment of the requirements for the M.Sc. degree in Earth Sciences

OTTAWA–CARLETON GEOSCIENCE CENTRE
AND
UNIVERSITY OF OTTAWA
OTTAWA, CANADA

© 2005 Sean Bradley Farrell

Library and Archives Canada

Published Heritage Branch

395 Wellington Street
Ottawa ON K1A 0N4
Canada

Bibliothèque et Archives Canada

Direction du Patrimoine de l'édition

395, rue Wellington
Ottawa ON K1A 0N4
Canada

Your file Votre référence
ISBN: 0-494-11269-7
Our file Notre référence
ISBN: 0-494-11269-7

NOTICE:
The author has granted a non-exclusive license allowing Library and Archives Canada to reproduce, publish, archive, preserve, conserve, communicate to the public by telecommunication or on the Internet, loan, distribute and sell theses worldwide, for commercial or non-commercial purposes, in microform, paper, electronic and/or any other formats.

The author retains copyright ownership and moral rights in this thesis. Neither the thesis nor substantial extracts from it may be printed or otherwise reproduced without the author's permission.

AVIS:
L'auteur a accordé une licence non exclusive permettant à la Bibliothèque et Archives Canada de reproduire, publier, archiver, sauvegarder, conserver, transmettre au public par télécommunication ou par l'Internet, prêter, distribuer et vendre des thèses partout dans le monde, à des fins commerciales ou autres, sur support microforme, papier, électronique et/ou autres formats.

L'auteur conserve la propriété du droit d'auteur et des droits moraux qui protège cette thèse. Ni la thèse ni des extraits substantiels de celle-ci ne doivent être imprimés ou autrement reproduits sans son autorisation.

In compliance with the Canadian Privacy Act some supporting forms may have been removed from this thesis.

While these forms may be included in the document page count, their removal does not represent any loss of content from the thesis.

Conformément à la loi canadienne sur la protection de la vie privée, quelques formulaires secondaires ont été enlevés de cette thèse.

Bien que ces formulaires aient inclus dans la pagination, il n'y aura aucun contenu manquant.

Canada

The undersigned hereby recommend to the Faculty of Graduate and Postdoctoral Studies acceptance of this thesis, submitted by Sean Bradley Farrell, B.Sc.(Hons) in partial fulfillment of the requirements for the M.Sc. degree in Earth Sciences.

Dr. Ian Clark, Thesis Co-Supervisor
Department of Earth Sciences,
University of Ottawa

Dr. Keith Bell, Thesis Co-Supervisor
Department of Earth Sciences,
Carleton University

Dr. Keiko Hattori, Chairperson
Department of Earth Sciences,
University of Ottawa

ABSTRACT

Thirty-five sulphur isotopic analyses have been obtained from six carbonatite-alkalic rock complexes ranging in age from 1906 Ma to 1008 Ma located within the Ontario portion of the Superior Province. Pyrrhotite, chalcopyrite and pyrite mineral separates were used. The overall range of $\delta^{34}S_{CDT}$ values are from +3.4 to −4.5‰. Each complex shows its own distinct range and mean sulphur isotopic composition. The range for the Schryburt Lake complex is −4.5 to −3.4‰ (avg. = −3.9‰), for the Big Beaver House complex −3.6 to −1.5‰ (avg. = −2.2‰), for the Cargill complex −1.5 to +0.5‰ (avg. = −0.7‰), for the Spanish River complex −0.1 to +0.1‰ (avg. = 0.0‰), and for the Firesand River complex +1.3 to +3.4‰ (avg. = +1.7‰). A single sample from the "Carb" Lake complex yielded a $\delta^{34}S_{CDT}$ value of +2.8‰.

Petrological and petrochemical observations suggest that the differences between the sulphur isotopic compositions for each of these carbonatite-alkalic rock complexes can be attributed to different modes of emplacement and degrees of melt differentiation rather then to source heterogeneities. In most of the complexes the carbonatites are associated with ultramafic rocks and these silicate rocks invariably possess a similar, but more primitive sulphur isotopic signature than the carbonatitic rocks. This relationship suggests that not only are the carbonatites and ultramafic rocks within a complex intimately related, but that the ultramafic rocks may have been the ultimate source of the carbonatitic sulphur. This relationship is also consistent with field and petrological observations which demonstrated that the carbonatites cross-cut the ultramafic rocks within an individual carbonatite-alkalic rock complex.

The overall range in the sulphur isotopic composition in conjunction with carbon and oxygen isotopic data suggests that these carbonatites and associated silicate rocks were derived from a relatively primitive mantle source. This is consistent with previously published Sr and Nd isotopic data that suggest that the mantle source underlying the Superior Province has remained essentially a closed system from about 2700 Ma to at least 1008 Ma. The sulphur isotopic data reported here is the first ever for carbonatites from the Superior Province.

ACKNOWLEGMENTS

First and foremost I would like to extend my deepest appreciations to both of my thesis co-supervisors. Thanks to Dr. Ian Clark, for his always positive attitude, cheerfulness and willingness to take me on with a project that is not directly related to his own research and to Dr. Keith Bell, who first introduced me to the strange and wonderful world of carbonatites and taught me about the world of scientific research, and his readiness to drop everything and engage into in-depth discussions about anything from carbonatites to world politics. This has kept me going these last few years.

My parents, whose love and financial support make this thesis as much theirs as it is mine. To the crew at the G.G. Hatch Stable Isotope Laboratories, especially Wendy, Paul and Gilles, thank you for your time and patience in teaching me the ins and outs of stable isotope analysis. To Helene de Gouffe, wow, you made sure I didn't die of administrative "stuff". Thanks also to Peter Jones for help with the electron microprobe and Lew Ling with the SEM analyses.

Dr. Don Hogarth, Department of Earth Sciences (University of Ottawa) who helped me make sense of my mysterious apatite data and the carbonatite and mineral nomenclature (I like 'sövites' and 'sphene'.....).

Vincent Vertolli, from the Royal Ontario Museum who graciously allowed me to sample the very comprehensive collection of carbonatites and associated silicate rocks from the Superior Province. Thanks also to Dr. Ron Sage (OGS – retired) whose work on these carbonatite-alkalic rock complexes was invaluable.

Mike Jackson, you're the crustiest and most generous Englishmen I know and I love it. All my fellow grad students at U of O and Carleton, especially J.O. (never stop being a CD...). To the brothers of S.P. Productions, most notably J.B. (do it... do it...).

Finally, I would like to thank my grandfather and also my grandmother who passed away before the completion of this thesis. Nanny, it was you who nurtured my love of geology and I dedicate this work in your memory. I hope I made you proud.

TABLE OF CONTENTS

LIST OF FIGURES

List of Tables

LIST OF PLATES

Chapter 1: Introduction

1.1 Carbonatites – General Overview

The general definition of a carbonatite is an igneous rock that contains at least 50% carbonate minerals (Streckeinsen, 1980). Carbonatite magmas differ significantly from most silicate magmas not only in their geochemical composition, but also in their rheological properties. Carbonatitic melts are composed of individual ions that are not bound covalently (Treiman, 1989), and thus do not form polymerized chains as in silicate melts. This lack of polymerization results in carbonatitic magmas having extremely low viscosities, which are similar to, and even lower then the most fluid basaltic melts. Their extremely low viscosities imply that carbonatitic magmas can migrate very rapidly and turbulently with flow rates up to 1 m/s (Treiman, 1989). Although volumetrically insignificant, carbonatites are found on every continent (including Antarctica) and range in age from the early Archaean to the present.

Mineralogically, carbonatites are mainly composed of calcite [$CaCO_3$] and dolomite [$CaMg(CO_3)_2$], with ankerite [$Ca(Fe,Mg,Mn)(CO_3)_2$] and siderite [$FeCO_3$] being important mineral phases in some occurrences. Important non-carbonate minerals present in carbonatites are: apatite, magnetite, aegirine, aegirine-augite and pyrochlore [$(Na,Ca)_2Nb_2O_6(OH,F)$] (Le Bas, 1981). In addition, Hogarth (1989) estimated that over 275 minerals have been found in carbonatites and he also provides an excellent summary of both the major carbonatitic minerals, as well as the minor and trace minerals. Accessory minerals include arfvedsonite, orthoclase, olivine, fluorite, barite, strontianite, bastnäsite [$(Ce,La,Y)CO_3F$], parisite [$Ca(Nd,Ce,La)_2(CO_3)_3F_2$], zircon and baddeleyite [ZrO_2] (Le Bas, 1981). Sulphide minerals that have been found in carbonatites include

pyrrhotite, pentlandite, pyrite, chalcopyrite, galena, arsenopyrite, bornite, cubanite [$CuFe_2S_3$], marcasite, millerite, molybdenite and sphalerite, of which chalcopyrite and pyrite are known to be the most abundant (Hogarth, 1989). Sulphate minerals that are commonly found in carbonatites include barite, gypsum and jarosite [$KFe_3(SO_4)_2(OH)_6$] (Hogarth, 1989). In terms of economic geology, carbonatites are important sources of thorite [$ThSiO_4$] (thorium), pyrochlore (niobium), apatite (phosphate), fluorite and REEs (Mariano, 1989). In addition, the carbonatite-ultramafic intrusion at Phalaborwa (South Africa) hosts one of the largest Cu deposits in the world, and although carbonatites contain late-stage sulphide mineralization (Mariano, 1989), the degree of mineralization seen at Phalaborwa seems to be unique.

The genesis and evolution of carbonatites has received much attention and is still a very intensive area of research among petrologists and isotope geochemists. There are essentially three principal models that have been put forth in the literature for the formation of carbonatitic melts, which are summarized by Gittins (1989): (1) crystal fractionation at crustal pressures of a mantle-derived parental magma, usually a 'carbonated' nephelinite; (2) liquid immiscibility of carbonate and silicate liquids from a nephelinitic or phonolitic liquid; (3) direct partial melting of a partially carbonated metasomatized mantle. However, radiogenic isotopic studies, e.g. Bell (1989) have demonstrated that carbonatites are mantle-derived melts and thus provide a unique insight into the geochemical evolution of the mantle through time, regardless of their petrogenetic origin.

1.2 Scope of this Study

The aim of this study is to evaluate the sulphur isotopic composition of carbonatites from the Superior Province in terms of their source(s) and/or emplacement mechanisms and to examine the relationship between the carbonatites and their associated silicate rocks. In order to obtain a representative suite of carbonatites and associated silicate rocks from the Superior Province, a literature review was undertaken which focussed primarily on studies of the Ontario Geological Survey relating to carbonatite-alkalic rock complexes. It was Mitchell and Krouse (1975) who first pointed out that although carbonatites often contain abundant sulphide and sulphate minerals, there exists very little published data on the isotopic composition of carbonatitic sulphur. In fact, since their study, very little additional data has been published. This study will present the first ever data on the sulphur isotopic composition of Superior Province carbonatites and associated silicate rocks. The goal was to choose complexes which not only showed evidence of sulphide mineralization, but which were also dissimilar in terms of age, geographic location and geological setting. Additional details on sampling methodology can be found in Appendix B. In addition, the sulphur isotopic data will be complemented by a detailed petrographic and petrochemical examination of these carbonatites and associated silicate rocks in order to ascertain whether their sulphur isotopic compositions represent source heterogeneities, crustal contamination, emplacement mechanisms, or a combination of each.

1.3 Previous Work

Papers relating to the isotopic composition of sulphur in carbonatites are listed in Table 1-1, and the data are shown in Figure 1-1.

Table 1-1. Localities and references for sulphur isotope data of carbonatites.

Name and Locality	Reference
Phalaborwa, South Africa	von Gehlen (1967)
Phalaborwa, South Africa	Hoefs et al. (1968)
Bol'shoy Sayan, former USSR Kovdor, Kola-Karelia, former USSR Maly Sayanski, East Sayan, former USSR Vuorijarvi, Kola-Karelia, former USSR	Grinenko et al. (1970a, b)
Bailundo, Angola (1975) Magnet Cove, USA (1975) Mountain Pass, California, USA Oka, Quebec, Canada (1975) Phalaborwa, South Africa (1975)	Mitchell and Krouse (1971, 1975)
Sokli, Finland	Mäkelä and Vartiainen (1978)
Lelyaki, Dnieper-Donets, former USSR	Panov et al. (1981)
Chernigovsk Zone, Azov Sea Coastal Region, former USSR	Bagdasarov and Grinenko (1981)
Dalbykha, Maimecha-Kotui, former USSR Yessey, Maimecha-Kotui, former USSR Yraas, Maimecha-Kotui, former USSR	Bagdasarov and Grinenko (1983)
Southern Siberia, former USSR	Bolonin and Zhukov (1983)
Nyanza Rift, western Kenya	Onuong'a et al. (1995)

Note that most of these data are from carbonatites now located within countries that were formerly included in the Soviet Union. The only data from Canada are from the carbonatite-ultramafic intrusion at Oka, Quebec.

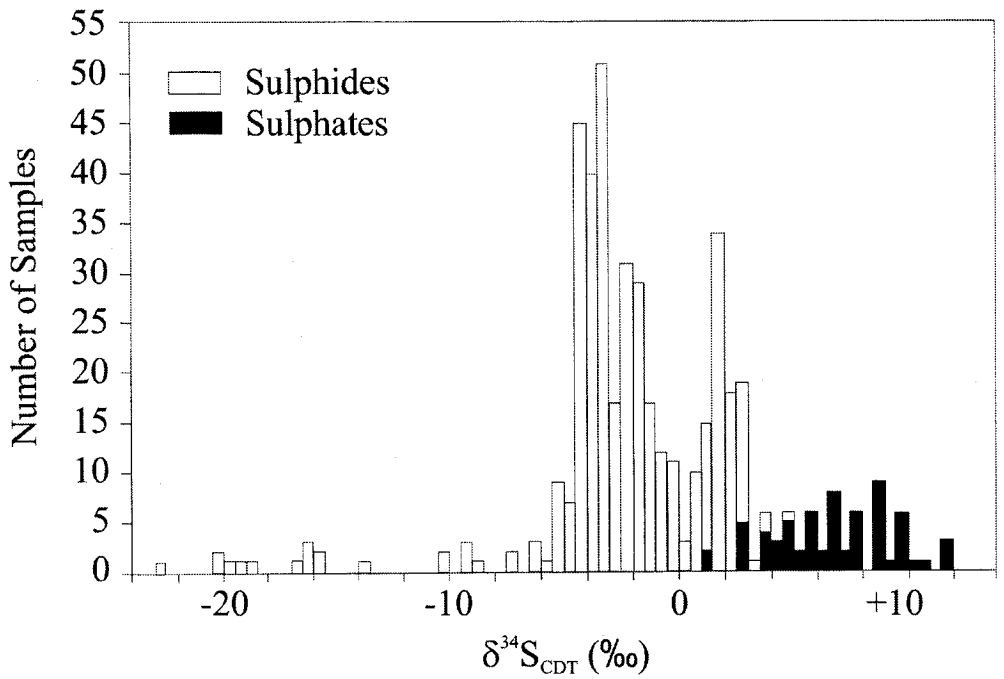

Figure 1-1. The sulphur isotopic composition of sulphides and sulphates from 14 carbonatite complexes compiled and plotted by Deines (1989). Data is from Hoefs et al. (1968); Grinenko et al. (1970a, b); Mitchell and Krouse (1971, 1975); Mäkelä and Vartiainen (1978); Panov et al. (1981); Bagdasarov and Grinenko (1983), Bolonin and Zhukov (1983). Figure is modified after Deines (1989).

Figure 1-1 shows a compilation made by Deines (1989) for 462 analyses from 14 carbonatite complexes. The sulphides include chalcopyrite, galena, pyrrhotite and pyrite. The sulphates are all barite except for one sample of celestite [$SrSO_4$]. From this Figure one can see the apparent ^{34}S enrichment in the sulphates compared to the sulphides. In addition, the apparent bimodality in the $\delta^{34}S_{sulphide}$ is not linked to sulphide mineralogy (Deines, 1989). In addition, Deines (1989 and references therein) found a trend of increase in negative $\delta^{34}S_{CDT}$ sulphide values from early to later stage carbonatites within a single complex. This trend was ascribed to an increase in oxidizing conditions from the

earlier to the later stages of formation. Deines (1989) also postulated that some of the differences in terms of sulphur isotopic composition between different carbonatite complexes are due to sulphur isotopic heterogeneity within the mantle. Also noteworthy was the observation that each carbonatite complex tends to possess its own distinct mean sulphur isotopic composition, but whether these differences are due to source or to the effects of carbonatite formation or crystallization is not known (Deines, 1989). Additional discussions on previously published studies relating to the sulphur isotope geochemistry of carbonatites can be found in Chapter 2.

1.4 Alkaline-Carbonatite Magmatism in the Superior Province

The Archaean Superior Province is the largest tectonothermal province that forms the Canadian Shield. In general, the Superior Province is made up of east-west trending belts which alternate between volcanic-rich and sedimentary-rich character and which are known as Subprovinces (Percival and Card, 1983). In addition, these east-west trending belts have been interrupted by a northeast-trending structural zone known as the Kapuskasing Structural Zone (KSZ) (refer to Figure 1-2). The Ontario portion of the Superior Province contains more than twenty alkaline-carbonatite intrusions which range in age from about 2700 Ma to 1000 Ma, e.g. Sage (1987a). Figure 1-2 shows the localities of those intrusions that were examined in this study. Allen (1972) and Sharpe (1987) noted that within 30 km of the 600 km long axis of the KSZ there exists eleven alkalic rock complexes of two distinct age groups, with one occurring ca. 1800 Ma and the other ca. 1075 Ma (Gittins et al., 1967). Burke and Dewey (1973) suggested that the

association of the 1000 – 1100 Ma alkalic-carbonatitic magmatism within the KSZ could mean that the Kapuskasing structure is a failed arm of the Keweenawan rift structure. Furthermore, Kumarapeli and Saull (1963) postulated that some of the Precambrian alkaline magmatism seen in Ontario (in addition to the Mesozoic Monteregian Alkaline Province near Montreal, QC) may be related to St. Lawrence rift valley.

Radiogenic isotope studies (Rb-Sr, Sm-Nd, U-Th-Pb) of alkaline-carbonatite intrusions from the Canadian Shield e.g. Bell et al. (1982), Blenkinsop and Bell (1983), Kwon (1986), Bell and Blenkinsop (1987), Bell et al. (1987) and Kwon et al. (1989), have shown that at ca. 2900 Ma ago there was a large-scale differentiation event within the mantle below the Superior Province which produced two complementary reservoirs in terms of Sr and Nd isotope systematics. The "enriched" reservoir is delineated by granitoid rocks (the Superior Province), while the "depleted" mantle is evidenced by the Sr and Nd isotopic composition of the carbonatites contained within the Superior Province. More significant is the fact that this "depleted" reservoir appears to have been preserved from at least 2900 Ma to about 110 Ma ago and that it also remained coupled to the continental crust until at least 110 Ma ago (Bell and Blenkinsop, 1987). Bell and Blenkinsop (1987) also postulated that by retaining its geochemical signature since the Archaean, this depleted reservoir may have avoided "complete convection disruption" and could indeed represent ancient lithospheric mantle.

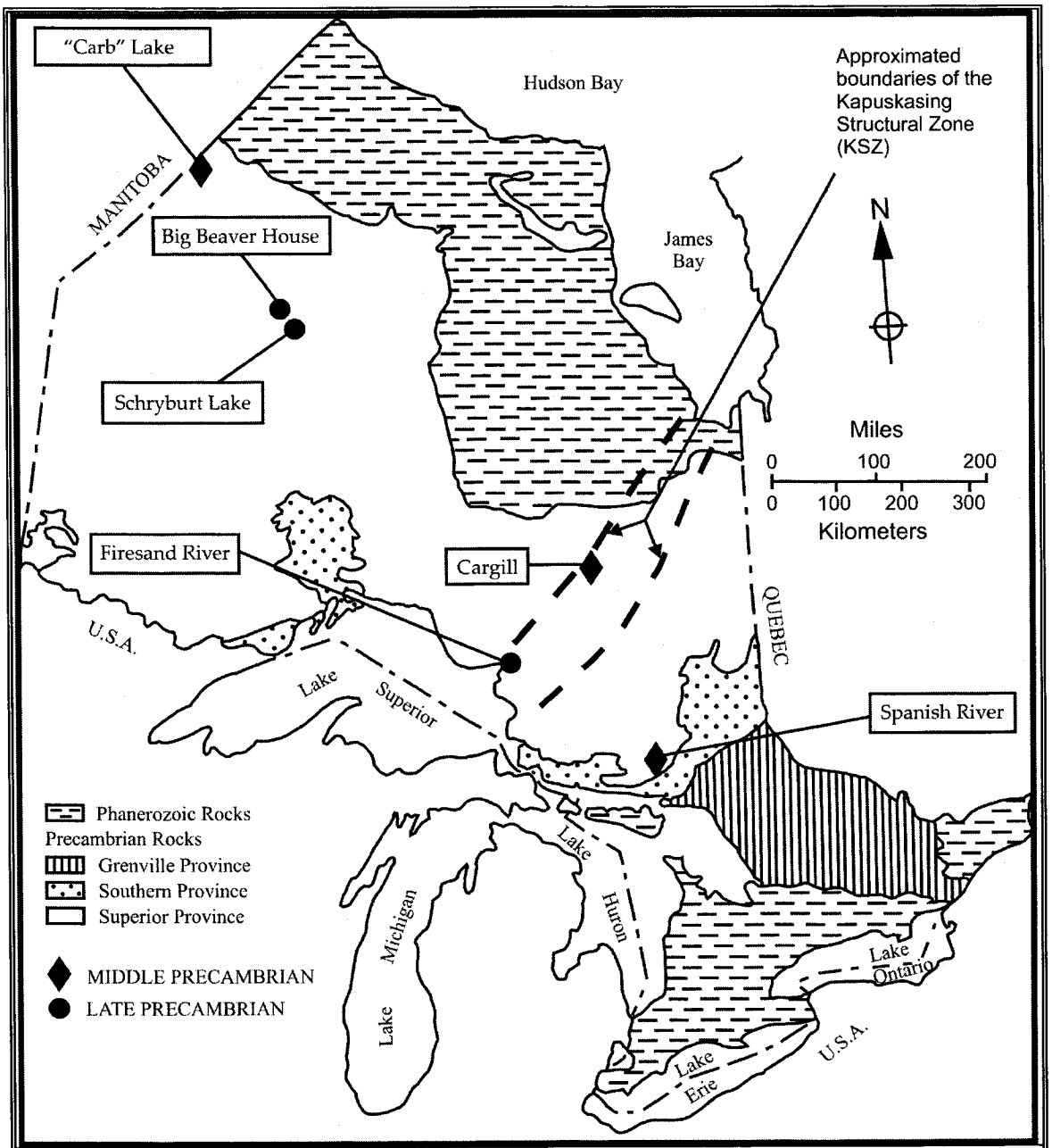

Figure 1-2. Simplified geological map of Ontario showing the localities of carbonatite complexes examined in this study. Map is modified after Sage (1987a).

Chapter 2: Stable Isotope Geochemistry

2.1 Overview - Sulphur

Sulphur is a group VI element (the same as oxygen) and has four stable isotopes with the following natural abundances: ^{32}S (94.93%), ^{33}S (0.76%), ^{34}S (4.29%) and ^{36}S (0.02%). The typical isotopic ratio measured in mass spectrometers is the $^{34}S/^{32}S$ ratio. This is because of the difference in mass and the percent abundances of the isotopes being measured. As with other stable isotope measurements, the results are reported using the δ-notation as per mil (‰) deviations from a standard of known isotopic composition. In the case of sulphur, this standard is a mineral phase called troilite (FeS) found in a meteorite from the Diablo Canyon located in Arizona, USA (note that CDT = Canyon Diablo Troilite). Thus,

$$\delta^{34}S_{CDT} = \left[\frac{^{34}S/^{32}S_{sample} - ^{34}S/^{32}S_{CDT}}{^{34}S/^{32}S_{CDT}} \right] \times 10^3 \qquad (2\text{-}1)$$

In addition to native sulphur, sulphides and sulphates are the two principal mineral types which host sulphur. In contrast to oxygen, which usually has only one oxidation state (–2), sulphur can exist in multiple oxidation states (–2, –1, 0, +2, +6). In sulphides, sulphur exists in its most reduced forms (–2, –1), whereas it is in its most oxidized form in sulphates (+6).

2.2 Mechanisms for Sulphur Isotope Fractionation

Isotopic fractionation results from the fact that certain thermodynamic properties of molecules are dependent on the masses of the atoms from which they are constituted

(Faure, 1986). One important consequence is that the lighter isotope of an element will form weaker bonds than the heavier isotope. Therefore, the phase containing the lighter isotope will be more reactive (Faure, 1986). In general, isotope fractionation occurs during several types of physical and chemical reactions (Faure, 1986):

(i) Isotope exchange reactions, which involve the re-distribution of isotopes of an element among the different molecules present which contain that element.

(ii) Single-directional reactions in which the reaction rates are dependent on the isotopic compositions of the reactants and products.

(iii) Physical reactions such as evaporation, condensation, melting and crystallization. Other mechanisms include adsorption and desorption and diffusion of ions or molecules caused by concentration or temperature gradients.

Sulphur is also known to undergo isotopic fractionation during bacterial reduction of sulphate into sulfide (Hoefs, 1997). Laboratory experiments have demonstrated that the resultant sulphide can be depleted in ^{34}S by between 4 to 46‰ when compared to the initial sulphate (Hoefs, 1997 and references therein).

In magmatic systems, sulphur can coexist as solid and vapour phases, as well as dissolved species. The solid phases present are different forms of sulphides and sulphates, e.g. FeS_2, $CuFeS_2$, $BaSO_4$, $CaSO_4$, and native sulphur [S_8]. The vapour and dissolved phases present can be SO_2, SO_3, H_2S and SO_4^{2-} and S^{2-} respectively. Because isotopic fractionation is inversely proportional to increasing temperature, one would not expect significant sulphur isotopic fractionation to occur at magmatic temperatures, e.g. ($T > 600°C$). However, experimental studies (e.g. Miyoshi et al., 1984) have shown that fractionation at high temperatures is significant for sulphur. In addition to temperature, there are many other factors, which affect the isotopic composition of sulphur within a

magma. These include, but are not limited to, the thermodynamic conditions (e.g. water vapour pressure in the melt P_{H_2O}, oxygen fugacity fo_2, and others) during cooling of the magma and the initial isotopic composition of the magma, $\delta^{34}S_{initial}$ (Zheng, 1990). Since sulphur can exist as gaseous SO_2 and H_2S in addition to sulphate and sulfide within a melt, Zheng (1990) proposed three different possible scenarios for sulphur isotopic fractionation within a magma:

i. A process of Rayleigh distillation involving bulk equilibrium fractionation between all of the magmatic sulphur species (which are in isotopic and chemical equilibrium), i.e. between degassed sulphur and residual sulphur, and between SO_2 and H_2S, and between sulfide and sulphate.

ii. Bulk disequilibrium fractionation, i.e. total disequilibrium fractionation among all sulphur species present.

iii. Partial equilibrium fractionation. This assumes that an equilibrium fractionation exists between sulfide and sulphate in the melt, but not between the degassed sulphur and the remaining sulphur, i.e. a selective flux of sulphur occurring during the emplacement of the magma.

These processes are evaluated in detail by Zheng (1990) who also suggests that temperature and fo_2 at the time of melt solidification control both the magnitude and direction of the $\delta^{34}S$ shift in the solidified rocks. Zheng (1990) summarized the processes that are often invoked in interpreting the sulphur isotopic composition of igneous rocks when their values fall outside the range of $0 \pm 2‰$. These are:

i. Contamination/assimilation (Shima et al., 1963; Cheney and Lange, 1967; Gorbachev and Grinenko, 1973; Ripley, 1981; Ohmoto, 1986)

ii. Alteration by seawater (Grinenko et al., 1975; Sakai et al., 1978)

iii. Outgassing of SO_2 (Sakai et al., 1982; Taylor, 1986)

iv. Outgassing of H_2S (Coleman, 1977; Rye et al., 1984)

Zheng (1990) goes on to comment that even these processes are often insufficient in explaining abnormally light or heavy $\delta^{34}S_{CDT}$ values in igneous rocks. Other factors that some authors have used to discuss certain $\delta^{34}S_{CDT}$ values are the oxidation state of the magma, e.g. Coleman (1979) and temperature and oxygen fugacity, e.g. Ohmoto and Rye (1979). In addition, Mitchell and Krouse (1975) demonstrated that fluctuations in the concentration of sulphur within a hydrothermal fluid can cause significant isotopic variations in the precipitated sulphur-bearing minerals. The process of Rayleigh distillation in terms of sulphur isotope systematics can be expressed quantitatively (Zheng, 1990) by:

$$\delta^{34}S = \delta^{34}S_o + 10^3 \ln \alpha_{melt}^{gas} \ln f \qquad (2\text{-}2)$$

where: $\delta^{34}S_o$ = the initial sulphur isotopic composition of the melt
α_{melt}^{gas} = the fractionation factor between gas and melt
f = fraction of sulphur remaining in the melt

In addition, taking into account the fractionation relationship between the gas and the melt in terms of quantitatively assessing the $\delta^{34}S$ values of igneous rocks that have lost varying proportions of sulphur during outgassing, the following approximation (Zheng, 1990) can be made:

$$10^3 \ln \alpha_{melt}^{gas} \approx \delta^{34}S_{gas} - \delta^{34}S_{melt} = \Delta^{34}S_{melt}^{gas} \qquad (2\text{-}3)$$

In addition, the dissolved volatiles such as H_2S and SO_2 must also be taken into account. This relationship (Zheng, 1990) can be expresses by:

$$\delta^{34}S_{melt} = x\delta^{34}S_{sulphide} + (1-x)\delta^{34}S_{sulphate} \qquad (2\text{-}4)$$

and

$$\delta^{34}S_{gas} = y\delta^{34}S_{SO_2} + (1-y)\delta^{34}S_{H_2S} \qquad (2\text{-}5)$$

where: x = the mole fraction of sulphur in the sulphide component of the melt

y = the mole fraction of sulphur in the SO_2 component of the magmatic volatiles

Subtracting equation (2-5) from equation (2-4) and introducing equation (2-3), the following (Zheng, 1990) is obtained:

$$\Delta^{34}S^{gas}_{melt} = 10^3 \ln \alpha^{SO_2}_{sulphide} - (1-y)10^3 \ln \alpha^{SO_2}_{H_2S} - (1-x)10^3 \ln \alpha^{sulphate}_{sulphide} \quad (2\text{-}6)$$

It becomes evident from equation (2-6) that trying to model the sulphur isotopic evolution of a melt can be quite complex because of all the variables and possible unknowns involved.

A simple example demonstrating a process of equilibrium fractionation between different sulphur species present within a melt is shown in Figure 2-1 below. In this example, isotopic enrichment occurring within the sulphate (SO_4^{2-}) with decreasing temperature is balanced by an equal isotopic depletion within the sulphide (S^{2-}).

Figure 2-1. Sulphur isotope fractionation between sulphate and sulphide in a melt with decreasing temperature. Modified after Zheng (1990); fractionation factors from Miyoshi et al. (1984).

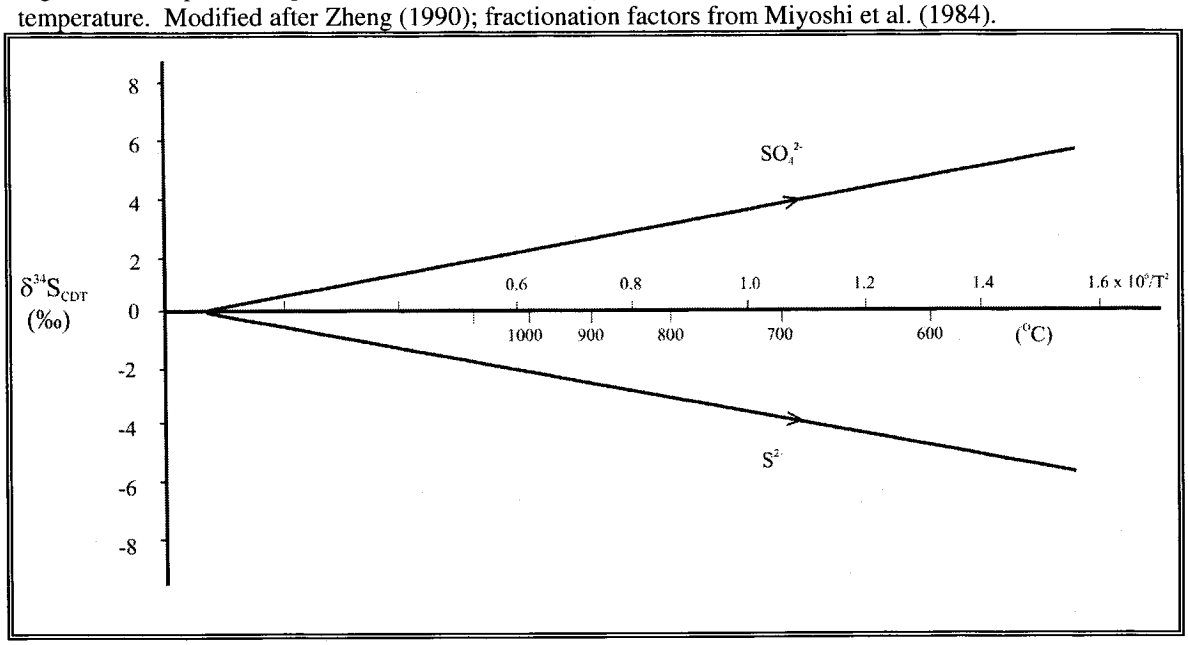

Another factor which has an indirect effect on sulphur isotopic fractionation is the mole fraction of a given sulphur species and its response to even small changes in pH and oxygen fugacity. Using data from Ohmoto (1972), Mitchell and Krouse (1975) noted that when the mole fraction of a given sulphur species is > 0.99, the isotopic composition of precipitating minerals is constant and unaffected by changes in pH or fo_2. When the mole fraction of a given sulphur species is < 0.99 it would seem that even small changes in pH or fo_2 will cause significant production of different sulphur species, which results in the precipitating minerals displaying a range in sulphur isotopic compositions (Mitchell and Krouse, 1975). Mitchell and Krouse (1975) also postulated that with falling temperatures within a carbonatite magma, oxidized sulphur species, e.g. HSO_4^-, SO_4^{2-} are formed at the expense of reduced sulphur species, e.g. H_2S, S^{2-}. This process could be attributed to an increase in oxygen fugacity with decreasing temperature. Therefore, high temperature carbonatites (≈ 700°C), for which sulphides are the dominant phase, will have $\delta^{34}S_{sulphide} \approx \delta^{34}S_{\Sigma S}$ because of mass balance considerations and the small isotopic fractionation (≈ 2.0‰) between H_2S and S^{2-} at 700°C (Mitchell and Krouse, 1975). In the case of low temperature carbonatites (≈ 300°C) sulphur is contained in both sulphates and sulphides, meaning that the sulphur is distributed between oxidized and reduced species and as a consequence of this neither the mean $\delta^{34}S_{sulphate}$ nor the mean $\delta^{34}S_{sulphide}$ will be indicative of $\delta^{34}S_{\Sigma S}$ (Mitchell and Krouse, 1975). Another important finding made by Mitchell and Krouse (1975) for part of the low temperature (≈ 300°C) carbonatite at Mountain Pass (California), was that a decrease in the total sulphur concentration from 0.1 m S/Kg H_2O to 0.001 m S/Kg H_2O within the calcitic carbonatite may explain the intra-unit $\delta^{34}S_{barite}$ variations from +9 to +1‰. An alternative

explanation for the calcitic carbonatite at Mountain Pass was non-equilibrium deposition, supported by the observation that the isotopic fractionation between galena and barite within this unit was not constant (Mitchell and Krouse, 1971). Mitchell and Krouse (1975) also noted that with an increase in the amount of oxidized sulphur species due to falling temperature, one would expect that the precipitating barites should in fact be progressively enriched in ^{32}S and not ^{34}S, as was noted for the carbonatites at Mountain Pass. This observation was attributed to either a decrease in the total sulphur concentration with sequence of intrusion, or to non-equilibrium deposition.

2.3 Isotopic Composition of Mantle Sulphur

Early studies on meteoritic sulphur (e.g. MacNamara and Thode, 1950; Thode et al., 1961) revealed that its isotopic composition was quite uniform when compared to terrestrial sulphur. In addition, the coincidence of the median terrestrial sulphur with that of meteoritic sulphur (which also fell into the approximate range of presumed igneous rocks) led MacNamara and Thode (1950) to postulate that meteoritic sulphur ($\approx 0‰$) represents the isotopic composition of primordial terrestrial sulphur. They also postulated that formation of the Earth's crust has fractionated the primordial sulphur above and below this baseline value.

$\delta^{34}S_{CDT}$ values of basic sills, ocean floor basalts and meteorites mostly fall into the narrow range of –1 to +1‰, which is generally considered to be characteristic of pristine mantle (Deines, 1989). There are, however, some sulphur isotopic values from basic intrusions which display mean $\delta^{34}S_{CDT}$ values that are above and outside of the

meteoritic mean, e.g. Muskox: +5‰ (Sasaki, 1969), Noril'sk: +9‰ (Godlevskii and Grinenko, 1963) and Sudbury: +2.1‰ (Schwarcz, 1973). Continental basalts may also show elevated $\delta^{34}S_{CDT}$ values, e.g. Schneider (1970), Hubberten et al. (1977), and Ueda and Sakai (1984). Schneider (1970) analyzed a large number of continental tholeiitic and olivine-alkali basalts from Europe and found a range of $\delta^{34}S_{CDT}$ values between +3.0 and –3.1‰. Based on these results, it was proposed that the mantle has a $\delta^{34}S_{CDT}$ value of +1.3 ± 0.5‰. Deines (1989) attributed these elevated $\delta^{34}S_{CDT}$ values to possible crustal contamination, changing fo_2 values, and degassing processes. In addition, Chaussidon and Lorand (1990) suggested that the sub-continental lithospheric mantle has two isotopically distinct sulphur reservoirs (+3‰ and –3‰). These authors analyzed sulphides from orogenic spinel lherzolite massifs, which displayed differences between the isotopic composition of the peridotites and the pyroxenites, the overall range being between –7.2 and +6.0‰. Based on their ion-microprobe study of sulphide inclusions within diamonds, Chaussidon et al. (1987) proposed that sulphur isotopic heterogeneity exists within the mantle, which they interpreted as evidence for recycling of crustal material into the lithospheric mantle.

On the other hand, the isotopic composition of the asthenospheric mantle seems more restricted and closer to the meteoritic mean. Fresh MORB lavas have $\delta^{34}S_{CDT}$ values of 0 ± 2‰ e.g. Grinenko et al., 1975; Sakai et al., 1982, 1984, which is a generally accepted range for the asthenospheric mantle (Ripley, 1999). Rollinson (1993) postulated that the best estimate for the sulphur isotopic composition of the primitive mantle is ≈ +0.5‰, which was proposed by Chaussidon et al. (1989) using a combination of sulphur isotopic analyses from mantle-derived rocks and mass balance calculations.

Considering all these data, a conservative estimate for the sulphur isotopic composition of the primitive mantle is proposed to be 0 ± 1.5‰ for the purposes of this study.

2.4 Overview – Carbon and Oxygen

Oxygen, like sulphur, is a group VI element and consists of three stable isotopes with the following natural abundances: ^{16}O (99.757%), ^{17}O (0.038%) and ^{18}O (0.205%) with the $^{18}O/^{16}O$ being the isotopic ratio most typically measured by most stable isotope ratio mass spectrometers. Carbon is a group IV element and consists of two stable isotopes with the following natural abundances: ^{12}C (98.93%) and ^{13}C (1.07%). Like sulphur, both oxygen and carbon isotopic ratios are reported as per mil deviations from a standard of precisely known isotopic composition using the conventional δ-notation. The standard for oxygen is V-SMOW (Vienna-Standard Mean Ocean Water) while the standard for carbon is V-PDB (Vienna-Peedee Belemnite).

The carbon isotopic composition of the mantle is thought to be approximately −5‰ (Kyser, 1986). Deines (1989) found that 91% of $\delta^{13}C_{V\text{-}PDB}$ values from intrusive carbonatites lie in the narrow range of −2 to −8‰. Deines (1989) also found that on average the carbon isotopic composition of carbonatites is slightly more enriched when compared to diamonds and meteoritic C, which was attributed to the isotopic effects concentrating ^{13}C in a carbonatitic melt during its formation.

The oxygen isotopic composition of the mantle is thought to lie between +5 and +7‰ (Kyser, 1986). The oxygen isotopic composition of carbonatites in contrast to carbon can be quite variable with a general range of +5 to +25‰. However, about 50%

of the analyses fall into the narrow range of +6 to +9‰ (Deines, 1989). Deines (1989) also demonstrated that carbonatite with an oxygen isotopic composition between +7 and +8‰ could be produced by isotopic fractionation at 1000°C of an average peridotite ($\delta^{18}O_{V\text{-}SMOW}$ = +5 to +6‰) that is in equilibrium with this carbonate melt.

2.5 Mechanisms for Oxygen and Carbon Isotopic Fractionation in a Carbonatitic System

In terms of oxygen isotope systematics, Deines (1989) proposed five mechanisms which could cause isotopic enrichment beyond the upper limit of +9.5‰:

1. the loss of fluids during pressure reduction at the time of emplacement;
2. exchange with magmatic fluids possessing a high ^{18}O content;
3. retrograde exchange with magmatic waters;
4. exchange with ^{18}O-rich hydrothermal fluids;
5. influx of meteoric water and isotope exchange at low temperatures.

With respect to carbon isotope systematics, Deines (1989) demonstrated that $\delta^{13}C_{V\text{-}PDB}$ tends to increase from earlier to later stages in a given carbonatitic intrusion, which was attributed to a process of Rayleigh fractionation.

Ray and Ramesh (2000) considered the effects of a fluid phase on the isotopic fractionation and isotopic composition of a precipitating carbonatite magma. In their study these authors examined two cases involving different fluid compositions. One case involved CO_2 as the dominant fluid phase while the other case involved H_2O as the dominant fluid phase. When CO_2 is the principle fluid phase, isotopic evolution in carbon and oxygen space tends to be nearly diagonal with the extent of the fractionation

dependent on the initial molar ratio of H_2O to CO_2 (Ray and Ramesh, 2000). In contrast, when H_2O is the principle fluid phase, isotopic evolution in carbon and oxygen is sub-vertical. The calculated extent of isotopic fractionation in this model was such that $\delta^{13}C_{V\text{-}PDB}(final) \approx -1‰$ when $\delta^{13}C_{V\text{-}PDB}(initial) \approx -5.5‰$, Ray and Ramesh (2000). Ray and Ramesh (2000) go on to point out that for calcite carbonatite complexes the slopes of the correlated $\delta^{13}C$ and $\delta^{18}O$ variations that are less than 1.0 are consistent with their model for which CO_2 is the dominant fluid phase. This, they go on to discuss, is also consistent with the suggestion that CO_2 is likely the major fluid phase associated with primary carbonate magmas (Kjarsgaard and Hamilton, 1989). In addition, even if H_2O was the dominant fluid phase the model involving CO_2 as the dominant fluid phase could still be applied if an H_2O-rich phase were expelled from the magma in the form of fenitizing fluids which in turn produced a residual CO_2-rich fluid prior to the onset of crystallization (Ray and Ramesh, 2000). It will be subsequently demonstrated that most of the carbonatite complexes examined in this study show relatively horizontal trends in carbon and oxygen isotopic space, suggesting that if the carbonate phases in these complexes were crystallizing in the presence of a fluid phase, it was likely dominated by CO_2 rather than H_2O.

Chapter 3: Results and Discussion

3.1 Chapter Format

This chapter contains a geological description and discussion on the isotopic geochemistry of each of the individual carbonatite complexes. Also contained is a section which relates the Schryburt Lake and Big Beaver House carbonatite complexes. Chapter 3 then ends with a section on mineral chemistry. Stable isotopic data are presented in tabular form for each complex and includes rock type, sulphide mineral species and sample ID. In addition, sample ID's with an asterisk denote samples which have also been examined in thin-section for which descriptions of sulphide and oxide mineralogy are found in Appendix C.

3.2 Schryburt Lake Complex – Geological Overview

The Schryburt Lake carbonatite complex, located within the Gods Lake Subprovince of the Superior Province of the Canadian Shield, is late Proterozoic in age and has been dated at 1145 ± 74 Ma by K-Ar (Bell and Watkinson, pers. comm. 1977 in Sage, 1988b). Combined outcrop and aeromagnetic data suggest that the complex has a surface area of approximately 4.5 km^2 (Sage, 1988b). The complex is composed of sövites, silicocarbonatites and dolomite-carbonatites that intruded early Precambrian gneissic granodiorites. Fenitized and brecciated granitic rocks are found on the north flank of the complex (Sage, 1988b).

The sövites at the Schryburt Lake complex are fine – medium grained, massive equigranular to inequigranular-seriate and hypidiomorphic, with some samples being

allotriomorphic with curved to straight grain boundaries and consist of carbonate, biotite-phlogopite, apatite, amphibole and magnetite (Sage, 1988b). Minor to trace minerals include perovskite, pyrochlore, titanite, pyrrhotite and chlorite. Higgins (1977) also reported the presence of fluorite, chalcopyrite and pentlandite.

The silicocarbonatites at the Schryburt Lake complex were found to display both gradational and sharp contacts with the sövites. In addition, Sage (1988b) postulated that these silicocarbonatites may represent either: (1) cumulate phases, (2) altered screens and xenolithic blocks of granitic gneiss, or (3) carbonated mafic dykes. Platt (1994) stressed that the term "silicocarbonatite" does not seem justifiable for many of the samples from the Schryburt Lake complex and proposed that some the samples could be classified as mica-rich, alkaline ultramafic rocks. In terms of texture and mineralogy, the silicocarbonatites are fine to medium grained, massive, equigranular to inegranular-seriate, hypidiomorphic to allotriomorphic, with curved to straight grain boundaries and composed of amphibole, magnetite, biotite-phlogopite, chondrodite, carbonate, olivine, apatite, perovskite, clinopyroxene and minor sericite and pyrochlore. Beforsite at the Schryburt Lake complex is relatively rare and appears to have taken the form of a dyke cross-cutting the sövites and silicocarbonatites (Sage, 1988b).

In terms of carbonate mineralogy, the Schryburt Lake complex is the only one in this study for which there are two distinct carbonate phases identified within the sample. Calcite and dolomite were identified on the basis of heavy liquid separation. Both Sage (1988b) and Higgins (1977) confirmed the presence of dolomite at Schryburt Lake using both X-ray diffraction and staining techniques. Higgins (1977) found that the dolomite occurs as either isolated grains, intergrowths with calcite, and as bands within the calcite.

Fenitization at the Schryburt Lake complex consists of Fe-Na-carbonate metasomatism in the altered granitic country rocks northeast of the complex (Sage, 1988b). Sage (1988b) found no petrographic evidence of metamorphism within the Schryburt Lake carbonatite complex.

3.3 Schryburt Lake Complex – Isotope Geochemistry and Discussion

$\delta^{34}S_{CDT}$ values were obtained from sulphides in six samples from the Schryburt Lake carbonatite complex. In addition, $\delta^{18}O_{V\text{-}SMOW}$ and $\delta^{13}C_{V\text{-}PDB}$ values were also obtained from carbonates from the same samples using both calcite and dolomite separates. The sulphur, oxygen and carbon isotopic compositions for the analysed samples from Schryburt Lake are listed in Table 3-1 and Table 3-2.

Table 3-1. Sulphur isotope values for carbonatites from the Schryburt Lake complex.

Sample ID	Rock Type	Mineral Separate	$\delta^{34}S_{CDT}$
SR18-4	sövite	pyrrhotite	–4.5‰
SR18-5*	sövite	pyrrhotite	–3.9‰
SR18-7*	sövite	pyrrhotite	–3.4‰
SR18-8*	sövite	pyrrhotite	–4.2‰
HEF 13-1	sövite	pyrrhotite	–3.7‰
HEF 13-1A1	sövite	pyrrhotite	–3.8‰

Table 3-2. Oxygen and carbon isotope values for carbonatites from the Schryburt Lake complex.

Sample ID	Rock Type	Mineral Separate	$\delta^{18}O_{V\text{-}SMOW}$	$\delta^{13}C_{V\text{-}PDB}$
SR18-4	sövite	calcite	+6.98‰	–4.91‰
SR18-4	sövite	dolomite	+5.28‰	–4.35‰
SR18-5*	sövite	calcite	+6.84‰	–4.95‰
SR18-5*	sövite	dolomite	+5.15‰	–4.38‰
SR18-7*	sövite	calcite	+6.85‰	–5.10‰
SR18-7*	sövite	dolomite	+5.21‰	–4.53‰
SR18-8*	sövite	calcite	+6.94‰	–5.01‰
SR18-8*	sövite	dolomite	+5.04‰	–4.49‰
HEF 13-1	sövite	calcite	+6.83‰	–5.10‰
HEF 13-1	sövite	dolomite	+5.08‰	–4.53‰
HEF 13-1A1	sövite	calcite	+6.95‰	–5.10‰

The sulphides within the carbonatites at the Schryburt Lake complex are mainly pyrrhotite with trace amounts of chalcopyrite. In addition, Platt (1994) identified chalcopyrite, sphalerite, pyrrhotite, pentlandite [$(Fe,Ni)_9S_8$] and millerite within the alkaline ultramafic rocks and minor amounts of djerfisherite [$K_6Na(Fe,Cu,Ni)_{25}S_{26}Cl$], possibly a metasomatic replacement of the pentlandite. In general, the crystals of pyrrhotite are euhedral to subhedral (see plate 1.1), range in size from about 0.1 mm to 4 mm, and occur as discontinuous sulphide-rich streaks in the banded host carbonatite (Sage, 1988b).

In terms of sulphur isotopic composition, the carbonatites from the Schryburt Lake complex represent the most depleted isotopic signature of all the carbonatite complexes examined in this study. As previously discussed, the primitive mantle is assumed to have a sulphur isotopic composition of $0 \pm 1.5‰$. Given this range, processe(s) other than simple source heterogeneity must be called upon to explain the sulphur isotopic values of these carbonatites.

There are at least four possibilities that could have caused the depleted sulphur isotopic signature in the carbonatites at the Schryburt Lake complex. These are: crustal contamination, source heterogeneity, isotopic exchange between reduced and oxidized sulphur species in the magmatic system and variations in f(x), where x = fo_2, fs_2, T(°C), $[S]^{conc.}$ and the FeO/Fe_2O_3 ratio or a combination of each one of these mechanisms.

The fact that the pyrrhotite occurs as distinct euhedral crystals in well defined layers implies that they formed as a primary cumulate phase during the crystallization of the carbonatitic magma. Mitchell and Krouse (1975) proposed that when the dominant sulphide within a carbonatite is pyrrhotite, it reflects higher temperatures of formation

(500 – 700°C) and that only carbonatites formed at high temperature will provide estimates of mantle $\delta^{34}S_{CDT}$.

The first possible way to explain the variation in sulphides from the Schryburt Lake complex is isotopic heterogeneity within the source of the source of the parental melt. Referring back to Chapter 2 on stable isotope geochemistry, it was demonstrated that there does indeed exist heterogeneity within the mantle in terms of sulphur isotope systematics (e.g. Chaussidon et al., 1987).

The possibility of source heterogeneity is difficult to evaluate, because the actual spatial distribution of potential pockets of heterogeneous material is not well constrained. The best clue may come from the study of radiogenic isotope systematics, which is known to be a useful tool in monitoring the geochemical evolution of the mantle through time. In fact, carbonatites are an ideal rock type for this kind of research because they are able to "buffer" their isotopic composition (in terms of Sr, Nd and sometimes Pb) from the effects of crustal contamination, e.g. Bell and Blenkinsop (1987). Analysis of Superior Province carbonatites has demonstrated that the mantle source below the Superior Province, for which these carbonatites were derived, has behaved as a relatively closed system from about 2900 Ma to approximately 110 Ma in terms of Sr isotope systematics (Bell and Blenkinsop, 1987). This of course does not necessarily mean that this mantle source has also remained a closed system in terms of sulphur, but it does demonstrate that for a large period of geological time, the mantle below the Superior Province may have avoided large scale differentiation events.

Another mechanism that can cause fluctuations in the sulphur isotopic composition of mantle-derived rocks is assimilation of crustal sulphur during

emplacement. On a broad scale, the continental crust possesses two sulphur isotopic reservoirs. The first is seawater sulphate, e.g. gypsum. Claypool et al. (1980) and Strauss (1997) have shown that seawater $\delta^{34}S_{CDT}$ has varied between ~ +10 and +30‰ from the Neoproterozoic to the present. The second principal reservoir is caused by bacterial reduction of this sulphate reservoir, which under different conditions can yield two reservoirs with quite different sulphur isotopic compositions. Bacterial reduction of sulphate under open-system conditions (meaning that the rate of sulphate reduction is slow with respect to sulphate supply, i.e. that the product sulphide does not remain in the system), results in $\delta^{34}S_{CDT}$ values that will be shifted in a negative direction, up to about 40‰ less than that of the parent seawater (Ripley, 1999 and references therein). On the other hand, if the rate of sulphate reduction is fast with respect to the supply of sulphate (e.g. slow diffusion of sulphate into the pores of seafloor sediments; finite supply of sulphate in a restricted basin), this results in $\delta^{34}S_{CDT}$ values that may approach or even exceed that of the source sulphate (Ripley, 1999; Zabach et al., 1993 and Goodfellow and Jonasson, 1984).

Crustal contamination and/or interaction with seawater sulphate are difficult to assess at Schryburt Lake especially since only about 3% of the complex has been studied because of limited outcrops (Sage, 1988b). However, Higgins (1977) proposed that the limited fenite zone associated with this carbonatite complex can be viewed as evidence for little, if any, magma contamination by the surrounding country rocks. In addition, the carbon and oxygen isotopic data (Table 3-2), which represents relatively pristine mantle-like isotopic signatures seem to rule out any interaction between the carbonatitic magma and circulating seawater, meteoric water or crustal material. It is, however, very

important to point out that the use of sulphur isotopes in delineating magma contamination by country rocks that are Archaean in age may be ambiguous. This is mainly because these country rocks tend to possess sulphur isotopic compositions similar to those expected for many mantle-derived igneous rocks, i.e. close to 0‰ e.g. Ohmoto (1986).

Source heterogeneities and crustal contamination can be considered external mechanisms which could alter the isotopic composition of primitive, mantle-derived sulphur. As was alluded to earlier, it is difficult to rigorously assess these two possibilities, but based on the carbon and oxygen isotope data and field observations presently available, it would appear that both source heterogeneity and crustal contamination can be ruled out. Therefore other mechanisms related to the emplacement and differentiation of the carbonatites at the Schryburt Lake complex (internal causes), will now be evaluated.

Isotopic exchange between reduced and oxidized sulphur species in the magmatic system could also explain the observed sulphur isotopic composition of pyrrhotite. If the sulphur isotopic compositions of the sulphide phases at the Schryburt Lake complex are to be modelled in terms of some kind of isotopic exchange model, then an estimate of the temperature of crystallization is required. The carbonatites examined at the Schryburt Lake complex are essentially mono-mineralic in terms of their sulphide composition, being principally composed of pyrrhotite with only very minor amounts of chalcopyrite. Because pyrrhotite is known to crystallize over a large temperature range (e.g. from 1100°C in magmatic sulphides deposits to 300°C in hypothermal deposits), it is difficult to evaluate crystallization temperatures based solely on the presence of pyrrhotite. Other

methods must therefore be in order to obtain a reasonable estimate of the crystallization temperature of the pyrrhotite.

Higgins (1977) proposed the following mineral sequence for crystallization of the Schryburt Lake carbonatites (earliest → latest): olivine → pyroxene → tremolite → phlogopite → apatite → oxides → calcite. It should be noted that Higgins also found that the crystallization intervals of most of the minerals overlapped during the crystallization process. Higgins (1977) does not mention where pyrrhotite fits into the petrogenetic sequence, but it would seem reasonable to assign its position to that of the oxides. This is logical because in both the study of Higgins (1977) and this study there is evidence that both magnetite and pyrrhotite are closely associated with one another (see Plate 1.2). Therefore, it would seem that the pyrrhotite within these carbonatites formed relatively late in the evolution of this carbonatitic melt.

Using the carbon and oxygen isotope data from coexisting dolomite and calcite it is possible to estimate crystallization temperature, which may also be indicative for the crystallization temperature of the pyrrhotite. The dolomitic phase was effectively separated from the calcitic phase using bromoform ($\rho \approx 2.90$ g/cm^3). Both minerals were analysed separately (see Table 3-2) for carbon and oxygen isotopes. The dolomite component was also further purified of any calcite using the carbonate extraction line before its CO_2 component was collected for analysis (see Appendix B). Thus, variations in the carbon and oxygen isotopic compositions between the calcite and dolomite phases from the same samples can be considered meaningful. Deines (1989) has demonstrated that when both calcite and dolomite are present in the same carbonatite, both the $\delta^{18}O_{V\text{-}SMOW}$ and $\delta^{13}C_{V\text{-}PDB}$ values of the dolomite phases are expected to be slightly more

enriched then the corresponding values for the calcite. This relationship seems to be more reliable for carbon than for oxygen. In any event, Deines (1989) attributed negative fractionation values (i.e. calcite is the isotopically enriched phase), to possible isotopic disequilibrium. Table 3-2 demonstrates that in terms of $\delta^{18}O_{V\text{-}SMOW}$ all of the dolomites are considerably depleted with respect to the coexisting calcites, in some cases by almost −2.0‰. The difference between the oxygen isotopic composition of the coexisting calcite and dolomite phases likely represents either some kind of isotopic disequilibrium process, or that the dolomites are a second and distinct magmatic phase (Deines, 1989). In their studies on Brazilian carbonatites, Santos and Clayton (1995) attributed negative oxygen isotopic fractionation between coexisting calcite and dolomite to secondary processes. Northrop and Clayton (1966) found that under laboratory conditions, calcite exchanges oxygen isotopes much faster then dolomite, and on this basis Santos and Clayton (1995) suggested that calcite would be more susceptible to isotope exchange with other phases in the system, such as hydrothermal fluids. Northrop and Clayton (1966) also stressed that all of the fractionations were initially negative but would become more positive with time. Therefore, it would seem that oxygen isotope exchange between calcite and dolomite is rather sluggish and requires considerable time to equilibrate. Since carbonatite magmas tend to exist at lower temperatures and cool more quickly than most other igneous rocks, it is possible that there was not enough time to achieve oxygen isotope equilibrium. This could explain why the $\delta^{18}O_{V\text{-}SMOW}$ of the calcite, on average, is enriched by ~ +1.7‰ compared to coexisting dolomite. Conversely, the $\delta^{13}C_{V\text{-}PDB}$ values of dolomite are slightly enriched when compared to the coexisting calcite $\delta^{13}C_{V\text{-}PDB}$ values. Assuming that dolomite does not represent a second

and distinct magmatic phase, this positive fractionation allows for a geothermometric calculation using the $\delta^{13}C_{V\text{-}PDB}$ values of the coexisting calcite and dolomite phases. Using the empirically derived equation of Sheppard and Schwarcz (1970):

$$10^3 \ln \alpha_{calcite}^{dolomite} = 0.18(10^6 T^{-2}) + 0.17 \qquad (3\text{-}1)$$

carbon isotope equilibrium temperatures between the coexisting dolomites and calcites were obtained and are listed in Table 3-3.

Table 3-3. Calcite-dolomite carbon isotope geothermometry for the Schryburt Lake carbonatites. The errors were calculated using a analytical mass spectrometer precision of ± 0.1‰ and then averaged. Both the $\delta^{13}C_{dolomite}$ and the $\delta^{13}C_{calcite}$ were measured versus V-PDB.

Sample ID	$\delta^{13}C_{dolomite}$	$\delta^{13}C_{calcite}$	Temperature
SR18-4	–4.35‰	–4.91‰	677 ± 209°C
SR18-5	–4.38‰	–4.95‰	669 ± 200°C
SR18-7	–4.53‰	–5.10‰	669 ± 199°C
SR18-8	–4.49‰	–5.01‰	715 ± 260°C
HEF 13-1	–4.53‰	–5.10‰	669 ± 199°C

The calculated temperatures are evidence that the carbonatites at the Schryburt Lake complex should be considered high-temperature carbonatites as defined by Mitchell and Krouse (1975) i.e. forming in the range of 500 – 700°C. Because pyrrhotite crystallized before calcite, then they may also have crystallized as high temperature mineral phases. Referring to Figure 2-1 (p.13), it can be seen that one possibility for the sulphur isotopic evolution in a melt is isotopic fractionation between coexisting sulphide and sulphate, represented by the S^{2-} and SO_4^{2-} ions, respectively. This however is a rather simplistic scenario because it does not take into account the possible effects of isotopic exchange with outgassing H_2S and/or SO_2, and it assumes the presence of both S^{2-} and SO_4^{2-} throughout the entire evolution of the melt. However, it does demonstrate that as a melt cools, isotopic depletion in the sulphide ion is balanced by isotopic enrichment in the coexisting sulphate ion. If the initial sulphur isotopic composition of

the melt was ~ 0‰ and pyrrhotite crystallized at approximately 680°C (see Table 3-3), then the expected isotopic composition of the S^{2-} ion, from which pyrrhotite crystallized would be about –4‰ as interpolated from Figure 2-1, and hence similar to the average $\delta^{34}S_{CDT}$ value of –3.9‰ from the Schryburt Lake carbonatites. Therefore the sulphur isotopic composition of the sulphides from the Schryburt Lake carbonatites could be explained by isotopic fractionation between coexisting sulphate and sulphide during the cooling of the melt down to a temperature of about 700°C.

A measurement of temperature and oxygen fugacity was also obtained using the petrochemistry of coexisting magnetite and ilmenite. A temperature of ~ 451°C and a fo_2 value of $\sim 10^{-22.34}$ were obtained (see Section I in Mineral Chemistry for a detailed discussion). This calculated temperature is about 200°C below the temperature calculated from the carbon isotopic compositions of coexisting calcite and dolomite, but is still within the range of analytical uncertainty. Of greater significance is the calculated value for the oxygen fugacity of $\sim 10^{-22.34}$, which along with the calculated temperature of ~ 451°C would put the conditions of magnetite-ilmenite crystallization very close to the stability boundary of H_2S and SO_2 (refer to Figure 3-6). The consequence of this, as discussed in Section 3.13.1 suggests that the rather depleted sulphur isotopic composition of pyrrhotite from the Schryburt Lake complex could have been the result of isotopic fractionation during magma outgassing, due to the presence of sulphur species possessing markedly different valences, i.e. –2 in H_2S and +4 in SO_2. The rarity of a sulphate-bearing mineral phase e.g. barite, in the carbonatites at the Schryburt Lake complex may signify that SO_2 was mostly removed (after isotopic exchange with H_2S) from the system

via outgassing, while H_2S remained in the system, being the principal source of sulphur for the formation of pyrrhotite.

Considering the evolved nature of the sulphur isotopic compositions of the carbonatites at the Schryburt Lake complex, it seems counterintuitive that both the carbon and oxygen isotopic compositions of the calcite and dolomite phases within these carbonatites are observed to be extremely uniform, in addition to possessing mantle-like isotopic signatures. If most of the carbonatites at the Schryburt Lake complex had crystallized from a volatile-rich melt then one would expect to find, at the very least, more evolved oxygen isotopic compositions than those observed at the Schryburt Lake complex. Higgins (1977) suggested that the limited fenite zone associated with the Schryburt Lake carbonatite complex indicates very little chemical reaction between the carbonatitic melt and the surrounding country rock during the intrusive event. All of this suggests that the melt which produced the Schryburt Lake carbonatite complex did not expel its volatile phase during emplacement, which would explain both the uniformity and mantle-like signature in terms of carbon and oxygen isotopic compositions.

An indirect method that might help piece together the sulphur isotopic evolution of the carbonatites is the geochemical signature of apatite [$Ca_5(PO_4)_3(F,OH,Cl)$] present in many samples. Apatite, a very common mineral in carbonatites (see Hogarth, 1989), can be present in sufficient quantity in some carbonatites to be of economic interest since it is one of the principal sources of phosphorus. Apatite from carbonatites can also be enriched in REEs and because it is usually on the liquidus during the entire evolution of carbonatite crystallization (e.g. Timmermans, 2003), its geochemical signature can be a good indicator of how evolved the melt was when it crystallized. A detailed petrographic

and petrochemical examination of apatite from the Schryburt Lake carbonatites (see Section 3.12.2 in Mineral Chemistry) reveals the following: (1) the apatite is compositionally zoned with REE contents that increase from core to rim (see Plate 1.3), (2) the apatite is fluorapatite, i.e. $Ca_5(PO_4)_3F$, (3) pyrrhotite formed after the apatite (e.g. Plate 1.4). Referring to Figure 3-7 (Section 3.12.2, p.77) it is evident that geochemical signatures for the apatite from the Schryburt Lake complex are generally more evolved than the apatite from the Cargill, Spanish River, Big Beaver House and Firesand River complexes, and also correlate well with the sulphur isotopic signatures of the sulphide phases from these different carbonatite complexes. Additional discussion on the petrochemistry of apatite from the different carbonatite complexes can be found in Section 3.12.2 on Mineral Chemistry.

The simplest interpretation of the sulphur isotopic compositions of pyrrhotite from the Schryburt Lake carbonatites is that isotopic fractionation took place between reduced and oxidized sulphur species, which resulted in ^{32}S enrichment in the reduced species and ^{34}S enrichment in the oxidized species. This interpretation would be best confirmed by isotopic analyses of coexisting sulphate minerals, e.g. barite in the same samples. Unfortunately, no sulphate mineral was detected during mineral separation procedures, but its presence within the Schryburt Lake carbonatites was confirmed using SEM techniques (see Plate 1.5). Although it is difficult to ascertain whether there was sufficient dissolved SO_4^{2-} present during the precipitation of pyrrhotite at the Schryburt Lake complex, the data obtained from the magnetite-ilmenite petrochemistry does suggest the presence of an oxidized sulphur species during the crystallization of the pyrrhotite. Another explanation for the sulphur isotope geochemistry of the sulphides at

the Schryburt Lake complex is discussed in Section 3.12, which involves a petrogenetic scheme involving the concomitant formation of the adjacent Big Beaver House carbonatite complex.

3.4 Big Beaver House Complex – Geological Overview

The Big Beaver House carbonatite complex is located within the Gods Lake sub-province in the Superior Province. The complex has been dated by K-Ar, which yielded an age of 1109 ± 61 Ma (Watkinson and Bell, 1977, pers. comm. in Sage, 1987a). Aeromagnetic data (ODM-GSC, 1970) suggest it may have been emplaced into an inferred NW-trending fracture and the intrusion is interpreted to have a surface area of 16km^2 (Sage, 1987a; ODM-GSC, 1960). It is interesting to note that the Big Beaver House carbonatite complex is located only 15 km northwest of the Schryburt Lake carbonatite complex and both complexes are late Precambrian in age. Because of this Higgins (1977) postulated that these two complexes may have been co-genetic; this is also discussed in Section 3.12

The Big Beaver House carbonatite complex consists of sövites, silicocarbonatites and ultramafic rocks (Sage, 1987a), that intruded early Precambrian, gneissic migmatitic rocks composed of massive to foliated biotite and biotite-hornblende trondhjemite to quartz monzonite (Thurston et al., 1979), and some medium-coarse grained pegmatites (Sage, 1987a).

Sage (1987a) found that the dominant mafic phase at Big Beaver House is pyroxenite and with increasing nepheline content grades into ijolite. The pyroxenites are fine-grained, massive, equigranular, allotriomorphic with curved to straight grain

boundaries and are composed predominantly of clinopyroxene, phlogopite-biotite, apatite, magnetite, amphibole and in some cases up to 25% carbonate (Sage, 1987a). The ijolites are fine to medium-grained, inequigranular, seriate and hypidiomorphic and contain clinopyroxene, phlogopite-biotite, magnetite, and nepheline and can contain up to 25% carbonate (Sage, 1987a).

The sövites at the Big Beaver House complex appear to have intruded the more mafic silicocarbonatitic phases of the complex (Sage, 1987a). The sövites are fine to medium-grained, massive, equigranular to inequigranular, seriate, allotriomorphic with curved to straight grain boundaries and are composed mainly of carbonate, phlogopite-biotite, amphibole, magnetite and apatite, with trace amounts of clinopyroxene, chlorite, rutile, limonite and fluorite (Sage, 1987a). Sage (1987a) noted that the mineralogy of the silicocarbonatites is highly variable, which he interpreted to be the result of: (1) being gradational phases into the sövites (2) interaction between the pyroxenitic and carbonatitic melts, and (3) being a carbonate-rich phase of the pyroxenite. The silicocarbonatites are fine to medium-grained, equigranular to inequigranular, seriate, allotriomorphic with curved to straight grain boundaries and are composed of phlogopite-biotite, amphibole, carbonate, magnetite, apatite and pyroxene (Sage, 1987a). In terms of structural setting, Sage (1987a) noted that due to lack of outcrop both within the complex and the surrounding terrain, it is very difficult to comment on the structural relationships within the complex and between the complex and the surrounding country rocks. Carbonate veining and in some cases, carbonate-related brecciation within the pyroxenitic phases, suggest that the intrusion of the carbonatite took place after the crystallization of the pyroxenites (Sage, 1987a).

3.5 Big Beaver House Complex – Isotope Geochemistry and Discussion

$\delta^{34}S_{CDT}$ values were obtained from seven samples from the Big Beaver House carbonatite complex. In addition, $\delta^{18}O_{V\text{-}SMOW}$ and $\delta^{13}C_{V\text{-}PDB}$ values were obtained on four of the seven samples for which $\delta^{34}S_{CDT}$ values were obtained. The sulphur, oxygen and carbon isotopic compositions for the analysed samples from Big Beaver House are listed in Table 3-4 and Table 3-5.

Table 3-4. Sulphur isotope values for carbonatites and associated silicate rocks from the Big Beaver complex.

Sample ID	Rock Type	Mineral Separate	$\delta^{34}S_{CDT}$
BB2	pyroxenite	pyrrhotite	−2.0‰
BB9*	pyroxenite	pyrrhotite	−1.9‰
BB16	sövite	pyrrhotite + chalcopyrite	−3.6‰
BB35	silicocarbonatite	pyrrhotite	−2.5‰
BB78*	ijolite	pyrrhotite	−1.5‰
HED7-14	sövite	pyrrhotite	−2.3‰
HED7-36*	pyroxenite	pyrrhotite	−1.6‰

Table 3-5. Oxygen and carbon isotope values for carbonatites and associated silicate rocks from the Big Beaver House complex.

Sample ID	Rock Type	Mineral Separate	$\delta^{18}O_{V\text{-}SMOW}$	$\delta^{13}C_{V\text{-}PDB}$
BB9*	pyroxenite	calcite	+8.45‰	−5.77‰
BB16	sövite	calcite	+6.61‰	−5.83‰
HED7-14	sövite	calcite	+6.94‰	−5.77‰
HED7-36*	pyroxenite	calcite	+7.20‰	−6.09‰

First order observations indicate that on average, the sulphur isotopic signature of the carbonatites is slightly more depleted than for the ultramafic rocks, and the carbonate within the pyroxenites have a more enriched oxygen isotopic signature than the carbonatites.

Samples BB78 and HED7-36 have essentially the same sulphur isotopic composition (−1.5‰ and −1.6‰, respectively), which also represent the most enriched isotopic signatures for all the analysed samples from the Big Beaver House complex. In addition, demonstrates that there were at least two distinct stages of sulphide formation

within one of the ijolitic rocks (see Plate 2.1). Another interesting finding was that sample HED7-36 (ijolite) contained pyrite with inclusion of stringers of chalcopyrite (see Plate 2.2); barite was adjacent to pyrite. These petrographic observations demonstrate the difficulty in obtaining an analysis of a single, homogeneous sulphide mineral from some of the samples (see also Appendix B).

The sulphur isotopic signature for the Big Beaver House carbonatites and associated silicate rocks is less depleted when compared to the sulphur isotopic signature of the carbonatites from the Schryburt Lake complex. The sulphur isotopic composition of the primitive mantle is within the range of the average isotopic composition (~ −1.8‰) of the ultramafic rocks from the Big Beaver House complex. The average sulphur isotopic composition of the carbonatites, however, falls outside of this range, and has an average value of −2.8‰. The most significant observation from the sulphur isotopic composition of these sulphides is that the carbonatites possess a more depleted isotopic signature than the associated silicate rocks. Grinenko et al. (1970a, b) and Mäkelä and Vartiainen (1978) observed that during the emplacement of multi-stage carbonatite massifs, there is a general decrease in $\delta^{34}S_{sulfide}$ from early to late stage. Mäkelä and Vartiainen (1978) ascribed this observed decrease in $\delta^{34}S_{sulfide}$ to isotopic redistribution among oxidized and reduced sulphur species caused by an increase in pH and/or fo_2.

The field relationships between the carbonatites and associated silicate rocks at the Big Beaver House complex seem to indicate that the carbonatites were intruded after the emplacement of the ultramafic silicate rocks (Sage, 1987a), since the pyroxenites were seen to be either veined and/or brecciated by a carbonate phase.

On the basis of the $\delta^{34}S_{CDT}$ values it is proposed that the ultramafic rocks at the Big Beaver House complex represent the earliest phases of the intrusion, whose sulphides possess a sulphur isotopic signature that is compatible with derivation from a primitive mantle. This was followed by the emplacement of the carbonatitic rocks. The more depleted sulphur isotopic composition of the sulphides contained in the carbonatites may have been the result of sulphur isotopic fractionation, e.g. Mäkelä and Vartiainen (1978). It should be noted, however, that this assumes that both the carbonatites and the associated ultramafic rocks both extracted their sulphur from either the same source, or that the carbonatites extracted their sulphur from the ultramafic rocks, in other words, the sulphur contained within the carbonatites and the pyroxenites originated from an isotopically similar source.

Also of interest in evaluating the sulphur isotopic composition and evolution of the carbonatites and silicate rocks from Big Beaver House are the redox conditions that existed when the sulphides were precipitated. The sulphur mineralogy at the Big Beaver House complex (pyrrhotite, pyrite and barite) would seem to indicate quite variable oxidizing/reducing conditions. Mitchell and Krouse (1975) demonstrated that higher temperature carbonatites (500 – 700°C) tend to have pyrrhotite as their dominant sulphide mineral, which also indicates sulphide formation under more reducing conditions. In addition, with decreasing temperature the abundance of the oxidized sulphur species becomes more abundant at the expense of the reduced species (Mitchell and Krouse, 1975). Therefore, the presence of pyrrhotite, pyrite and barite within the same sample implies that both reduced sulphur species, e.g. S^{2-} for the pyrrhotite and more oxidized sulphur species, e.g. S^{-} for the pyrite and SO_4^{2-} for the barite, were present

either at the same time (concomitant crystallization) and/or during distinct stages of sulphide/sulphate crystallization.

When sulphur species of different oxidation states are present at the same time within a melt, appreciable sulphur isotopic fractionation can occur, e.g. Ripley (1999). Because of the difficulties in analyzing either pure sulphide or sulphate minerals, it is difficult to evaluate to what degree, if any, sulphur isotopic fractionation took place between sulphur species possessing different valences. In terms of petrogenesis, pyrite commonly rims pyrrhotite (see Plate 2.1), and this is consistent with the theory that under higher temperatures and more reducing conditions, the principal sulphide to crystallize was pyrrhotite. As the melt cooled, the oxidation state under which sulphides were precipitating increased, thus pyrite became the dominant sulphide. Finally, under the most oxidizing conditions the dominant sulphur-bearing mineral would be barite. Whether the sulphur isotopic composition of the sulphides within some of the ultramafic rocks is representative of any one specific sulphide mineral is not known with certainty. The rather limited spread in the $\delta^{34}S_{CDT}$ values (−2.0‰ to −1.5‰) for the ultramafic rocks, coupled with the variable sulphide mineralogy and in some cases, the presence of a sulphate mineral phase (e.g. Plate 2.2), seem to rule out any sulphur isotopic fractionation brought about by changes in sulphur oxidation state. Additional isotopic analyses on pure mineral separates, especially pyrrhotite, pyrite and sulphate minerals (e.g. barite), are needed in order to better understand the sulphur isotopic evolution of the Big Beaver House carbonatite complex.

Also noteworthy is the observation that the carbonate phases within the pyroxenitic rocks possess a more enriched oxygen isotopic signature than those within

the carbonatitic rocks (refer to Table 3-5). The relatively enriched $\delta^{18}O_{V\text{-}SMOW}$ values observed within these carbonate-bearing pyroxenitic rocks is most likely related to a process of carbonate-silicate oxygen isotopic fractionation, which will be discussed in more detail in Chapter 4, Section 4.1.

In conclusion, the sulphur isotopic composition of the Big Beaver House carbonatites and associated silicate rocks is compatible with a model that involves derivation of sulphur from a mantle source with an isotopic composition close to −1‰. The variations in $\delta^{34}S_{CDT}$ values between the carbonatites and associated ultramafic silicate rocks can be attributed to sulphur isotopic fractionation related to timing of emplacement. Another possibility that could explain the sulphur isotopic composition of the Big Beaver House complex is a model that relates the isotopic compositions to the formation of the adjacent Schryburt Lake carbonatite complex. This is discussed in detail in Section 3.12

3.6 Cargill Complex – Geological Overview

The 9.6 km^2 Cargill Township carbonatite complex is located in the Kapuskasing Subprovince of the Superior Province of the Canadian Shield. It was emplaced along regional faults associated with the Kapuskasing Subprovince (Sage, 1988c). Kwon (1986) obtained a U-Pb age of 1907 ± 4 Ma age for the complex. Aeromagnetic mapping (ODM-GSC, 1962) shows that the complex consists of two distinctive magnetic anomalies which Bennett et al. (1967) and Sandvik and Erdosh (1977) interpreted to be the result of post-intrusion faulting giving the complex a dumb-bell shape (north and south sub-complexes). The complex consists of a pyroxenite rim and a carbonatitic core,

made up of calcitic, dolomitic and sideritic phases, all intruded into Archaean quartz diorite gneisses and amphibolites (Sage, 1988c). An apatite-rich residuum that formed during late-Cretaceous to early-Tertiary weathering of the carbonatite is also present (Sage, 1988c).

The pyroxenites at the Cargill complex are mineralogically quite diverse and were the subject of a M.Sc. thesis by Allen (1972). Sage (1988c) noted the presence of the following rock types in the pyroxenitic rim: amphibole-olivine clinopyroxenite, olivine-phlogopite-bearing clinopyroxenite, amphibole rock, clinopyroxenite, amphibole clinopyroxenite and biotite-carbonate amphibole rock. Mineralogically, the clinopyroxene-rich rocks contain clinopyroxene, olivine, amphibole and opaques (Sage, 1988c). Allen (1972) identified the following oxide phases: titanomagnetite, magnetite with ilmenite lamellae, magnetite with exsolved ulvöspinel, ilmenite, ilmenite plus magnetite and magnetite with exsolved ulvöspinel and hercynite. In addition, Allen (1972) also identified pyrrhotite and chalcopyrite as the sulphide phases, which can make up to 15% of the rock. The sövites at Cargill are fine to medium-grained, inequigranular, seriate, hypidiomorphic to allotriomorphic with straight to curved grain boundaries and mineralogically consist of: phlogopite, magnetite, clinohumite, carbonate, apatite, olivine, pyrrhotite and amphibole (Sage, 1988c). Allen (1972) reported that dolomite in the sövites at the Cargill complex is ubiquitous and Twyman (1983) noted that it is also present, although rarely, as exsolution lamellae in the calcite. The sövites at the Cargill complex grade into silicocarbonatites with increasing accessory mineral content and are similar in texture to the silicocarbonatites. Mineralogically, the silicocarbonatites are composed of phlogopite, magnetite, clinohumite, carbonate, apatite, olivine, and

amphibole (Sage, 1988c). Dolomite-carbonatites are present within the central core of the complex and consist mostly of dolomite with minor amounts of apatite and biotite (Sage, 1988c). These dolomite-carbonatites have a cataclastic texture displaying rounded porphyroclasts, some fractured, of carbonate set in a matrix of recrystallized carbonate (Sage, 1988c).

In terms of petrology, the Cargill complex has been one of the most studied carbonatite complexes in Ontario, e.g. Gittins et al. (1967), Gasparrini et al. (1971), Allen (1972), Gittins et al. (1975), Twyman (1983), Kwon (1986), Sharpe (1987) and Sage (1988c). Twyman (1983) proposed that the Cargill carbonatite complex was derived from a carbonated, mafic, alkalic, silicate magma that underwent immiscible separation at approximately 27 kb in the upper mantle. This in turn produced an olivine sövite magma containing about 8% alkalies at 1100 – 1200°C, which then differentiated to a natrocarbonatite magma by crystal fractionation (Twyman, 1983). Gittins et al. (1975) proposed that the Cargill carbonatite complex formed from a carbonated, aqueous, alkali-rich magma that intruded the pyroxenite. This intrusion metasomatized the pyroxenite producing phlogopite and hence loss of the aqueous phase, halides and alkalies from the melt. This loss of the alkali-rich aqueous fluids caused the precipitation of both calcitic and dolomitic carbonate phases. Both Twyman (1983) and Sharpe (1987) did, however, propose that there is a genetic link between the carbonatites and silicate rocks at Cargill. Sage (1988c) did not find any evidence for regional scale metamorphism within the Cargill carbonatite complex and any alteration was attributed to the emplacement of the complex.

Cargill also hosts minor Cu-Ni mineralization within the pyroxenitic border of the intrusion (Sage, 1988c and references therein), which has been evaluated for its economic potential. Although the samples that were assayed indicate that the copper and nickel contents are generally less then 0.10%, Sage (1988c) points out that the possibility exists for local accumulations of disseminated sulphide mineralization of economic potential within the pyroxenitic phases.

3.7 Cargill Complex – Isotope Geochemistry and Discussion

$\delta^{34}S_{CDT}$ values were obtained from nine samples from the Cargill carbonatite complex. In addition, $\delta^{18}O_{V\text{-}SMOW}$ and $\delta^{13}C_{V\text{-}PDB}$ values were obtained on seven of the nine samples for which $\delta^{34}S_{CDT}$ values were obtained. The sulphur, oxygen and carbon isotopic compositions for the analysed samples from Cargill are listed in Table 3-6 and Table 3-7.

Of all of the carbonatite complexes examined in this study, the sulphur values from the Cargill carbonatite complex represent the most primitive, mantle-like composition. The average $\delta^{34}S_{CDT}$ value for all of the samples is −0.7‰.

Table 3-6. Sulphur isotope values for carbonatites and associated silicate rocks from the Cargill complex.

Sample ID	Rock Type	Mineral Separate	$\delta^{34}S_{CDT}$
CCM6 102.9 – 103.3	silicocarbonatite	pyrrhotite	−1.5‰
CCM29 136.85 – 137.2*	hornblendite	pyrrhotite + chalcopyrite	−0.3‰
H24 IMC 28.6 – 29.0	sövite	pyrrhotite	−1.2‰
H24 IMC 101 – 101.4	sövite	pyrrhotite	−1.5‰
H35 IMC 128.9 – 129.3*	silicocarbonatite	pyrrhotite	+0.1‰
H49 IMC 190.2 – 190.7	sövite	pyrrhotite	−0.7‰
H49 IMC 294.1 – 294.45	sövite	pyrrhotite	−0.9‰
H49 IMC 332.5 – 332.9	sövite	pyrrhotite	−0.6‰
CCM 135 IMC 179.3 – 179.7*	hornblendite	pyrrhotite	+0.5‰

Table 3-7. Oxygen and carbon isotope values for carbonatites and associated silicate rocks from the the Cargill complex.

Sample ID	Rock Type	Mineral Separate	$\delta^{18}O_{V\text{-}SMOW}$	$\delta^{13}C_{V\text{-}PDB}$
CCM29 136.85 – 137.2*	hornblendite	calcite	+7.58‰	–4.39‰
H24 IMC 101 – 101.4	sövite	calcite	+6.73‰	–4.29‰
H35 IMC 128.9 – 129.3*	silicocarbonatite	calcite	+8.26‰	–4.15‰
H49 IMC 190.2 – 190.7	sövite	calcite	+6.01‰	–4.45‰
H49 IMC 294.1 – 294.45	sövite	calcite	+6.70‰	–4.48‰
H49 IMC 332.5 – 332.9	sövite	calcite	+6.93‰	–4.14‰
CCM 135 IMC 179.3 – 179.7*	hornblendite	calcite	+8.04‰	–4.61‰

Both hornblendites for which sulphur, oxygen and carbon isotopic analyses were obtained were also examined in thin-section. The opaques from the CCM 135 IMC 179.3 – 179.7 consist of 60% magnetite and ilmenite, 35% pyrrhotite and ~ 5% chalcopyrite. The pyrrhotite is generally associated with magnetite and commonly mantle and/or is subophitic to the magnetite, e.g. Plate 3.1. The reaction rims around some of the magnetite may imply disequilibrium between the magnetite and the melt, e.g. Plate 3.2. There is also pyrrhotite that is not in contact with the magnetite, and commonly occurs as bleb-like inclusions in silicate minerals, e.g. Plate 3.3. The other hornblendite (CCM29 136.85 – 137.2), shows that both oxides and sulphides occur as an interstitial phase to the surrounding silicate minerals. In this sample the sulphides not only rim the oxides (e.g. Plate 3.4), but are also poikilitically enclosed within oxide oikocrysts (e.g. Plate 3.5). Allen (1972) attributed the formation of the sulphide phase to an immiscible sulphide liquid.

The Cargill carbonatite complex seems to have the characteristics of a high-temperature carbonatite (~ 700°C) as described by Mitchell and Krouse (1975), see Table 3-8. The presence of pyrrhotite and magnetite as dominant phases, coupled with the absence of pyrite and especially barite, are indicative of a high temperature carbonatite.

Table 3-8. Approximate temperatures of formation and mineral assemblages of some carbonatites. Modified after Mitchell and Krouse (1975).

Temperature (°C)	Iron Oxide-Sulphide Mineralogy in order of relative abundance	Barite	Example
300	haematite, magnetite, pyrite	abundant	Mountain Pass
400 – 500	pyrite, magnetite	present	Oka, Magnet Cove
400 – 500	pyrite, magnetite, pyrrhotite	rare	Kovdor, Bearpaw
500 – 600	pyrrhotite, pyrite, magnetite	rare	Sayan
700	pyrrhotite, magnetite, Cu-Fe sulphides	absent	Phalaborwa, Cargill?

Mitchell and Krouse (1975) demonstrated that pyrrhotite-bearing carbonatites have mean $\delta^{34}S$ sulphide values closer to $\delta^{34}S_{\Sigma S}$ than carbonatites in which pyrite is the dominant iron sulphide because of higher temperatures of formation and the more reduced nature of the magma. If the oxide phases formed concomitantly with the sulphides it follows that their mineralogy should also be indicative of precipitation under similarly reducing conditions. Earlier it was noted that Allen (1972) had found many oxide minerals within the pyroxenitic phases at the Cargill complex. These included magnetite [$Fe^{3+}(Fe^{2+}Fe^{3+})O_4$], ilmenite [$Fe^{2+}TiO_3$], ulvöspinel [$Fe^{2+}(Fe^{2+}Ti^{4+})O_4$], and hercynite [$Fe^{2+}Al_2O_4$]. These minerals show the reduced nature of the magma.

On the basis of the mineral assemblages shown in Table 3-8, the Cargill carbonatites seem to fit into the highest temperature category (~ 700°C). In addition, no pyrite or barite was detected, although Twyman (1983) found pyrite, but only in the arfvedsonite sövites. It is interesting to note that both the Phalaborwa carbonatite-ultramafic complex (see Eriksson, 1989) and the Cargill carbonatite complex are geologically similar. Both complexes possess a pyroxenitic rim and a carbonatite core, and both intrusions show evidence for Cu-mineralization. It should, however, be

mentioned that the amount of Cu-mineralization seen at Phalaborwa is extreme, and seems to be unique among carbonatites. The average $\delta^{34}S_{CDT}$ value for 33 analyses from Phalaborwa is ~ +0.9‰ (data from: von Gehlen, 1967, Hoefs et al., 1968, Mitchell and Krouse, 1975). Therefore both complexes deviate only slightly from the primitive mantle mean of ~ 0‰.

As with the carbonatites and ultramafic rocks from the Big Beaver House complex, there also appears to be a similar relationship in terms of oxygen isotope systematics between the carbonatites and ultramafic rocks at the Cargill complex. Referring to Table 3-7 it can be seen that the carbonate phases within the ultramafic rocks possess a more enriched oxygen isotopic signature than the carbonate phases within the carbonatites. As with the pyroxenitic rocks at the Big Beaver House complex, the relatively enriched oxygen isotopic signatures observed in the carbonate phase of the ultramafic rocks at the Cargill complex was most likely the result of carbonate-silicate oxygen isotopic fractionation.

In conclusion, the sulphur isotopic composition of the Cargill carbonatite complex represents derivation from a primitive mantle source very close to 0‰. As with the Big Beaver House intrusion, the sulphur isotopic compositions of the ultramafic rocks are more primitive than the carbonatitic rocks. This is consistent with the carbonatites being younger than the ultramafic rocks.

3.8 Firesand River Complex – Geological Overview

The Firesand carbonatite complex is located within the Wawa Subprovince of the Superior Province, immediately adjacent to the Kapuskasing Subprovince (refer to Figure

1-2). The complex has been dated at 1008 and 1047 Ma by K-Ar dating (Gittins et al., 1967). The surface area of the complex is approximately 4.5 km^2 in size as inferred by the aeromagnetic maps 2191G and 2192G (ODM-GSC, 1963a, b; Sage, 1988a). Structurally, this carbonatite complex is located at the intersection of two faults, one of which is related to Kapuskasing Structural Zone (Sage, 1988a). More specifically, the Firesand carbonatite complex was intruded where the Wawa Lake, Hawk Lake and Firesand River faults intersect (Sage et al., 1982; Sage, 1988a; Sage, 1993).

The Firesand River complex consists of a dolomite-carbonatite core and a rim of sövite, silicocarbonatite and ijolite intruded into Archaean supracrustal rocks of the Michipicoten greenstone belt (Sage, 1988a). The latter consists of intermediate – mafic metavolcanics, intermediate – felsic metavolcanics and quartz-feldspar porphyritic felsic intrusive rocks. Sage (1988a) also noted some diabase dykes that cross-cut the supracrustal rocks, but which were truncated by the carbonatites. Sage (1988a) provided a detailed description of all the carbonatites within the Firesand River carbonatite complex, which is summarized in Table 3-9. The reader should also refer to Appendix D for a detailed reflective-light petrographic description of selected thin sections.

The carbonatite intrusion is unmetamorphosed (Sage, 1988a). In addition, Sage (1988a) found that the Firesand River carbonatite complex is surrounded by a fenitized zone that exceeds 1 km in width. The fenitizing fluid was found to be initially Fe and Na-rich and later carbonate- and K-rich (Sage, 1988a). Using the petrochemistry of coexisting magnetite-ulvöspinel and ilmenite-haematite solid solutions, Teal (1979) estimated that the minimal temperature of emplacement of the Firesand River carbonatite complex was approximately 600°C with an fo_2 value of $10^{-22.5}$. These values were

revised using the QUILF95 program (Andersen et al., 1993) to: T = 580 ± 25°C and fo_2 = $10^{-21.95 \pm 0.47}$ (see also Figure 3-6).

Table 3-9. Textures and mineralogy of the carbonatites found at the Firesand River complex (Modified after Sage, 1988a). Note: apt = apatite, amp = amphibole, bt = biotite, carb = carbonate, cpx = clinopyroxene, gt = garnet, mgt = magnetite, ol = olivine, phlog = phlogopite, plag = plagioclase, po = pyrrhotite, py = pyrite, qz = quartz.

Carbonatite	Texture	Modal mineralogy	Minor/trace minerals
Sövite	Fine to medium grained, massive, equigranular, allotriomorphic with curved to straight grain boundaries	apt: 0 – 10%, cpx: 0 – 30%, mgt: 0 – 10%, carb: 50 – 100%, bt, bt-phlog: 0 – 30%, amp: 0 – 10%, unknown brown alteration mineral: 0 – 15%, ± ol: up to 15%	qz, barite, chlorite, serpentine, titanite, pyrochlore, perovskite, garnet and po
Ferruginous sövite	Essentially the same as the sövite unit	Essentially the same as the sövite unit, also there accumulation of iron oxide on the rock surface due to the weathering of the iron-bearing carbonate	Not available
Silicocarbonatite	Fine to medium grained, massive, equigranular, allotriomorphic with curved to straight grain boundaries	apt: 0 – 10%, cpx: 0 – 30%, mgt: 0 – 15%, carb: 10 – 50%, bt, bt-phlog, phlog: 0 – 55%, amp: 0 – 30%, ol: 0 – 30%, gt: 0 – 30%	chlorite, perovskite, analcite(?), albite and nepheline
Dolomite-carbonatite	Fine grained, massive, equigranular, allotriomorphic with curved to lobate grain boundaries	carb: 75 – 95%, mgt + apt: 5 – 25%	bt, barite
Sövite dykes	Same as the sövite	Same as the sövite	Same as the sövite
Silicocarbonatite dykes	Same as the silicocarbonatite	Same as the silicocarbonatite	Same as the silicocarbonatite
Ferruginous carbonate dykes	Fine grained, massive, equigranular, allotriomorphic with curved boundaries	qz: 5%, plag: 10%, carb: 85%	py (up to 1 – 2%)

3.9 Firesand River Complex – Isotope Geochemistry and Discussion

$\delta^{34}S_{CDT}$ values were obtained from nine samples from Firesand River carbonatite complex. In addition, $\delta^{18}O_{V\text{-}SMOW}$ and $\delta^{13}C_{V\text{-}PDB}$ values were obtained on carbonate

phases from eight of the nine samples for which $\delta^{34}S_{CDT}$ values were determined. The sulphur, oxygen and carbon isotopic compositions for the analysed samples from Firesand River are listed in Table 3-10 and Table 3-11.

Table 3-10. Sulphur isotope values for carbonatites and associated silicate rocks from the Firesand River Complex.

Sample ID	Rock Type	Mineral Separate	$\delta^{34}S_{CDT}$
H5 21.95 – 22.45	malignite	pyrite	+1.3‰
H8 135.65 – 136.05*	sövite	pyrrhotite	+1.4‰
H8 285.4 – 285.85	silicocarbonatite	pyrrhotite	+1.5‰
FS1 147	silicocarbonatite	pyrrhotite	+1.6‰
FS1 150.8	silicocarbonatite	pyrrhotite	+1.4‰
FS2 157.8 – 158.2	ijolite	pyrite	+1.7‰
ST-34*	silicocarbonatite	pyrite	+1.3‰
ST-62*	ijolite	pyrrhotite and pyrite	+1.3‰
F 384-A*	carbonatitic dyke rock	pyrite	+3.4‰

Table 3-11. Oxygen and carbon isotope values for carbonatites and associated silicate rocks from the Firesand River complex.

Sample ID	Rock Type	Mineral Separate	$\delta^{18}O_{V\text{-}SMOW}$	$\delta^{13}C_{V\text{-}PDB}$
H5 21.95 – 22.45	malignite	calcite	+5.40‰	−6.49‰
H8 135.65 – 136.05*	sövite	calcite	+5.58‰	−6.47‰
H8 285.4 – 285.85	silicocarbonatite	calcite	+6.95‰	−5.80‰
FS1 147	silicocarbonatite	calcite	+7.24‰	−5.58‰
FS1 150.8	silicocarbonatite	calcite	+7.31‰	−5.99‰
ST-34*	silicocarbonatite	calcite	+6.05‰	−5.95‰
ST-62*	ijolite	calcite	+5.99‰	−6.27‰
F 384-A*	carbonatitic dyke rock	calcite	+2.98‰	−4.71‰

Other than sample F 384-A, there is very little variation in the $\delta^{34}S_{CDT}$ values obtained for the samples from the Firesand River complex. In addition, there also does not appear to be any variation between $\delta^{34}S_{CDT}$ and rock type or sulphide mineralogy. The general variation in $\delta^{34}S_{CDT}$ of between +1.3 and +1.7‰ is well within the range of 0 ± 1.5‰, previously discussed as being representative of the primitive mantle. In addition, most of the carbon and oxygen isotopic data are compatible with this carbonatitic melt being derived from the mantle.

In light of its dissimilar stable isotopic composition compared to the other samples from the Firesand River complex, a brief discussion of sample F 384-A seems justified. Both the $\delta^{34}S_{CDT}$ (+3.4‰) of the pyrite and the $\delta^{18}O_{V\text{-}SMOW}$ (+2.98‰) of the calcite for this sample deviate substantially from both other values from the Firesand River complex and indeed from any of the other samples examined in this study. It was difficult to ascertain how this sample was classified in the OGS report of Sage (1988a) but based on other samples from the same outcrop; it would appear that this sample represents a late-stage dyke rock, related to the intrusion of the Firesand River complex. Many of these dyke rocks intruded the surrounding country rock (Sage, 1988a). Since dykes typically possess a small surface area relative to the rocks into which they intrude, they are more likely to record the possible effects of secondary processes. If sample F 384-A does represent a late-stage dyke rock that was related to the intrusion of the Firesand River carbonatite complex, then its stable isotopic composition may reflect secondary processes such as interaction with circulating hydrothermal fluids or even country rock contamination.

The sulphides from the Firesand River complex consist mainly of pyrrhotite and pyrite; with some pyrrhotite rimmed by pyrite and possibly marcasite (see Plate 4.1). In addition, pyrite is also present as distinct crystals, some of which are euhedral (see Plate 4.2). Interestingly enough, pyrite seems to be absent from the one sample of sövite that was examined under reflective light (H8 135.65 – 136.05); only pyrrhotite and minor chalcopyrite are present. In both the silicocarbonatite (ST-34) and the ijolite sample (ST-62) the dominant sulphide is pyrite.

Most of the samples possess sulphur isotopic compositions compatible with derivation from a primitive mantle source, i.e. in the range of 0 ± 1.5‰. However, there is evidence that this particular carbonatite complex may have been contaminated by the surrounding country rocks. Sage (1988a) delineated the presence of highly altered xenolithic fragments within the silicocarbonatite rim of the complex. In addition, Sage (1988a) proposed that the presence of plagioclase feldspar in some of the samples implies contamination. However, considering that the sulphur, carbon and oxygen isotopic compositions of both the carbonatitic and the silicate rocks are indicative of a pristine, mantle-derived melt, this would seem to preclude any large scale magma-country rock interaction at the Firesand River complex.

On the basis of the above discussions, the sulphur isotopic compositions for most of the samples from the Firesand River complex seem to represent derivation from a primitive mantle source possessing a sulphur isotopic composition in the range of 0 ± 1.5‰. The similarity between the sulphur isotopic compositions of pyrite and pyrrhotite is compatible with isotopic fractionation between these two phases at 580°C (e.g. Kajiwra and Krouse, 1971), which was the calculated temperature of emplacement for the Firesand River carbonatite complex. In addition, this calculated temperature of 580°C coupled with the calculated fo_2 value of $10^{-21.95}$ signifies that in terms of redox conditions, H_2S would have dominated over SO_2. Consequently, unlike for the carbonatites at the Schryburt Lake complex, there would not have been any significant sulphur isotopic fractionation due to fluctuating sulphur redox conditions. Given these data and observations, it is possible to estimate the field of crystallization for the majority of the samples at the Firesand River complex in $fs_2 - fo_2$ space, which is depicted in

Figure 3-1. This estimation is based on the calculated T(°C) and fo_2 values from the magnetite-ulvöspinel, ilmenite-haematite petrochemistry of Teal (1979) and the previously discussed petrographic observations.

The enriched $\delta^{34}S_{CDT}$ value of +3.4‰ for the pyrite within the carbonatitic dyke rock could have been produced by isotopic fractionation at about 170°C between dissolved H_2S possessing a $\delta^{34}S_{CDT}$ value of about +1.4‰ (sample average, excluding F 384-A and using data from Ohmoto and Rye, 1979), with the dissolved H_2S being produced by the breakdown of pyrrhotite within the main carbonatitic intrusion. The possibility of the presence of a dissolved H_2S phase is supported by the postulated field of crystallization in $fs_2 - fo_2$ space for the sulphide-bearing carbonatites and associated silicate rocks depicted in Figure 3-1. The field of crystallization is located such that the mole fraction of H_2S (X_{H_2S}) is at its maximum value. The fact that the isotopic composition of this late stage dyke rock is markedly enriched (compared to sulphides from the main intrusion) as opposed to depleted suggests that the sulphur redox conditions continued to be relatively reducing even down at these hydrothermal temperatures.

In addition, using the isotopic fractionation factor between calcite and water ($\alpha_{H_2O}^{calcite}$) calculated by Zheng (1999), the depleted $\delta^{18}O_{V\text{-}SMOW}$ value of about +3.0‰ for the calcite fraction from this same dyke rock could have been produced by isotopic exchange, also at about 170°C with meteoric water possessing an oxygen isotopic composition of about –8.6‰. Considering that the position of Laurentia at about 1100 Ma ago was close to the equator (Scotese, 2003), an oxygen isotopic composition for meteoric water of about –8.6‰ is not unreasonable.

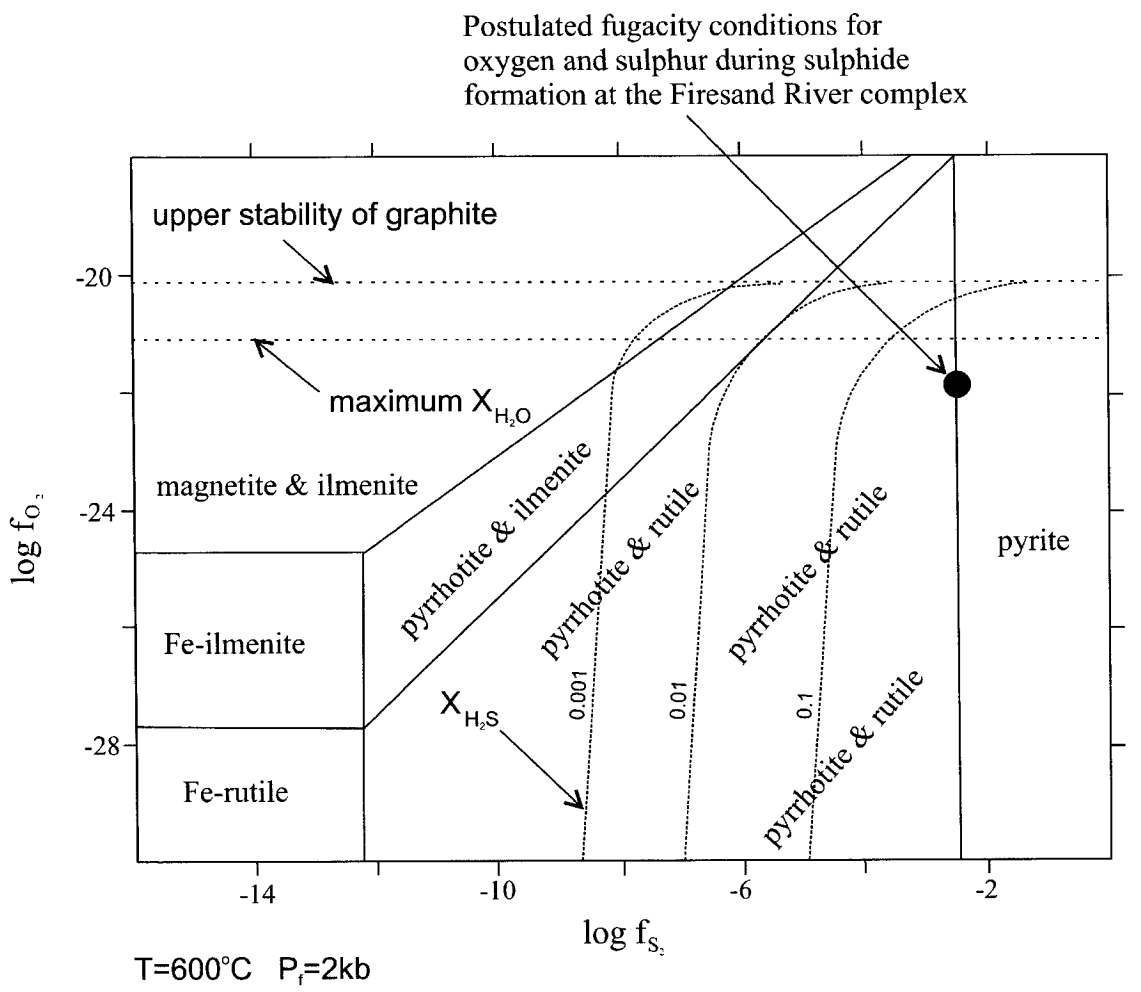

Figure 3-1. Plot of fo_2 versus fs_2 showing mineral stability fields, contours of X_{H_2S} and the field of sulphide formation at the Firesand River complex. Figure is modified after Ripley (1999).

This estimation is based on the calculated T(°C) and fo_2 values from the magnetite-ulvöspinel, ilmenite-haematite petrochemistry of Teal (1979) and the previously discussed petrographic observations.

In conclusion, the primitive mantle-like sulphur isotopic composition of the Firesand River carbonatite complex can be explained by a model involving both intra-

isotopic exchange between the different sulphide phases at magmatic temperatures (T ~ 580°C) and inter-isotopic exchange between the carbonatitic magma and circulating meteoric water at hydrothermal temperatures (T ~ 170°C). This model is depicted below in Figure 3-2.

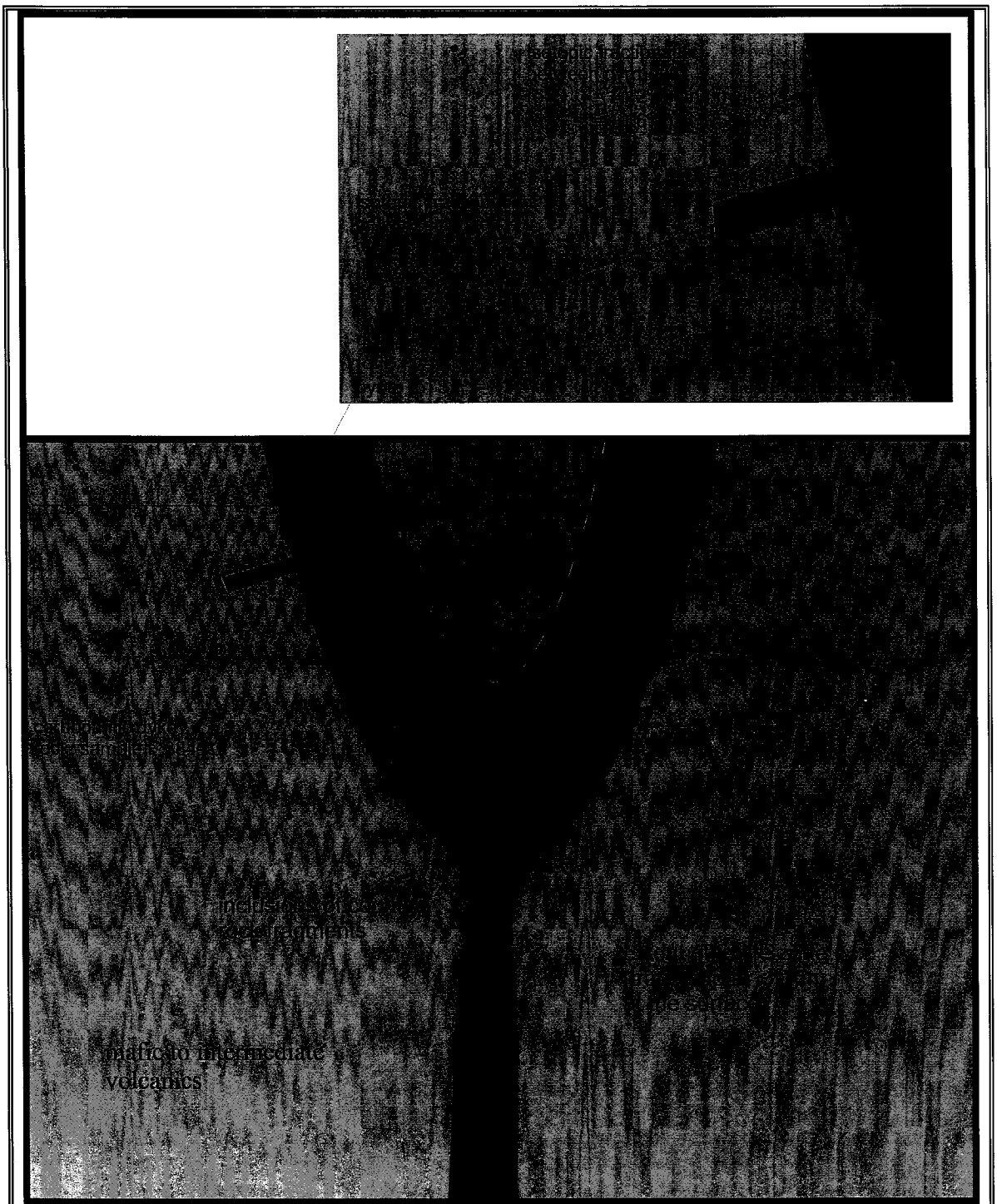

Figure 3-2. Simplified cross-section of the Firesand River carbonatite complex based on observations from Teal (1979) and references therein and Sage, (1988a), and petrogenetic model delineating the stable isotopic compositions of carbonatites and associated silicate rocks.

3.10 Spanish River Complex – Geological Overview

The Spanish River carbonatite complex is located within the Abititbi Subprovince of the Superior Province of the Canadian Shield, about 55 km north-west of Sudbury. The complex was emplaced within a fault zone, possibly an offshoot of the Ottawa-Bonnechere Graben (Sage, 1987b). The complex has been dated at 1835 ± 95 Ma by Rb-Sr (Bell and Blenkinsop, 1980), and has a surface area of about 2 km^2 (Sage, 1987b). The complex consists of sövites, silicocarbonatites, ijolites, pyroxenites and syenites and is surrounded by fenitized, Archaean quartz monzonite (Sage, 1987b). As with other complexes chosen for this study, it appears as though the carbonatitic phase is the youngest of all the units.

The pyroxenites at the Spanish River complex are fine grained, equigranular to inequigranular, seriate, hypidiomorphic to allotriomorphic with straight to lobate grain boundaries and are composed of nepheline, cancrinite, clinopyroxene, carbonate, apatite, biotite, titanite, and magnetite (Sage, 1987b). The silicocarbonatites present at Spanish River may in fact be carbonate-rich pyroxenite and separation between the two is somewhat ambiguous (Sage, 1987b).

Petrographically, the silicocarbonatites are fine to medium grained, equigranular, allotriomorphic with curved to straight grain boundaries and consist of nepheline, clinopyroxene, apatite, carbonate, cancrinite, magnetite and biotite, with trace amounts of titanite and albite (Sage, 1987b). The sovitic phase at Spanish River occurs towards the core of the complex. The sövites are generally composed of calcite, clinopyroxene, biotite-phlogopite, olivine, apatite and magnetite (Sage, 1987b).

3.11 Spanish River Complex – Isotope Geochemistry and Discussion

$\delta^{34}S_{CDT}$ values were obtained from three samples from the Spanish River carbonatite complex. In addition, $\delta^{18}O_{V\text{-}SMOW}$ and $\delta^{13}C_{V\text{-}PDB}$ values were obtained on carbonate phases from the same three samples. The sulphur, oxygen and carbon isotopic compositions for the analysed samples from the Spanish River complex are listed in Table 3-12 and Table 3-13.

Table 3-12. Sulphur isotope values for carbonatites and associated silicate rocks from the Spanish River complex

Sample ID	Rock Type	Mineral Separate	$\delta^{34}S_{CDT}$
107-108 1201.0	silicocarbonatite	pyrrhotite	+0.1‰
107-108 1223.5	pyroxenite	pyrrhotite	+0.1‰
107-108 1376.0*	pyroxenite	pyrrhotite	−0.1‰

Table 3-13. Oxygen and carbon isotope values for carbonatites and associated silicate rocks from the Spanish River complex

Sample ID	Rock Type	Mineral Separate	$\delta^{18}O_{V\text{-}SMOW}$	$\delta^{13}C_{V\text{-}PDB}$
107-108 1201.0	silicocarbonatite	calcite	+7.54‰	−4.43‰
107-108 1223.5	pyroxenite	calcite	+8.13‰	−4.19‰
107-108 1376.0*	pyroxenite	calcite	+8.66‰	−4.24‰

Because only three samples were analysed from the Spanish River complex it is difficult to make many assertions about either the source or emplacement of this carbonatite complex based on the sulphur isotopic composition of such a small data set. The limited sulphur isotopic data does suggest however that the sulphur contained within the Spanish River carbonatite complex was derived from a primitive mantle source with a sulphur isotopic composition of ~ 0‰. It is also noteworthy to mention that all three isotopic systems, i.e. sulphur, oxygen and carbon are similar to those from the Cargill complex, which is also an early Proterozoic carbonatite-ultramafic complex that also appears to have obtained its sulphur from a primitive mantle source, also close to 0‰.

The proximity of the Spanish River carbonatite complex to the Sudbury Igneous Complex, coupled with their similar ages of emplacement, may suggest contemporaneous emplacement, which was suggested by Sage (1987b). The limited sulphur isotopic data from Spanish River is consistent with data obtained for the Sudbury Igneous Complex. Naldrett (1981) and Ripley (1999) found $\delta^{34}S_{CDT}$ values from 0 to +4‰. Table 3-12 demonstrates that the sulphur isotopic data from the Spanish River complex fall into the lower end of the range obtained for the Sudbury Igneous Complex.

In conclusion, the limited sulphur isotopic from the Spanish River carbonatite complex suggests that the sulphur was derived from a primitive mantle source with an isotopic composition of ~ 0‰. The sulphur isotopic of the Spanish River carbonatite complex is similar to the $\delta^{34}S_{CDT}$ of the Sudbury Igneous Complex, which is also mid Proterozoic in age.

3.11 Petrogenetic Relationship between the Big Beaver House and the Schryburt Lake carbonatite complexes

The sulphur isotopic data from the Big Beaver House carbonatite complex warrants additional discussion due to the evidence that suggest that there may be a petrogenetic association with the Schryburt Lake carbonatite complex located only 15 km to the southeast of Big Beaver House. Higgins (1977) was the first to propose a model suggesting a petrogenetic link between the Schryburt Lake and Big Beaver House carbonatite complexes. In addition to their geographic proximity both of these carbonatite complexes are late Proterozoic in age. Also, radiogenic isotopic studies (Bell and Blenkinsop, 1987) demonstrate that both carbonatite complexes may have originated

from a similar mantle source since they possess nearly identical $^{143}Nd/^{144}Nd_{initial}$ and $^{87}Sr/^{86}Sr_{initial}$ ratios (0.51144 and 0.70244 respectively, for the Big Beaver House complex and 0.51140 and 0.70234 respectively, for the Schryburt Lake complex).

In the model proposed by Higgins (1977) the formation of both of these carbonatite complexes involves differentiation from a single magma chamber located in the lower crust or upper mantle, (see Figure 3-3). The magma within this chamber fractionated to produce a volatile-rich, less mafic-rich phase above a mafic-rich, volatile poor phase. This more volatile-rich, less viscous phase ascended to form the Schryburt Lake intrusion, while the more mafic magma formed the Big Beaver House carbonatite complex (Higgins, 1977). Although Higgins (1977) does not mention what the initial starting material was, the presence of a pyroxenitic and carbonatitic phase at the Big Beaver House complex suggests that the parental magma was probably a carbonated ultramafic magma produced by partial melting of a carbonated peridotite. Assuming that these two carbonatite complexes are petrogenetically related, the stable isotope data obtained in this study will be used to evaluate such a model.

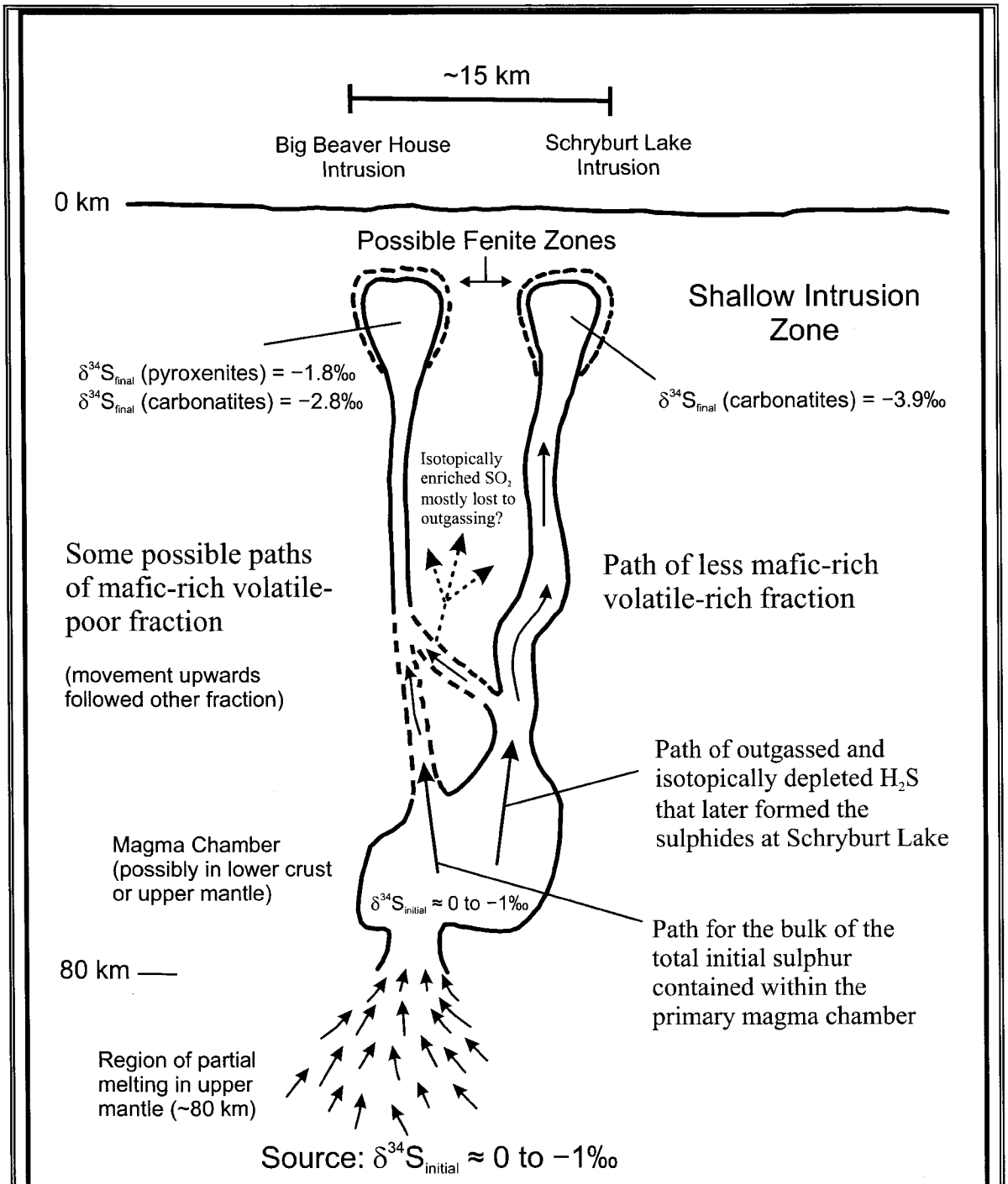

Figure 3-3. Proposed model for the concomitant sulphur isotopic evolution of the Big Beaver House and the Schryburt Lake carbonatite complexes superimposed on the model put forth Higgins (1977). Diagram is modified after Higgins (1977).

First consider the carbon and oxygen isotopic data for both of these carbonatite complexes (Figure 3-4). Although the isotopic data is somewhat limited, they do

demonstrate that carbonatites and associated silicate rocks from the Big Beaver House complex possess more primitive (lower, less fractionated) carbon isotopic signature than the carbonatites from the Schryburt Lake complex.

The model that is favoured is that formation of the volatile-rich, mafic-poor melt fraction (i.e. the Schryburt Lake complex) resulted in carbon isotopic fractionation with no appreciable amount of oxygen isotopic fractionation. This can be explained if the volatile phase associated with the formation of the Schryburt Lake complex was one in which H_2O was in excess of CO_2, e.g. Ray and Ramesh (2000). The carbonatites at the Schryburt Lake complex contain abundant biotite and amphibole (Sage, 1988b), which supports the proposal that this melt may have had a significant dissolved H_2O fluid phase present. In addition, the total H_2O content ($H_2O^+ + H_2O^-$) of the Schryburt Lake carbonatites is generally higher than the carbonatites found at the Big Beaver House complex (refer to Sage, 1987a, 1988b).

Figure 3-4. $\delta^{18}O_{V\text{-}SMOW}$ (cc) vs. $\delta^{13}C_{V\text{-}PDB}$ (cc) for the Schryburt Lake & Big Beaver House Complexes

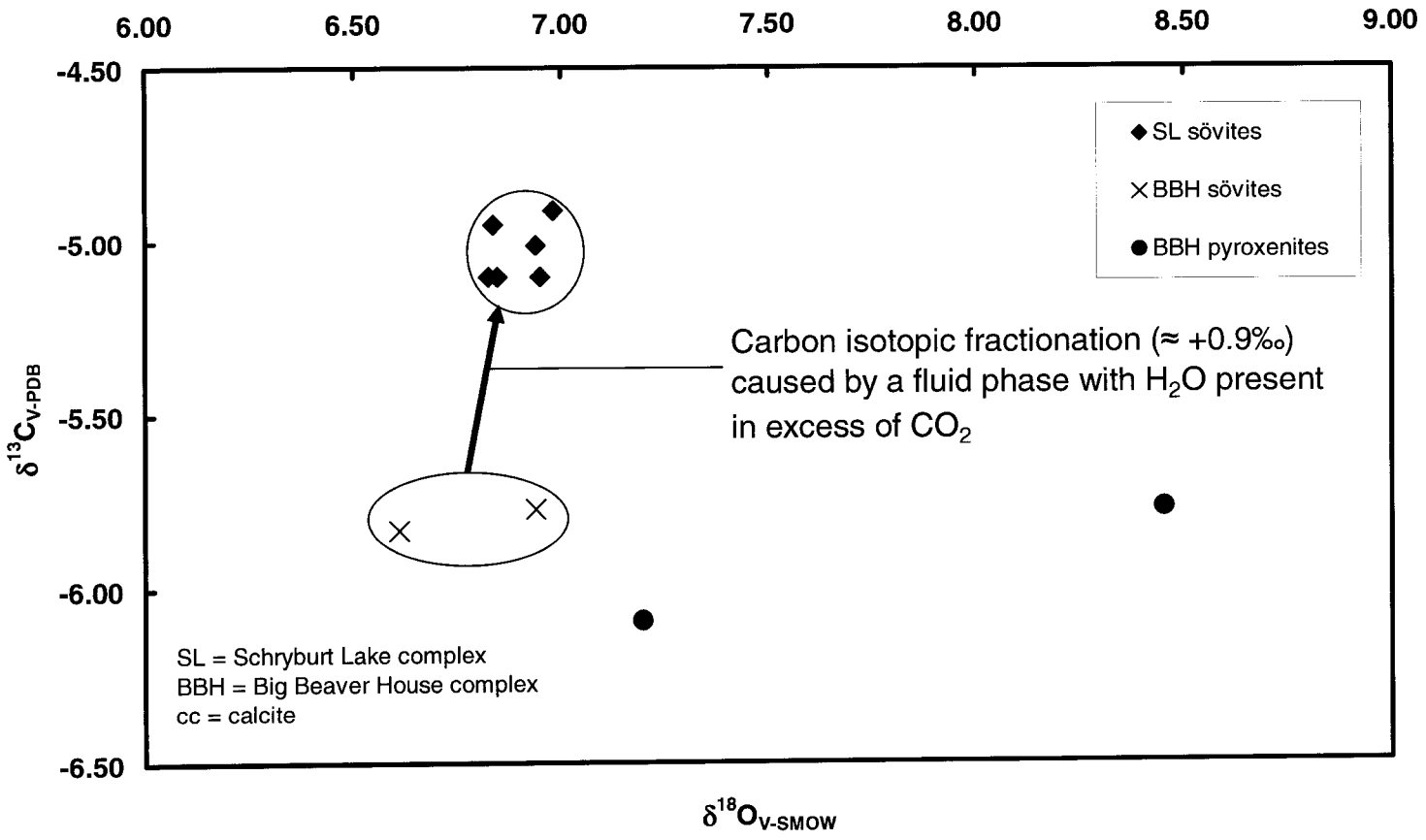

In terms of sulphur isotope systematics, the sulphides at the Schryburt Lake complex possess a more depleted (negative) isotopic signature than those at the Big Beaver House complex. More specifically, the sulphur isotopic compositions of the Schryburt Lake carbonatites ($\delta^{34}S_{CDT} = -4.5$ to $-3.4‰$) are more depleted than the sulphur isotopic compositions of the Big Beaver House pyroxenites ($\delta^{34}S_{CDT} = -2.0$ to $-1.5‰$). There is, however, an overlap between the sulphur isotopic compositions of the Schryburt Lake carbonatites and the Big Beaver House carbonatites ($\delta^{34}S_{CDT} = -3.6$ to $-2.3‰$). If the initial source of the sulphur found in the sulphides at both complexes was this carbonated mafic-rich, parental magma, then it is possible that when the Schryburt Lake melt fraction separated from this parental melt, it also assimilated the necessary sulphur as well. This sulphur extraction resulted in isotopic fractionation which is discussed in detail later in this chapter. In addition, the carbonatites from the Big Beaver House complex also possess a more depleted sulphur isotopic signature in comparison to the pyroxenites, which is also consistent with sulphur isotopic fractionation having taken place between these carbonatites and the more mafic parental magma.

Zheng (1990) demonstrated that in general, under high fo_2 conditions, the sulphate/sulphide ratio (can be qualitatively estimated using the whole-rock Fe_2O_3/FeO ratio) in a melt tends to increase with the melt becoming enriched in ^{34}S with progressive loss of either SO_2 or H_2S. Earlier it was postulated that the initial source of the sulphur contained within the Schryburt Lake carbonatites was the more mafic-rich phase which formed the pyroxenites at Big Beaver House. Petrographic and geochemical observations suggest that the ultramafic rocks at Big Beaver House formed under relatively oxidized conditions. The average Fe_2O_3/FeO ratio of these pyroxenitic rocks is more than two

times higher than both the Schryburt Lake carbonatites and the Big Beaver House carbonatites (refer to Sage, 1987a, 1988b). In addition, qualitative SEM analyses indicated the presence of both pyrite and barite within at least one of the pyrrhotite-bearing pyroxenite samples (see Plate 2.2). It, therefore, is postulated that the melt that formed the Schryburt Lake carbonatites contained a sulphur-bearing volatile phase, derived from the carbonated, mafic-rich parental magma. Higgins (1977) postulated that the melt which produced the Schryburt Lake intrusion was enriched in volatiles relative to the melt which produced the Big Beaver House intrusion. If the sulphides at Schryburt Lake were precipitated from a dissolved, sulphur-bearing volatile phase e.g. H_2S, then it is likely that this volatile phase had undergone isotopic fractionation (Rayleigh distillation) during the separation of the Schryburt Lake melt fraction from the parental magma. This sulphur isotopic fractionation is attributed to fluctuations in the sulphur redox conditions, with the isotopically enriched SO_2 phase having been lost to outgassing, while the correspondingly isotopically depleted H_2S remained in the system for later sulphide precipitation within the carbonatites at the Schryburt Lake complex. This process of Rayleigh distillation can best demonstrated using the observed correlation between $\delta^{34}S_{CDT}$ and whole-rock sulphur concentration as depicted in Figure 3-5. This plot readily demonstrates that the carbonatitic rocks at Schryburt Lake possess a lower sulphur concentration and a more depleted (evolved) sulphur isotopic composition then most of the carbonatitic and ultramafic rocks from the Big Beaver House complex. This is consistent with a process of Rayleigh distillation involving the outgassing of a sulphur-bearing volatile phase, in this case H_2S. Figure 3-3 shows the proposed model involving

the concomitant sulphur isotopic evolution of the Big Beaver House and the Schryburt Lake carbonatite complexes.

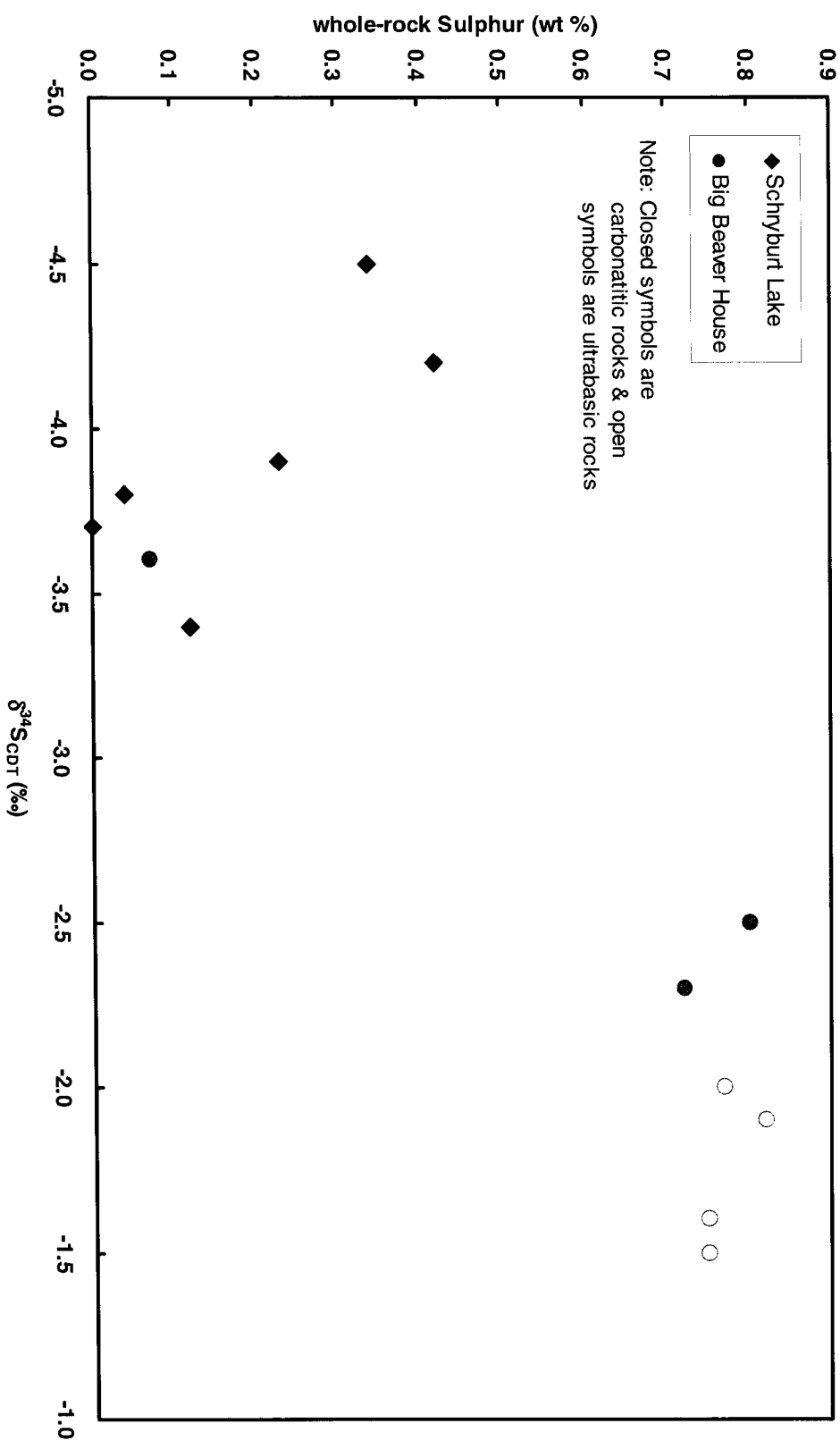

Figure 3-5. $\delta^{34}S_{CDT}$ vs. Whole-Rock Sulphur Concentration for Schryburt Lake Carbonatites & Big Beaver House Carbonatites and Associated Silicate Rocks

3.13.1 Mineral Chemistry – Oxides – Magnetite and Ilmenite

Electron microprobe analyses of coexisting magnetite [Fe_3O_4] and ilmenite [$FeTiO_3$] lamellae in samples from the Schryburt Lake and Cargill carbonatite complexes were performed in order to determine the temperature and oxygen fugacity conditions of their formation. Data are presented in Table 3-14. All of the uncorrected electron microprobe data for the analysed magnetite and ilmenite can be found in Appendix A.

Table 3-14. Corrected and averaged electron microprobe results on coexisting magnetite-ulvöspinel and ilmenite-haematite from the Schryburt Lake and Cargill complexes. Also listed are the recalculated FeO and Fe_2O_3 values and the mol % of ulvöspinel within the magnetite, the mol % of haematite within the ilmenite, and the calculated temperatures and oxygen fugacities for the magnetite-ulvöspinel, ilmenite-haematite solid solutions. NA = Not Applicable, b.d. = below detection limit (refer to Table B-2).

Sample ID Complex Rock Type	SR18-5 Schryburt Lake Sövite		H24 IMC 28.6 – 29.0 Cargill Sövite		CCM 135 IMC 179.3 – 179.7 Cargill Hornblendite	
	$magnetite_{ss}$ - $ilmenite_{ss}$		$magnetite_{ss}$ - $ilmenite_{ss}$		$magnetite_{ss}$ - $ilmenite_{ss}$	
Oxide (wt.%)	magnetite	ilmenite	magnetite	ilmenite	magnetite	ilmenite
SiO_2	b.d.	b.d.	b.d.	b.d.	b.d.	0.03
Al_2O_3	b.d.	b.d.	b.d.	b.d.	0.33	0.15
TiO_2	0.46	51.55	0.87	52.73	0.21	49.78
Cr_2O_3	0.08	b.d.	0.03	b.d.	0.05	b.d.
V_2O_5	1.13	0.48	0.94	0.59	0.62	0.40
FeO_{Total}	92.34	38.68	91.90	41.16	92.87	42.91
MgO	0.48	5.20	0.19	3.73	0.03	0.75
MnO	0.20	3.86	0.39	2.04	0.24	5.01
CaO	b.d.	b.d.	b.d.	0.12	b.d.	0.02
TOTAL	94.69	99.76	94.32	100.37	94.34	99.04
Recalculated						
Fe_2O_3	66.24	5.27	65.54	1.87	67.29	4.35
FeO	32.73	33.93	32.93	39.48	32.32	39.00
TOTAL	101.32	100.29			101.10	99.49
mole % ulvöspinel	1	NA	2	NA	0	NA
mole % haematite	NA	8	NA	3	NA	6
T(°C)	451 ± 32		442 ± 19		397 ± 26	
log fo_2	−22.36 ± 0.76		−25.78 ± 0.47		−23.55 ± 0.70	

Because the electron microprobe reports all of the Fe as FeO, a correction was made using the FORMULA program, version 96.9 (Ercit, 1996), which redistributes the Fe as both FeO and Fe_2O_3 based on 3 cations and 4 anions for magnetite and 2 cations and 3 anions for ilmenite. In addition, the mol %'s of ulvöspinel [$TiFe_2O_4$] within the

magnetite and the mol %'s of haematite [Fe_2O_3] within the ilmenite were determined using the QUILF95 program of Andersen et al. (1993). The QUILF95 program was also used to determine the T(°C) and fo_2 conditions for these coexisting magnetite-ulvöspinel and ilmenite-haematite solid-solutions. The calculations were made with pressure set at 1 kb. These data listed in Table 3-15 are computed averages derived from the data in Appendix A.

In terms of chemical composition, the magnetite from the sövites at the Schryburt Lake and the Cargill carbonatite complexes are consistent with those from other carbonatites e.g. (Prins, 1972), in that their stoichiometric compositions lie close to that of ideal magnetite that crystallized at low temperatures for igneous rocks. The trace element concentrations (MgO, MnO, Al_2O_3, V_2O_5 and CaO) magnetite from the carbonatitic rocks at Cargill and Schryburt Lake are also consistent with data from Prins (1972) in that they are depleted relative to magnetite from acidic igneous rocks, but enriched compared to magnetite from basic rocks. The exsolved ilmenite within the carbonatitic magnetite were found to contain much larger concentrations of Mn and Mg than the host magnetite, consistent with Prins's (1972) data and observation of considerable substitution of Mg^{2+} and Mn^{2+} for Fe^{2+} within the ilmenite structure.

The idea that coexisting magnetite-ilmenite can be used to evaluate temperature and oxygen fugacity was first recognized by Buddington and Lindsley (1962), involving the reaction magnetite + ilmenite = ulvöspinel + haematite, i.e.:

$$Fe_3O_4 + FeTiO_3 \leftrightarrow Fe_2TiO_4 + Fe_2O_3 \qquad (3\text{-}2)$$

This reaction governs the exchange of $Fe^{2+} + Ti^{4+}$ with $2Fe^{3+}$ (Andersen et al., 1993), which is controlled by temperature and oxygen fugacity. In addition, the QUILF95

program takes into account the presence of Al_2O_3, MgO and MnO within the magnetite and ilmenite. The experimental data can be plotted as surfaces in fo_2–T–X space for both the magnetite-ulvöspinel$_{ss}$ and the ilmenite-haematite$_{ss}$. This is followed by projecting portions of both of these surfaces (expressed by appropriate contours) on to a fo_2–T plane. The intersection of any two contours demonstrates both the temperature and oxygen fugacity at which the determined titaniferous magnetite and hematitic ilmenite can coexist (Buddington and Lindsley, 1962). It should be noted, however, that due to possible subsolidus cation exchange and re-equilibration e.g. Hammond and Taylor (1982), the extrapolated temperatures should be taken as minimum temperatures of crystallization.

The calculated temperatures and oxygen fugacities of the coexisting magnetite-ilmenite oxide pairs for the two sövites and the one hornblendite are reported in Table 3-14. The data for the two sövites are also plotted on Figure 3-6. The calculated temperature for the hornblendite is much lower than what one would expect for an intrusive ultramafic rock. This anomalous temperature may have been the result of the loss of Ti which is evidenced by the magnetite possessing rims of titanite [$CaTiSiO_5$], see Plate 3.2. The temperature and oxygen fugacity data from the carbonatitic magnetite from the Schryburt Lake and Cargill complexes are relatively low, even for carbonatite magmas, and may indicate that there was some subsolidus cation exchange between the magnetite and coexisting ilmenite. Both the magnetite from the Schryburt Lake and Cargill complexes gave the same temperatures of about 450°C, but markedly different fo_2 values. The magnetite-ilmenite from the Cargill complex appear to have equilibrated under much lower oxygen fugacity conditions than the magnetite-ilmenite from the

Schryburt Lake complex ($fo_2 = 10^{-25.78}$ vs. $fo_2 = 10^{-22.36}$). These values for fo_2 seem to correlate well with the overall sulphur isotopic compositions of the sulphides within these two carbonatite complexes. Using the log fo_2 vs. T(°C) diagram from Ohmoto (1986) (refer to Figure 3-6), it can be seen that the temperatures and fo_2 conditions for the magnetite-ilmenite from the Schryburt Lake complex were very close to the SO_2/H_2S boundary, which is the boundary for which either H_2S or SO_2 is the dominant S-bearing species present. Mitchell and Krouse (1975) demonstrated that when there is more than one dominant sulphur species present, even small changes in fo_2 or pH can cause the sulphur isotopic composition of precipitating minerals to be quite variable. If indeed, the sulphides precipitating at the Schryburt Lake complex were doing so under conditions such that there was both H_2S and SO_2 present, then significant isotopic fractionation could have taken place. This isotopic fractionation would have meant that ^{32}S preferentially entered the H_2S, and ^{34}S entered the SO_2. As a consequence, the precipitating sulphides (principally as pyrrhotite) at the Schryburt Lake complex would record a more 'depleted' isotopic signature because they obtained their sulphur from the reduced and isotopically depleted H_2S rather than from the oxidized and isotopically enriched SO_2. The $\delta^{34}S_{CDT}$ values from the Schryburt Lake sulphides do, in fact, retain such a depleted sulphur isotopic signature (see Table 3-1). The fo_2 value of $10^{-25.78}$ from the Cargill complex on the other hand is such that if sulphur was present under such conditions, it would occur as H_2S, i.e. fo_2 as recorded by the magnetite-ilmenite which is well within the H_2S stability field at T = 450°C. Therefore, sulphides precipitating under such conditions would not have had their sulphur isotopic signature affected by SO_2 – H_2S isotopic fractionation. As a consequence, the sulphur isotopic composition of these

sulphides would also be more likely to be representative of the initial sulphur isotopic composition of the melt, which in the case of the Cargill complex appears to have occurred. If the initial sulphur isotopic composition of the melt was close to that of the average, primitive mantle i.e. ~ 0‰, then it would appear that it was preserved at the Cargill complex, but not at the Schryburt Lake complex, where isotopic fractionation between H_2S and SO_2 may have caused the isotopic composition of the precipitating sulphides to be driven in the negative direction. All of this is supported by the calculated temperatures and oxygen fugacities of the coexisting magnetite-ilmenite from the Schryburt Lake and Cargill complexes (refer to Figure 3-6).

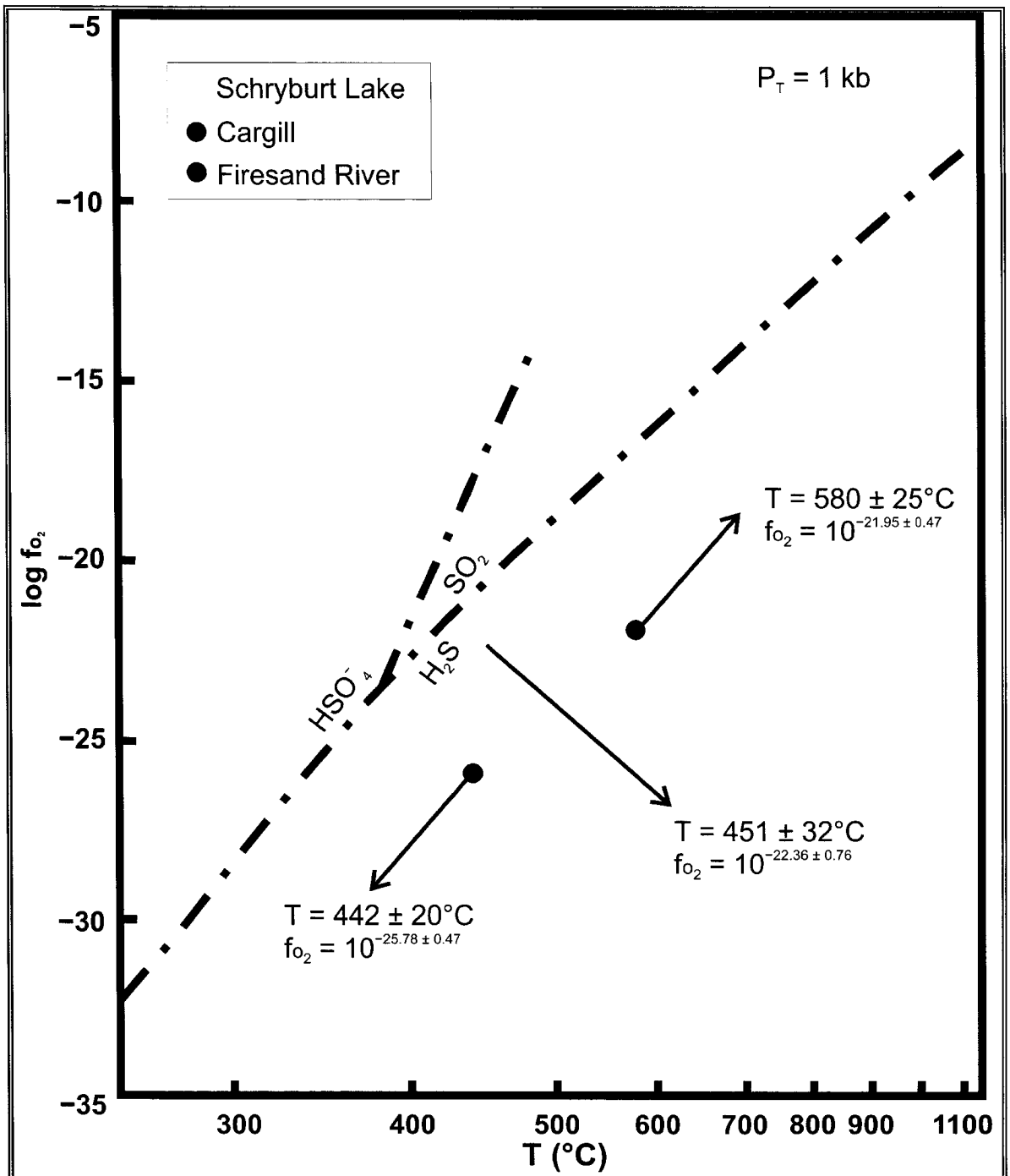

Figure 3-6. Plot of log fo_2 vs. T(°C) for the magnetite-ilmenite$_{ss}$ data for sövites from the Schryburt Lake, Cargill and Firesand River complexes. Also superimposed are the stability fields of HSO^-_4, SO_2 and H_2S (Ohmoto, 1986). Diagram is modified after Ohmoto (1986). Firesand River complex data originally from Teal (1979).

3.13.2 Mineral Chemistry – Phosphates – Apatite

Electron microprobe analyses (see Table 3-15) were carried out on apatite crystals from all five of the carbonatite complexes which were investigated for their sulphur isotopic compositions. All of the raw electron microprobe data and methodology can be found in Appendices A and B, respectively. It should be noted that many of the totals are quite low, even when recalculated taking H_2O into account. These low totals may be attributed to the presence of CO_2 which cannot be measured by the electron microprobe, see also Hogarth (1989).

Table 3-15. Electron microprobe analyses of apatite from carbonatites and associated silicate rocks from the Superior Province carbonatite complexes examined in this study. n.a. = not analysed, b.d. = below detection limit (refer to Table B-1). All Fe reported as FeO (i.e. $FeO_{Total} = Fe_2O_3 + FeO$). $\sum REE = La_2O_3 + Ce_2O_3 + Pr_2O_3 + Nd_2O_3 + Sm_2O_3$. TOTAL and TOTAL-O were calculated using the raw electron microprobe data (refer to Table A-2).

Complex	Schryburt Lake	Schryburt Lake	Schryburt Lake	Schryburt Lake	Schryburt Lake	Schryburt Lake
Sample ID	SR18-5	SR18-5	SR18-7	SR18-7	SR18-8	SR18-8
Oxide	avg. core	avg. rim	avg. core	avg. rim	avg. core	avg. rim
P_2O_5	40.62	41.44	41.21	40.74	41.40	40.79
SiO_2	b.d.	b.d.	0.12	b.d.	b.d.	b.d.
As_2O_5	b.d.	b.d.	b.d.	b.d.	b.d.	b.d.
SO_3	b.d.	b.d.	b.d.	b.d.	b.d.	b.d.
CaO	53.23	53.00	53.46	52.44	54.12	52.41
Na_2O	0.34	0.38	0.25	0.30	0.23	0.37
FeO_{Total}	b.d.	b.d.	b.d.	b.d.	b.d.	b.d.
MnO	b.d.	b.d.	b.d.	b.d.	b.d.	b.d.
SrO	0.84	1.02	0.67	0.83	0.84	1.01
BaO	b.d.	b.d.	b.d.	b.d.	b.d.	b.d.
Y_2O_3	b.d.	b.d.	b.d.	b.d.	b.d.	b.d.
La_2O_3	0.34	0.43	0.14	0.27	0.23	0.37
Ce_2O_3	0.77	1.06	0.42	0.75	0.51	0.96
Pr_2O_3	n.a.	n.a.	n.a.	n.a.	n.a.	n.a.
Nd_2O_3	0.37	0.48	b.d.	0.22	0.27	0.50
Sm_2O_3	0.10	0.12	b.d.	b.d.	b.d.	0.16
F	2.59	2.56	2.81	2.89	2.84	3.02
Cl	0.02	b.d.	0.03	b.d.	0.02	b.d.
TOTAL	99.41	100.62	99.26	98.62	100.69	99.76
TOTAL-O	98.31	99.54	98.07	97.41	99.49	98.48
∑REE	1.58	2.09	0.56	1.24	1.01	1.99

Complex	Big Beaver House	Big Beaver House	Big Beaver House	Big Beaver House	Spanish River	Spanish River
Sample ID	BB78	BB78	HED7-36	HED7-36	107-108 1376.0	107-108 1376.0
Oxide	avg. core	avg. rim	avg. core	avg. rim	avg. core	avg. rim
P_2O_5	40.33	40.32	40.85	41.02	41.44	41.32
SiO_2	0.28	0.22	0.41	0.20	0.09	0.13
As_2O_5	b.d.	b.d.	b.d.	b.d.	b.d.	b.d.
SO_3	b.d.	b.d.	b.d.	b.d.	b.d.	b.d.
CaO	54.97	54.81	53.63	52.93	54.75	54.46
Na_2O	0.06	0.14	0.07	0.10	0.11	0.10
FeO_{Total}	0.07	b.d.	b.d.	b.d.	b.d.	0.10
MnO	b.d.	b.d.	b.d.	b.d.	b.d.	b.d.
SrO	0.60	0.58	0.63	0.67	0.37	0.37
BaO	0.08	b.d.	b.d.	b.d.	0.08	b.d.
Y_2O_3	b.d.	b.d.	b.d.	b.d.	b.d.	b.d.
La_2O_3	0.09	0.14	b.d.	0.19	0.10	0.11
Ce_2O_3	0.19	0.34	0.13	0.22	0.21	0.21
Pr_2O_3	b.d.	0.10	b.d.	b.d.	b.d.	b.d.
Nd_2O_3	0.10	0.15	b.d.	b.d.	b.d.	b.d.
Sm_2O_3	b.d.	b.d.	b.d.	b.d.	b.d.	b.d.
F	2.25	2.42	2.46	2.46	2.51	2.44
Cl	b.d.	b.d.	b.d.	b.d.	b.d.	b.d.
TOTAL	99.21	99.35	98.50	98.13	99.88	99.40
TOTAL-O	98.26	98.33	97.47	97.09	98.82	98.38
∑REE	0.38	0.73	0.13	0.41	0.31	0.32

Complex	Cargill	Cargill	Cargill	Cargill	Cargill	Cargill
Sample ID	CCM29 136.85-137.2	CCM29 136.85-137.2	H24 IMC 28.6-29.0	H24 IMC 28.6-29.0	H35 IMC 128.9-129.3	H35 IMC 128.9-129.3
Oxide	avg. core	avg. rim	avg. core	avg. rim	avg. core	avg. rim
P_2O_5	40.26	40.26	40.65	40.25	41.05	40.99
SiO_2	0.15	b.d.	b.d.	b.d.	b.d.	b.d.
As_2O_5	b.d.	b.d.	b.d.	b.d.	b.d.	b.d.
SO_3	b.d.	b.d.	b.d.	b.d.	b.d.	b.d.
CaO	54.27	54.76	54.12	54.15	54.20	53.87
Na_2O	0.26	0.21	0.15	0.16	0.19	0.24
FeO_{Total}	b.d.	b.d.	b.d.	b.d.	b.d.	b.d.
MnO	0.10	0.09	b.d.	b.d.	b.d.	b.d.
SrO	0.34	0.42	0.33	0.34	0.41	0.39
BaO	b.d.	b.d.	b.d.	b.d.	b.d.	b.d.
Y_2O_3	b.d.	b.d.	b.d.	b.d.	b.d.	b.d.
La_2O_3	0.18	0.12	b.d.	b.d.	0.25	0.28
Ce_2O_3	0.42	0.29	0.18	0.19	0.34	0.51
Pr_2O_3	n.a.	n.a.	n.a.	n.a.	b.d.	b.d.
Nd_2O_3	b.d.	b.d.	b.d.	b.d.	0.19	0.40
Sm_2O_3	b.d.	b.d.	b.d.	b.d.	b.d.	b.d.
F	2.11	2.33	2.15	2.13	2.24	2.41
Cl	0.03	0.04	0.02	0.02	b.d.	b.d.
TOTAL	98.46	98.78	97.79	97.45	99.18	99.41
TOTAL-O	97.56	97.79	96.88	96.55	98.24	98.40
∑REE	0.60	0.41	0.18	0.19	0.78	1.19

Complex	Firesand River	Firesand River	Firesand River	Firesand River
Sample ID	H8 135.65-136.85	H8 135.65-136.85	ST-34	ST-34
Oxide	avg. core	avg. rim	avg. core	avg. rim
P_2O_5	40.60	40.34	41.82	41.28
SiO_2	0.14	0.13	0.17	0.19
As_2O_5	b.d.	b.d.	b.d.	b.d.
SO_3	b.d.	b.d.	b.d.	b.d.
CaO	54.53	54.47	53.35	52.09
Na_2O	0.09	0.13	0.14	0.22
FeO_{Total}	b.d.	b.d.	0.08	0.08
MnO	b.d.	b.d.	b.d.	b.d.
SrO	1.04	1.08	1.03	0.53
BaO	b.d.	b.d.	b.d.	0.12
Y_2O_3	b.d.	b.d.	0.10	0.21
La_2O_3	0.13	0.14	0.12	0.24
Ce_2O_3	0.23	0.28	0.25	0.46
Pr_2O_3	n.a.	n.a.	b.d.	b.d.
Nd_2O_3	b.d.	b.d.	0.11	0.21
Sm_2O_3	b.d.	b.d.	b.d.	b.d.
F	2.57	2.56	2.48	2.46
Cl	b.d.	0.03	b.d.	b.d.
TOTAL	99.37	99.27	99.79	98.20
TOTAL-O	98.29	98.19	98.75	97.17
∑REE	0.36	0.42	0.48	0.91

Geochemical investigations of apatite from carbonatites can be useful to the understanding of the evolution of a carbonatitic melt. Carbonatitic apatite are known to crystallize throughout nearly the entire magmatic history of a carbonatitic melt (Gittins, 1989), and thus they can be a good indicator as to how evolved the melt was on crystallization. In addition, Klemme and Dalpé (2003) demonstrated that the partition coefficients for La, Ce, Pr, Sm, Si, Sr and Y between apatite and a carbonatitic melt are close to 1, which means that carbonatitic apatite can be a good proxy of how enriched or depleted a carbonatitic melt was in REE's.

Timmermans (2003 and references therein) has demonstrated on the basis of data from apatite that the LREE abundances increase from the earlier to the later stages of carbonatite formation. The general mode of REE substitution (Timmermans, 2003; references therein) into apatite can be represented by:

$$Ca^{2+} + P^{5+} \leftrightarrow REE^{3+} + Si^{4+} \qquad (3\text{-}3)$$

where: REE^{3+} is best represented in carbonatitic apatite by: La^{3+} or Ce^{3+}

However, an examination of the apatite data from the electron microprobe revealed that the concentration of SiO_2 was generally quite low, and in many cases it was either below or barely above the probe detection limit. Also, it was found that in many instances the concentration of SiO_2 actually decreases from core to rim within a single crystal of apatite, which is inconsistent with equation 3-3 (see also Table 3-15). On the other hand Na, which is another trace element commonly found in carbonatitic apatite, is notably higher than Si. In addition, it was found that the concentration of Na_2O mostly increases from core to rim (refer to Table 3-15). Given these observations, a more plausible mode of substitution which involves the REE's (REE^{3+}) and Na^+ can be denoted by:

$$2Ca^{2+} \leftrightarrow REE^{3+} + Na^{+} \qquad (3\text{-}4)$$

This coupled substitution, the 'belovite scheme', is common in apatite from carbonatites (Hogarth, 1989).

Therefore, examining the relationship between 2Ca vs. La and Ce and Na is a good indicator as to how evolved the carbonatitic melt was when it crystallized. It would be difficult to directly evaluate how the geochemical signature of apatite and the sulphur isotopic composition of carbonatitic sulphides evolved together because of lack of empirical and experimental investigations. However, examination of the apatite data among some of the carbonatite complexes (notably those possessing the most dissimilar sulphur isotopic compositions), allows for a semi-quantitative evaluation as to whether the sulphur isotopic variations between the different carbonatite complexes are related to

melt evolution as opposed to source heterogeneities and/or crustal contamination. Working under the assumption that each of these carbonatite complexes originated from a similar mantle source in terms of LREE abundance, an examination of the relative LREE concentrations between the complexes allows for a comparison of how evolved each complex was upon crystallization. Figure 3-7, which is a plot of 2Ca (apfu) vs. La + Ce + Na (apfu), readily demonstrates that the carbonatitic apatite from the Schryburt Lake complex are the most evolved while those from the Cargill complex are the most primitive. This relationship also matches up fairly well with the sulphur isotope systematics of these rocks. Only the apatite data from carbonatitic rocks was used to construct this plot. Unfortunately, no apatite data were available from the Spanish River and Big Beaver House carbonatites.

The apatite data from sample ST-34 (a silicocarbonatite from the Firesand River complex) deviate significantly from the other data shown in Figure 3-7. It is interesting to note that the apatite from sample ST-34 was the only one to contain detectable amounts of Y_2O_3, up to 0.28 wt.%. In addition, the whole-rock $(La/Yb)_{CN}$ ratio for sample ST-34 is ~ 1.6 (normalizing values from Nakamura, 1974), which is the lowest of any of the samples analysed and is extremely low for a carbonatite e.g. Hornig-Kjarsgaard (1998).

Figure 3-7. 2Ca (apfu) vs. La+Ce+Na (apfu) for apatite from Superior Province carbonatites

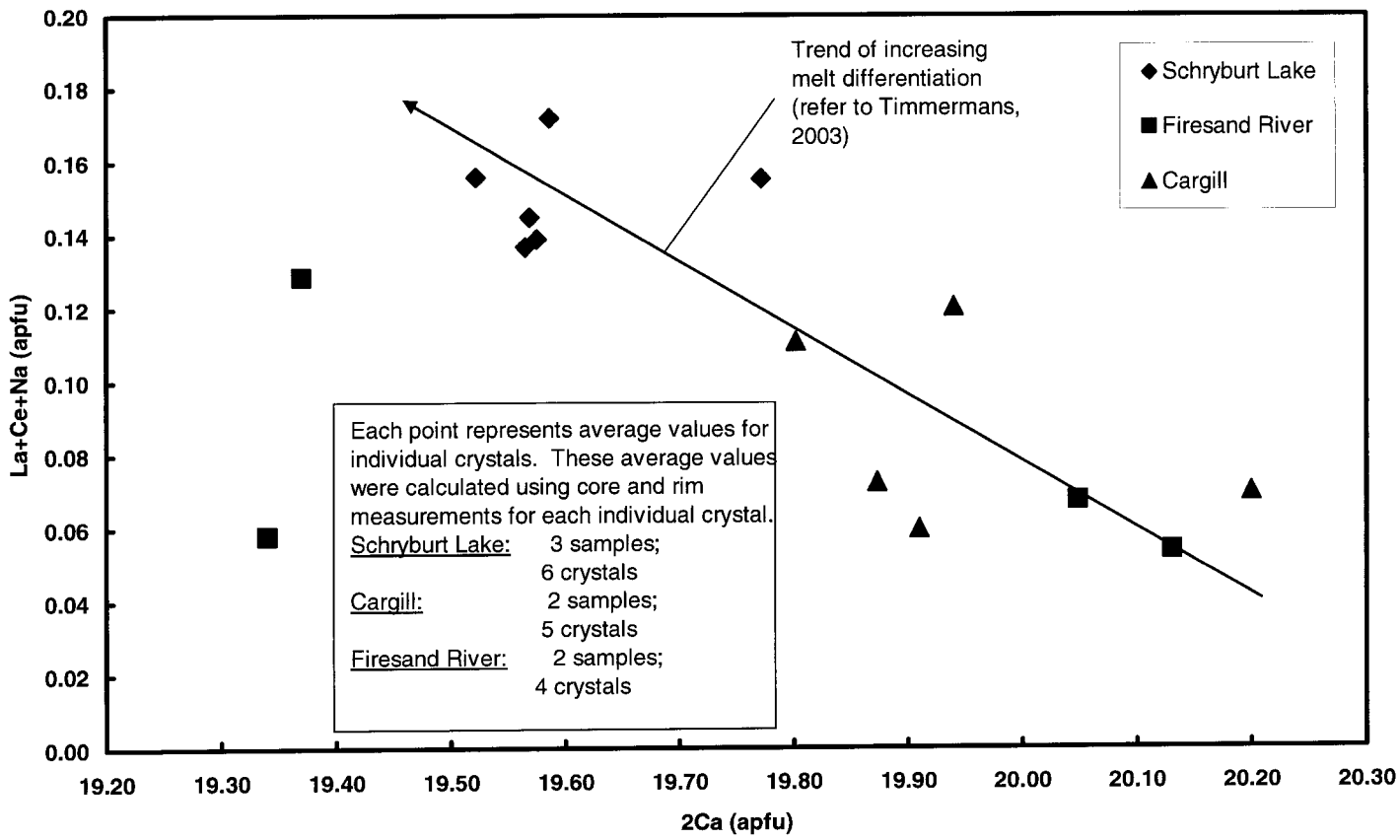

The sulphides from the Schryburt Lake complex possess both the most evolved $\delta^{34}S_{CDT}$ values and the most evolved apatite geochemical signatures, while the carbonatites from the Cargill complex have the most primitive $\delta^{34}S_{CDT}$ values and least differentiated apatite geochemical signatures. Although the plot shows some overlap between the different complexes, it does demonstrate that the complexes which possess the most primitive sulphur isotopic compositions, i.e. close to 0‰ also tend to have the least differentiated apatite compositions.

In terms of elemental zonation, most of the apatite that was probed possessed a rim that is enriched in LREE's relative to the core. This is consistent with the work of Timmermans (2003) suggesting that the LREE abundances tend to increase from the early to the late stages of carbonatite formation. The Sr content also generally increases from core to rim. The LREE abundances in the apatite can also be seen in BSE images (refer to AP plates). The apatite from the Schryburt Lake carbonatites appears to be the most strongly zoned (see Plates AP1 – AP6) whereas the apatite from the Spanish River and Cargill complexes is the most weakly zoned (see Plates AP10 – AP13, AP19 – AP25).

Apatite from the Schryburt Lake complex are the most enriched in the REE's while apatite from the Spanish River complex are the most impoverished in the REE's. Overall, the $\sum$REE content of all of the apatite do show a considerable amount of variation ($\sum$REE = 0.13 – 2.09 wt.%), which is consistent with different degrees of melt differentiation. In addition, all of the apatite is fluoroapatite (F (apfu) > 1.00) with some possessing a minor hydroxy component. The higher SiO_2 (up to 0.41 wt.%) content

within the Big Beaver House complex apatite probably reflects the fact that this apatite is contained within ultramafic rather than carbonatitic rocks.

3.13.3 Mineral Chemistry – Sulphides – Pyrrhotite, Pyrite and Chalcopyrite

Electron microprobe analyses were carried out on grain mounts of various sulphide minerals from the Schryburt Lake, Spanish River, Firesand River and "Carb" Lake complexes in order to determine whether or not there was a correlation between the sulphur isotopic composition of the sulphides and their mineralogy. The electron microprobe data for the analysed sulphides can be found in Appendix A. For the most part, the analysed sulphides did not contain any appreciable amounts of base metals other than Fe for the pyrrhotite and pyrite and Fe and Cu for the chalcopyrite. Only one sample (3-439-454B), a silicocarbonatite from the "Carb" Lake complex contains appreciable amounts of Ni. The pyrrhotite from this sample averaged approximately 0.5 wt.% Ni. Sample 3-439-454B was the only sample from the "Carb" Lake complex analysed in this study and hence was not included as a section within Chapter 3. It is, however, noteworthy to point out that the $\delta^{34}S_{CDT}$ value of the pyrrhotite from this sample is +2.8‰, which is by far the most enriched sulphur isotopic signature for any of the pyrrhotite-bearing samples analysed in this study. Ripley (1999) demonstrated that in certain mafic intrusions, the sulphide-rich zones tend to possess a more enriched $\delta^{34}S_{CDT}$ signature then the associated sulphide-poor zones. The elevated sulphur isotopic signatures in the sulphide-rich zones are often attributed to contamination by country rock sulphur. The Archaean country rocks surrounding this complex consist of hybrid

granite and granitic gneiss (Riley and Davies, 1967b). Whether or not these rocks contained enough sulphur to contaminate the "Carb" Lake intrusion is not known. It can be seen, however, that the sulphur isotopic value of +2.8‰ for this pyrrhotite-bearing silicocarbonatite falls outside of the range of values for the primitive mantle and given this rather elevated $\delta^{34}S_{CDT}$ value, there may have been a contribution of country rock sulphur into this carbonatitic magma. However, the country rocks surrounding the "Carb" Lake complex are Archaean in age, and therefore it is likely that their sulphur isotopic composition is close to 0‰ e.g. Ohmoto (1986). Thus, the use of sulphur isotopes in delineating crustal contamination by Archaean rocks can be somewhat ambiguous. Country rock contamination could be confirmed with a more in-depth analysis of this complex and of both the sulphur concentration and the sulphur isotopic composition of the surrounding granitic and gneissic country rocks.

Chapter 4: Additional Discussions and Concluding Remarks

4.1 Discussion of the $\delta^{13}C_{V\text{-}PDB}$ and $\delta^{18}O_{V\text{-}SMOW}$ variations

The fact that the both the carbon and oxygen isotopic composition (all mineral separates are calcite unless otherwise noted) of all of the carbonatite complexes examined in this study either fall into and/or are close to the carbon and oxygen isotopic composition of the upper mantle field (Chazot et al., 1997 and Cartigny et al., 1998) is quite remarkable (see Figure 4-1). Even the slightly elevated $\delta^{18}O_{V\text{-}SMOW}$ values of between +7 and +8‰ for some of the samples from the Cargill, Big Beaver and Spanish River complexes may still be representative of the oxygen isotopic composition of the mantle. Deines (1989) demonstrated that a carbonate melt with an oxygen isotopic composition of between +7 and +8‰ could be produced by equilibrium fractionation at 1000°C with a mantle peridotite possessing an oxygen isotopic composition of between +5 and +6‰.

A discussion related to the carbon and oxygen isotopic compositions of the silicate rocks associated with some of these carbonatites seems warranted because a great deal of this study has focussed on the comparative sulphur isotopic composition of the carbonatites and associated silicate rocks. Despite the wealth of oxygen and carbon isotopic data from carbonatites, Deines (1989) comments that there do not exist very many studies which have investigated the oxygen isotopic composition of silicate rocks found in association with sövites. Investigations of the Oka carbonatite complex by Deines (1967) demonstrated that most of the $\delta^{13}C_{PDB}$ values of the carbonate portions of silicate rocks associated with the carbonatites fall into a narrow range of between –4.8

and –5.8‰. In contrast, the $\delta^{18}O_{SMOW}$ values from the Oka complex were found to vary considerably and tended to be enriched in ^{18}O. The most important point made by Deines (1989) was that the ^{18}O enrichment observed in the carbonate portion of the silicate rocks was attributed to both the concentration and proportion of carbonate to silicate minerals within the silicate rock. Deines (1989) and references therein, demonstrated that at high temperatures calcite in the silicate rocks is generally enriched in ^{18}O by about 1-2‰ with respect to melilite and the pyroxenes. For example, the oxygen isotope fractionation factor between calcite and diopside at 700°C (as represented by: $1000 \ln \alpha_{diopside}^{calcite}$) is 1.0025 (Chiba et al., 1989). Therefore, even at 700°C calcite is enriched by approximately +3.5‰ when compared to the coexisting diopside, e.g. if $\delta^{18}O_{calcite}$ = +7.5‰, then $\delta^{18}O_{diopside}$ would ≈ + 4.0‰.

Figure 4-1. Carbon and oxygen isotopic composition of Superior Province carbonatites and associated silicate rocks

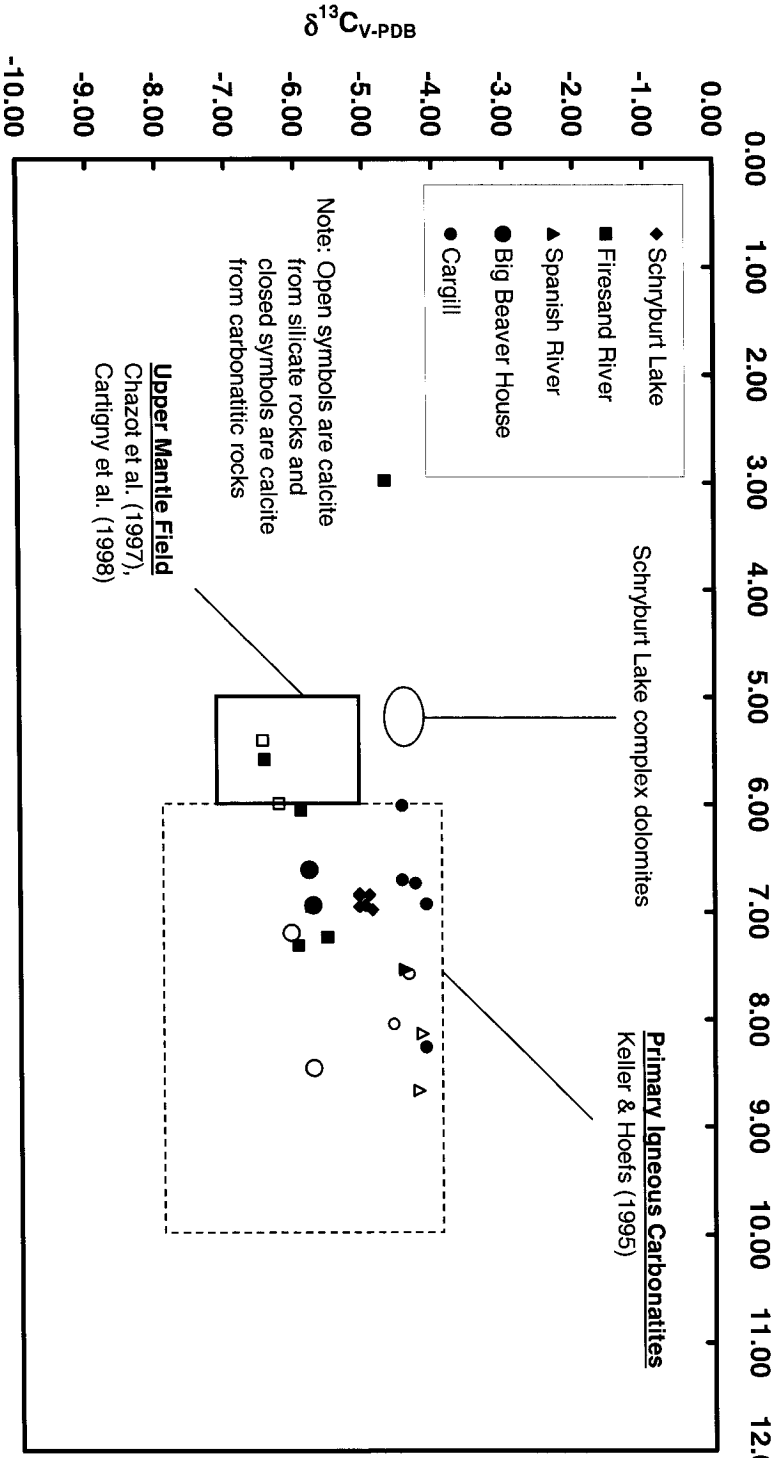

Overall, the carbon isotopic compositions of the carbonatites and carbonates contained within the associated silicate rocks from this study are very similar, and do not differ to any significant degree within each individual complex. The variation is well within the 1‰ range observed for the Oka carbonatites and associated silicate rocks (Deines, 1967). On the other hand, the oxygen isotopic composition of the carbonate portions of the silicate rocks examined in this study tended to be enriched by about +1‰ with respect to the carbonatitic carbonates. Because the oxygen isotopic composition of the silicate rocks examined in this study do not deviate substantially from the mantle range (+5 to +7‰) proposed by Kyser (1986), the most plausible explanation for their slightly elevated $\delta^{18}O_{V\text{-}SMOW}$ values is that high temperature fractionation (~ 700°C) took place between the silicate calcite and silicate minerals e.g. pyroxene, causing a slight ^{18}O enrichment in the calcite contained within the silicate rock. This could be most easily verified with an oxygen isotopic investigation of the silicate minerals. The coupled carbonate content and ^{18}O enrichment of the carbonate-bearing silicate rocks may be analogous to the ^{34}S enrichment and higher sulphur concentrations of the silicate rocks found associated with the carbonatites.

4.2 Conclusions

The main goal of this study was to ascertain whether the sulphur isotopic signatures within Superior Province carbonatites are representative of mantle-derived sulphur, and to place constraints on the genetic relationship between carbonatites and their associated silicate rocks.

For the most part, the sulphur isotopic data reported in this study lie close to or fall within the range of 0 ± 1.5‰, which was proposed to be the range for sulphur derived from the primitive mantle (see Table 4-1). In the simplest interpretation, this means that the carbonatitic melts obtained their sulphur from the mantle and that there was little, if any, input of country rock sulphur when these carbonatites were emplaced into the crust. This explanation seems satisfactory for the carbonatites and associated silicate rocks from both the Cargill and Spanish River complexes which possess mean sulphur isotopic compositions of –0.6‰ and 0.0‰, respectively. The sulphur isotopic compositions of the various sulphide-bearing samples from the Firesand River complex can be modelled in terms of isotopic fractionation at magmatic temperatures (T ~ 580°C) and at hydrothermal temperatures (T ~ 170°C). As with the Cargill and Spanish River complexes, the sulphur at the Firesand River complex was also derived from the primitive mantle. The low sulphur isotopic values of the sulphides at the Big Beaver House and the Schryburt Lake complexes are attributed to the effects of redox-related isotopic fractionation during the emplacement of these two complexes.

The results from this study seem to suggest that there is an intimate relationship between the sulphur contained within the carbonatites and the associated silicate rocks. The associated silicate rocks within the studied carbonatitic intrusions generally contain a higher sulphur concentration and a more primitive sulphur isotopic composition than the carbonatites. The more evolved sulphur isotopic compositions of the carbonatites, compared to their associated silicate rocks, is consistent with a model in which the carbonatites represent the final products of magmatic differentiation.

Table 4-1. Summary of the stable isotopic compositions of the Superior Province carbonatites and associated silicate rocks examined in this study.

Complex	Rock Type	Range in $\delta^{34}S_{CDT}$	Range in $\delta^{18}O_{V\text{-}SMOW}$	Range in $\delta^{13}C_{V\text{-}PDB}$
Schryburt Lake	carbonatite	−4.5 to −3.4‰ (n=6)	+6.83 to +6.98‰ (n=6)	−5.10 to −4.91‰ (n=6)
Big Beaver House	carbonatite	−3.6 to −2.4‰ (n=3)	+6.61 to +6.94‰ (n=2)	−5.83 to −5.87‰ (n=2)
	silicate	−2.0 to −1.5‰ (n=4)	+7.20 to +8.45‰ (n=2)	−6.09 to −5.77‰ (n=2)
Cargill	carbonatite	−1.5 to −0.1‰ (n=7)	+6.01 to +8.26‰ (n=5)	−4.48 to −4.14‰ (n=5)
	silicate	−0.3 to +0.5‰ (n=2)	+7.58 to +8.04‰ (n=2)	−4.61 to −4.39‰ (n=2)
Spanish River	carbonatite	+0.1‰ (n=1)	+7.54‰ (n=1)	−4.43‰ (n=1)
	silicate	−0.1 to +0.1‰ (n=2)	+8.13 to +8.66‰ (n=2)	−4.24 to −4.19‰ (n=2)
Firesand River	carbonatite	+1.3 to +1.6‰ (n=5)	+5.58 to +7.31‰ (n=5)	−6.47 to −5.58‰ (n=5)
	silicate	+1.3 to +1.7‰ (n=3)	+5.40 to +5.99‰ (n=2)	−6.49 to −6.27‰ (n=2)
"Carb" Lake	carbonatite	+2.8‰ (n=1)	----------	----------

Note: (1) All of the carbon and oxygen isotopic data are from calcite separates; (2) The sulphur isotopic data are from pyrrhotite, pyrite and chalcopyrite separates; (3) Isotopic data from the Firesand River complex excludes sample F 384-A (carbonatitic dyke rock) [$\delta^{34}S_{CDT}$ = +3.4‰, $\delta^{18}O_{V\text{-}SMOW}$ = +2.98‰, $\delta^{13}C_{V\text{-}PDB}$ = −4.71‰].

Sulphur isotopic variations both within and between the complexes can be attributed to different modes of emplacement and melt differentiation rather than to source heterogeneity. This study also demonstrates that stable isotopic investigations of carbonatites should also include both petrographic and petrochemical analyses in order to better evaluate the observed isotopic variations seen both within and between complexes. Figure 4-2 is a comparison between the sulphur isotopic composition of sulphide-sulphur for Superior Province carbonatites and associated silicate rocks and the compilation made by Deines (1989). Although there is an almost 8‰ spread in the data, the mean (−0.8‰)

and the median (–0.7‰) lie very close to the primitive mantle mean of ~ 0‰. This not only demonstrates that the ultimate source of the carbonatitic sulphur for the Superior Province was derived from the mantle, but that the mantle source below the Superior Province appears to have remained relatively closed with respect to sulphur over much of its geological history. Both the corresponding carbon and oxygen isotope data are also consistent with carbonatite derivation from a pristine mantle source. All of this is consistent with the findings of Bell et al. (1982), and Bell and Blenkinsop (1987), demonstrating that the mantle beneath the Superior Province, which was the source for these carbonatitic melts, has remained essentially a closed-system over most of its geological history. This study reports the first ever sulphur isotopic analyses of carbonatites from the Superior Province.

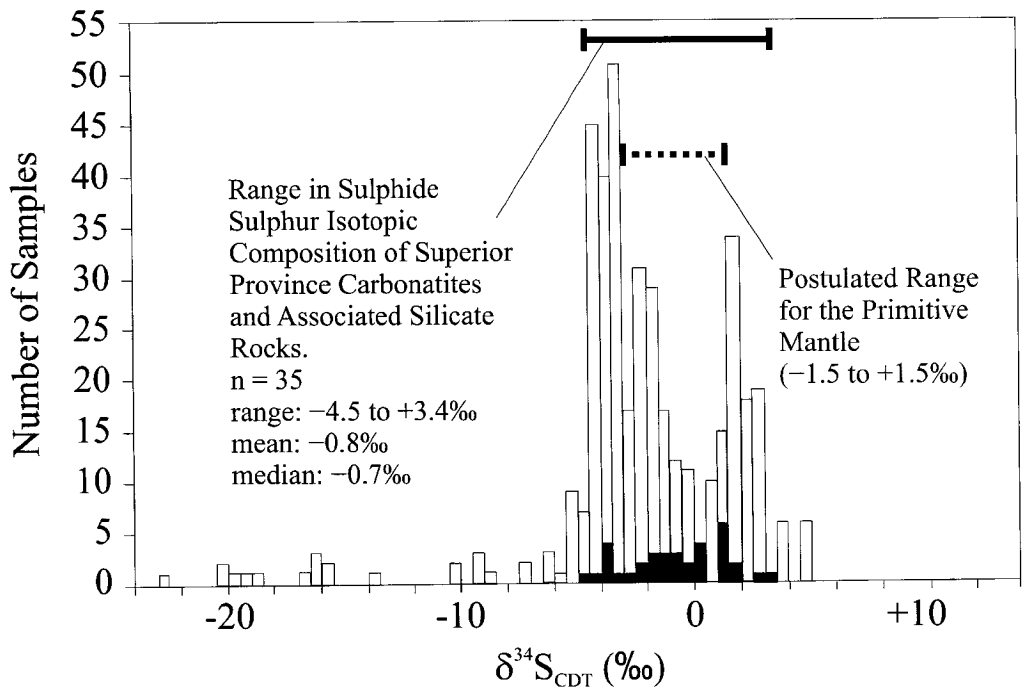

Figure 4-2. Bar chart which compares the isotopic composition of sulphide sulphur for Superior Province carbonatites and associated silicate rocks with carbonatites from other localities. Source of data: Hoefs et al. (1968); Grinenko et al. (1970a, b); Mitchell and Krouse (1971, 1975); Mäkelä and Vartiainen (1978); Panov et al. (1981); Bagdasarov and Grinenko (1983), Bolonin and Zhukov (1983). Figure is modified after Deines (1989).

On the basis of the findings in this thesis future work should involve obtaining:

1. additional sulphur isotopic data from each complex to ascertain the full degree of intracomplex isotopic variations.
2. isotopic analyses of the surrounding country rocks, which may yield clues about the possibility of contamination in certain complexes, most notably at the Firesand River complex.
3. further sulphur isotopic analyses in order to compare intrusions that only possess carbonatitic rocks (e.g. Valentine Township) and those that possess only alkaline-ultramafic rocks (e.g. Lackner Lake). This may produce additional insights into

the relationship between carbonatites and their associated alkaline-ultramafic rocks

References

Al-Aasm, I.S., Taylor, B.E. & South B. (1990). Stable Isotope Analysis of Multiple Carbonate Samples Using Selective Acid Extraction. *Chemical Geology* **80,** 119 – 125.

Allen, C. (1972). The Petrology of the Ultramafic Suite Associated with the Cargill Alkaline Ultramafic Carbonatite Complex, Kapuskasing, Ontario. *Unpublished M.Sc. Thesis,* University of Toronto.

Andersen, D.J., Lindsley, D.H. & Davidson, P.M. (1993). QUILF: A PASCAL Program to Assess Equilibria among Fe-Mg-Ti Oxides, Pyroxenes, Olivines, and Quartz. *Computers in Geosciences* **19,** 1333 – 1350.

Bagdasarov, Yu. A. & Grinenko, L.N. (1981). Isotopic Composition of Sulphur in Carbonatites of the Chernigovsk Zone Azov Sea Coastal Region and Reasons for its Variations in Carbonatite Complexes. *Doklady Akademii Nauk SSSR, Seriya Geologiya* **258,** 1192 – 1195.

Bagdasarov, Yu. A. & Grinenko, L.N. (1983). Isotopic Composition of Sulphur in Sulfides from Carbonatite Massifs of the Maimecha-Kotui Province and some Conditions of their Formation. *Doklady Akademii Nauk SSSR, Seriya Geologiya* **271,** 1484 – 1488.

Bell, K. & Blenkinsop, J. (1980). Ages and Initial $^{87}Sr - ^{86}Sr$ Ratios from Alkalic Complexes of Ontario. *In:* Geoscience Research Grant Program, Summary of Research, 1979-1980. *Ontario Geological Survey* Miscellaneous Paper **93,** 16 – 23.

Bell, K., Blenkinsop, J., Cole, T.J.S. & Menagh, D.P. (1982). Evidence from Sr Isotopes for Long-lived Heterogeneities in the Upper Mantle. *Nature* **298,** 251 – 253.

Bell, K., Blenkinsop, J., Kwon, S.T., Tilton, G.R. & Sage, R.P. (1987). Age and Radiogenic Isotopic Systematics of the Borden Carbonatite Complex, Ontario, Canada. *Canadian Journal of Earth Sciences* **24,** 24 – 30.

Bell, K. & Blenkinsop, J. (1987). Archaean Depleted Mantle: Evidence from Nd and Sr Initial Isotopic Ratios of Carbonatites. *Geochimica et Cosmochimica Acta* **51,** 291– 298.

Bell, K. (1989). Carbonatites Genesis and Evolution. *Unwin Hyman* 618 pages.

Bell, K. & Blenkinsop, J. (1989). Neodymium and Strontium Isotope Geochemistry of Carbonatites. *In:* Bell, K. (Ed.) Carbonatites Genesis and Evolution. *Unwin Hyman,* pp. 278 – 300.

Bennett, G., Brown, D.D., George, P.T. & Leahy, E.J. (1967). Operation Kapuskasing. *Ontario Department of Mines* Miscellaneous Paper **10,** 98p.

Blenkinsop, J. & Bell, K. (1983). Rb-Sr Geochronology of the Coldwell Complex, North-western Ontario, Canada; Discussion. *Canadian Journal of Earth Sciences* **20,** 1499 – 1500.

Bolonin, A.V. & Zhukov, F.I. (1983). Isotopic Composition of Carbon Oxygen and Sulphur of Carbonatites from Deposits in Southern Siberia. *Izvestiya Vysshikn Uchebnykn Zavedenii, Geologiya i Razvedka* **26,** 67 –72.

Buddington, A.F. & Lindsley, D.H. (1962). Iron-titanium Oxide Minerals and Synthetic Equivalents. *Journal of Petrology* **2,** 310 – 357.

Burke, K. & Dewey, J.F. (1973). Plume Generated Triple Junctions: Key Indicators in Applying Plate Tectonics to Old Rocks. *Journal of Geology* **81,** 406 – 433.

Cartigny, P., Harris, J.W., Phillips, D., Girad, M. & Javoy, M. (1998). Subduction-related Diamonds? – The Evidence for a mantle-derived Origin from Coupled $\delta^{13}C$- $\delta^{15}N$ Determinations. *Chemical Geology* **147,** 250 – 265.

Chaussidon, M., Albarède, F. & Sheppard, S.M.F. (1987). Sulphur Isotope Heterogeneity in the Mantle from Ion Microprobe Measurements of Sulfide Inclusions in Diamonds. *Nature* **330,** 242 – 244.

Chaussidon, M., Albarède, F. & Sheppard, S.M.F. (1989). Sulphur Isotope Variations in the Mantle from Ion Microprobe Analyses of Micro-sulphides Inclusions. *Earth and Planetary Science Letters* **92,** 144 – 156.

Chaussidon, M. & Lorand, J.-P. (1990) Sulphur Isotope Composition of Orogenic Spinel Lherzolite Massifs from Ariege (North-Eastern Pyrenees, France): An Ion Microprobe Study. *Geochimica et Cosmoschimica Acta* **54,** 2835 – 2846.

Chazot, G., Lowrey, D., Menzies, M. & Mattey, D. (1997). Oxygen Isotopic Composition of Hydrous and Anhydrous Peridotites. *Geochimica et Cosmochimica Acta* **61,** 161 – 169.

Cheney, E.S. & Lange, I.M. (1967). Evidence for Sulphurization and the Origin of some Sudbury – Type Ore. *Mineralium Deposita* **2,** 80 – 94.

Chiba H., Chacko T., Clayton R.N. & Goldsmith J.R. (1989). Oxygen Isotope Fractionations Involving Diopside, Forsterite, and Calcite: Applications to Geothermometry. Geochimica et Cosmochimica Acta **53,** 2985-2995.

Claypool, G.E., Holster, W.T., Kaplan, I.R., Sakai, H. & Zak, I. (1980). The Age Curves of Sulphur and Oxygen Isotopes in Marine Sulphate and their Mutual Interpretation. *Chemical Geology* **28,** 199 – 260.

Clayton, R.N., Jones, B.F. & Berner, R.A. (1968). Isotope Studies of Dolomite Formation Under Sedimentary Conditions. *Geochimica et Cosmochimica Acta* **32,** 415 – 432.

Coleman, M.L. (1977). Sulphur Isotopes in Petrology. *Journal of the Geological Society of London* **133,** 593 – 608.

Craig, H. (1965). The Measurement of Oxygen Isotope Paleotemperatures. *In:* Stable Isotopes in Oceanographic Studies and Paleotemperatures. Spoleto, July 26 – 27, 1965. Consiglio Nazionle delle Ricerche, Laboratorio di Geologia Nucleare, Pisa, pp. 1 – 24.

Deines, P. (1967). Stable Carbon and Oxygen Isotopes of Carbonatite Carbonates and their Interpretation. *Ph.D. Thesis,* The Pennsylvania State University, University Park.

Deines, P. (1989). Stable Isotope Variations in Carbonatites. *In:* Bell, K. (Ed.) Carbonatites Genesis and Evolution. *Unwin Hyman,* pp. 301 – 359.

Ercit, T.S. (1996). FORMULA: A General-Purpose Program for Formula Calculation, Version 96.9.

Eriksson, S.C. (1989). Phalaborwa: A Saga of Magmatism, Metasomatism, and Miscibility. *In:* Bell, K. (Ed.) Carbonatites Genesis and Evolution. *Unwin Hyman,* pp. 221 – 254.

Faure, G. (1977). Principles of Isotope Geology. *John Wiley and Sons,* 464 pages.

Faure, G. (1986). Principles of Isotope Geology. 2nd Edition. *John Wiley and Sons,* 589 pages.

Friedman, I. & O'Neil, J.L. (1977). Compilation of Stable Isotope Fractionation Factors of Geochemical Interest. *In:* Fleischer, M. (Ed.) Data of Geochemistry, 6th Edition. *United States Geological Survey Professional Paper* Report: **P 0440-KK,** 12p.

Gasparrini, J., Gittins, J. & Rucklidge, J.C. (1971). Chemical Variation among the Non-Carbonate Minerals of the Cargill Lake Carbonatite. *Canadian Mineralogist* **10,** 913. (Abstract).

Gehlen, K. von (1967). Sulphur Isotopes from the Sulfide-Bearing Carbonatite of Phalaborwa, South Africa. *Transactions, Institution of Mining and Metallurgy, Section B: Applied Earth Science* **76(B),** 223. (Abstract).

Gittins, J., McIntyre, R.M. & York, D. (1967). The Ages of Carbonatite Complexes in Eastern Canada. *Canadian Journal of Earth Sciences* **4,** 651 – 655.

Gittins, J., Allen, C.R. & Cooper, A.F. (1975). Phlogopitization of Pyroxenite; Its Bearing on the Composition of Carbonatite Magmas. *Geological Magazine* **112,** 503 – 507.

Gittins, J. (1989). The Origin and Evolution of Carbonatite Magmas. *In:* Bell, K. (Ed.) Carbonatites Genesis and Evolution. *Unwin Hyman,* pp. 580 – 600.

Godlevskii, M.N. & Grinenko, L.N. (1963). Some Data on the Sulphur Isotopic Composition of Sulphur in Sulfides of the Noril'sk Deposit. *Geokhimiya* **1963,** 35 – 40.

Goodfellow, W.D. & Jonasson, I.R. (1984). Ocean Stagnatin and Ventilation Defined by $\delta^{34}S$ Secular Trends in Pyrite and Barite, Selwyn Basin, Yukon. *Geology* **12,** 583 – 586.

Gorbachev, N.S. & Grinenko, L.N. (1973). Origin of the October Sulfide Ore Deposits, Noril'sk Region, in the Light of Sulfide and Sulphate Isotope Composition. *Geochemistry International* **12,** 132 – 137.

Grinenko, L.N., Kononova, V.A. & Grinenko, V.A. (1970a). Isotopic Composition of Sulphur in Sulfides from Carbonatites. *Geokhimiya* **1,** 66 – 75.

Grinenko, L.N., Kononova, V.A. & Grinenko, V.A. (1970b). Isotopic Composition of Sulfide Sulphur in Carbonatites. *Geochemistry International* **7,** 45 – 53.

Grinenko, V.A., Dimitriev, L.V. Migdisov, A.A. & Sharas'kin, A.Y. (1975). Sulphur Contents and Isotopic Composition for Igneous and Metamorphic rocks from Mid-Ocean Ridges. *Geochemistry International* **12,** 132 – 137.

Hammond, P.A. & Taylor L.A. (1982). The Ilmenite Titano-magnetite Assemblage: Kinetics of Re-equilibration. *Earth and Planetary Science Letters* **61,** 143 – 150.

Heinrich, E.W. & Vian, R.W. (1967). A Barite–Quartz Phase in the Firesand River Carbonatite, Wawa, Ontario. *Canadian Mineralogist* **9,** 252 – 257.

Higgins, C.S. (1977). Petrography and Petrology of the Schryburt Lake Carbonatite Intrusion. *Unpublished B.Sc. Thesis,* Carleton University 50 pages.

Hoefs, J., Nielsen, H. & Schidlowski, M. (1968). Sulphur Isotope Abundances in Pyrite from the Witwatersrand Conglomerates. *Economic Geology* **63,** 975 – 977.

Hoefs, J. (1997). Stable Isotope Geochemistry. 4th Edition. *Springer-Verlag,* 201 pages.

Hogarth, D.D. (1989). Pyrochlore, Apatite and Amphibole: Distinctive Minerals in Carbonatite. *In:* Bell, K. (Ed.) Carbonatites Genesis and Evolution. *Unwin Hyman,* pp. 105 – 148.

Hubberten, H.W., Nielsen, H. & Puchelt, H. (1977). Sulphur Isotope Investigations on Rocks and Ores of the Santorini Archipelago, Greece. *Annales Géologique des Pays Helléniques le Séries* **XXVIII-1976,** 334 – 348.

Kajiwra, Y. & Krouse, H.R. (1971). Sulphur Isotope Partitioning in Metallic Sulphide Systems. *Canadian Journal of Earth Sciences* **8,** 1397-1408.

Keller, J. & Hoefs J. (1995). Stable Isotope Characteristics of Recent Natrocarbonatite from Oldoinyo Lengai. *In:* Bell, K. & Keller, J. (Eds.) Carbonatite Volcanism; Oldoinyo Lengai and the Petrogenesis of Natrocarbonatites. IAVCE I, *Proceedings in Volcanology* **4,** pp. 113 – 123.

Kjarsgaard, B.A. & Hamilton, D.L. (1989). The Genesis of Carbonatites by Immiscibility. *In:* Bell, K. (Ed.) Carbonatites Genesis and Evolution. *Unwin Hyman,* pp. 388 – 404.

Klemme, S. & Dalpé, C. (2003). Trace-element Partitioning between Apatite and Carbonatite Melt. *American Mineralogist* **88,** 639 – 646.

Kumarapeli, P.S. & Saull, V.A. (1966). The St. Lawrence Valley System: A North American Equivalent of the East African Rift Valley System. *Canadian Journal of Earth Sciences* **3,** 639 – 658.

Kwon, S.T. (1986). Pb-Sr-Nd Isotope Study of the 100 to 2700 Ma Alkalic Rock-Carbonatite Complexes in the Canadian Shield: Inferences on the Geochemical and Structural Evolution of the Mantle. *Unpublished Ph.D. Thesis,* University of California at Santa Barbara 242 pages.

Kyser, K.T. (1986). Stable Isotope Variations in the Mantle. *In:* Valley, J.W., Taylor, H.P. and O'Neil, J.R. (Eds.) Stable Isotopes in High Temperature Geological Processes. *Reviews in Mineralogy* **16,** pp. 141 – 164.

Le Bas, M.J. (1981). Carbonatite Magmas. *Mineralogical Magazine* **44,** 133 – 140.

Mäkelä, M. & Vartianen, H. (1978). A Study of Sulphur Isotopes in the Sokli Multi-Stage Carbonatite (Finland). *Chemical Geology* **21,** 257 – 265.

Mariano, A.N. (1989). Nature of Economic Mineralization in Carbonatites and Related Rocks. *In:* Bell, K. (Ed.) Carbonatites Genesis and Evolution. *Unwin Hyman,* pp. 149 – 176.

McCrea, J.M. (1950). On the Isotopic Chemistry of Carbonates and a Paleotemperature Scale. *Journal of Chemical Physics* **18,** 849 – 857.

McNamara, J. & Thode H.G. (1950). Comparison of the isotopic constitution of terrestrial and meteoritic sulphur. *Physical Review* **78,** 307 – 308.

Mitchell, R.H. & Krouse, H.R. (1971). Isotopic Composition of Sulphur in Carbonatites at Mountain Pass, California. *Nature* **231,** 182.

Mitchell, R.H. & Krouse, H.R. (1975). Sulphur Isotope Geochemistry of Carbonatites. *Geochimica et Cosmochimica Acta* **39,** 1505-1513.

Myoshi, T., Sakai, H. & Chiba, H. (1984). Experimental Study of Sulphur Isotope Fractionation between Sulphate and Sulfide in High Temperature Melts. *Geochemical Journal* **18,** 75 – 84.

Nakamura, N. (1974). Determination of REE, Ba, Fe, Mg, Na and K in Carbonaceous and Ordinary Chondrites. *Geochimica et Cosmochimica Acta* **38,** 757 – 775.

Naldrett, A.J. (1981). Nickel Sulphide Deposits: Classification, Composition, and Genesis. *Economic Geology* **75th Anniversary Volume,** pp. 628 – 685.

Northrop, D.A. & Clayton, R.N. (1966). Oxygen-Isotope Fractionation in Systems Containing Dolomite. *Journal of Geology* **74,** 174 – 196.

ODM–GSC (1960). Big Beaver House. *Ontario Department of Mines – Geological Survey of Canada,* Aeromagnetic Map **939G,** Scale: 1:63 360.

ODM–GSC (1962). Lost River, Ontario. *Ontario Department of Mines – Geological Survey of Canada,* Aeromagnetic Map **2252G,** Scale: 1 inch to 1 mile.

ODM–GSC (1963a). Michipicoten Bay. *Ontario Department of Mines – Geological Survey of Canada,* Aeromagnetic Map **2191G,** Scale: 1:63 360.

ODM–GSC (1963b). Wawa. *Ontario Department of Mines – Geological Survey of Canada,* Aeromagnetic Map **2192G,** Scale: 1:63 360.

ODM–GSC (1970). Albany River. *Ontario Department of Mines – Geological Survey of Canada,* Aeromagnetic Compilation Map **P.578,** Scale: 1:1 013 760.

Ohmoto, H. (1972). Systematics of Sulphur and Carbon Isotopes in Hydrothermal Ore Deposits. *Economic Geology* **67,** 551 – 578.

Ohmoto, H. & Rye, R.O. (1979). Isotopes of Sulphur and Carbon. *In:* Barnes, H.L. (Ed.) Geochemistry of Hydrothermal Ore Deposits, 2nd Edition. *Wiley Interscience* pp. 509 – 567.

Ohmoto, H. (1986). Stable Isotope Geochemistry of Ore Deposits. *In:* Valley, J.W., Taylor, H.P. and O'Neil, J.R. (Eds.) Stable Isotopes in High Temperature Geological Processes. *Reviews in Mineralogy* **16,** pp. 491 – 560.

Onuong'a, I.O., Bowden, P. & Fallick, A.F. (1995). Carbon, Oxygen and Sulphur Isotope Investigations at Buru and Kuge Volcanic Carbonatite Centres, Nyanza Rift, Eastern Kenya. *Conference of the Geological Society of Africa, Conference Program* **10,** 124 – 125.

Panov, B.S., Lyashkevich, Z.M. & Pilot, I. (1981). Isotopic Sulphur, Oxygen and Carbon Content of Devonian Mineral Formations of the Dnieper Donetsk Basin. *Dopovidi Akademii Nauk Ukrains'koi RSR, Seriya B: Geologichni Khimichni ta Biologichni Nauki* **1981,** 21 – 23.

Percival, J.A. & Card, K.D. (1983). Archaean Crust as Revealed in the Kapuskasing Uplift, Superior Province, Canada. *Geology* **11,** 323 – 326.

Platt, R.G. (1994). Perovskite, Loparite and Ba-Fe Hollandite from the Schryburt Lake Carbonatite Complex, North-western Ontario, Canada. *Mineralogical Magazine* **58,** 49 – 57.

Prins, P. (1972). Composition of Magnetite from Carbonatites. *Lithos* **5,** 227 – 240.

Ray, J.S. & Ramesh, R. (2000). Rayleigh Fractionation of Stable Isotopes from a Multicomponent Source. *Geochimica et Cosmochimica Acta* **64,** 299 – 306.

Riley, R.A. & Davies, J.C. (1967b). Swan Lake Sheet, Operation Lingman Lake, District of Kenora (Patricia Portion). *Ontario Department of Mines* Map **P.427,** Geological Series, Scale: 1:126 720.

Ripley, E.W. (1981). Sulphur Isotopic Studies of the Dunka Road Cu – Ni Deposit, Duluth Complex, Minnesota. *Economic Geology* **76,** 610 – 620.

Ripley, E.M. (1999). Systematics of Sulphur and Oxygen Isotopes in Mafic Igneous Rocks and Related Cu-Ni-PGE Mineralization. *In:* Keays, R.R., Lesher, C.M., Lightfoot, P.C. and Farrow, C.E.G. (Eds.) Dynamic processes in Magmatic Ore Deposits and their Application to Mineral Exploration. *Geological Association of Canada, Short Course Volume* **13,** pp. 133 – 158.

Rollinson, H. (1993). Using Geochemical Data: Evaluation, Presentation, Interpretation. *Addison Wesley Longman Limited* 352 pages.

Rosenbaum, J. & Sheppard, S.M.F. (1986). An Isotopic Study of Siderites, Dolomites and Ankerites at High Temperatures. *Geochimica et Cosmochimica Acta* **50,** 1147 – 1150.

Rye, R.O., Luhr, J.F. & Wasserman, M.D. (1984). Sulphur and Oxygen Isotopic Systematic of the 1982 Eruptions of El Chichon Volcano, Chiapas, Mexico. *Journal of Volcanology and Geothermal Research* **23,** 109 – 123.

Sage, R.P., Sawitsky, K., Turner, J., Leeselleur, P. & Sagle, E. (1982). Precambrian Geology of McMurray Township, Wawa Area, Algoma District. *Ontario Geological Survey* Preliminary Map **P.2441,** Geological Series, Scale: 1:15 840. Geology 1979.

Sage, R.P. (1987a). Geology of Carbonatite – Alkalic Rock Complexes in Ontario: Big Beaver Carbonatite Complex, District of Kenora. *Ontario Geological Survey* Study **51,** 71p.

Sage, R.P. (1987b). Geology of Carbonatite – Alkalic Rock Complexes in Ontario: Spanish River Carbonatite Complex, District of Sudbury. *Ontario Geological Survey* Study **30,** 62p.

Sage, R.P. (1987c). Geology of Carbonatite – Alkalic Rock Complexes in Ontario: "Carb" Lake Carbonatite Complex, District of Kenora. *Ontario Geological Survey* Study **53,** 42p.

Sage, R.P. (1988a). Geology of Carbonatite – Alkalic Rock Complexes in Ontario: Firesand River Carbonatite Complex, District of Algoma. *Ontario Geological Survey* Study **47,** 82p.

Sage, R.P. (1988b). Geology of Carbonatite – Alkalic Rock Complexes in Ontario: Schryburt Lake Carbonatite Complex, District of Kenora. *Ontario Geological Survey* Study **50,** 43p.

Sage, R.P. (1988c). Geology of Carbonatite – Alkalic Rock Complexes in Ontario: Cargill Township Carbonatite Complex, District of Cochrane. *Ontario Geological Survey* Study **36,** 92p.

Sage, R.P. (1993). Geology of Chabanel, Esquega, Lastheels and McMurray Townships, District of Algoma. *Ontario Geological Survey* Report **5586,** 462p.

Sakai, H., Ueda, A. & Field C.W. (1978). $\delta^{34}S$ and Concentration of Sulphide and Sulphate Sulphurs on some Ocean – Floor Basalts and Serpentinites. *In:* Zartman, R.E. (Ed.) Short Papers of the Fourth International Conference on Geochronology, Cosmochronology and Isotope Geology. *U.S. Geological Survey* Open – File Report **78 – 701,** pp. 372 – 374.

Sakai, H., Casadevall, T.J. & Moore, J.G. (1982). Chemistry and Isotope Ratios of Sulphur in Basalts and Volcanic Gases at Kilauea Volcano, Hawaii. *Geochimica et Cosmochimica Acta* **46,** 929 – 938.

Sakai, H., Desmarais, D.J., Ueda, A. & Moore, J.G. (1984). Concentrations and Isotope Ratios of Carbon, Nitrogen and Sulphur in Ocean-Floor Basalt. *Geochimica et Cosmochimica Acta* **48,** 2433 – 2441.

Sandvik, P.O. & Erdosh, G. (1977). The Geology of the Cargill Phosphate Deposit, Northern Ontario. *Canadian Institute of Mining and Metallurgy Bulletin* **69,** 90 – 96.

Santos, R.V. & Clayton, R.N. (1995). Variations of Oxygen and Carbon Isotopes in Carbonatites: A Study of Brazilian Alkaline Complexes. *Geochimica et Cosmochimica Acta* **59,** 1339 – 1352.

Sasaki, A. (1969). Sulphur Isotope Study of the Muskox Intrusion, district of MacKenzie. *Geological Survey of Canada* Paper **68,** 68p.

Schneider, A. (1970). The Sulphur Isotopic Composition of Basaltic Rocks. *Contributions to Mineralogy and Petrology* **25,** 95 – 124.

Schwarcz, H.P. (1973). Sulphur Isotope Analysis of Some Sudbury, Ontario, Ores. *Canadian Journal of Earth Sciences* **10,** 1444 – 1459.

Scotese, C.R. (2003). PALEOMAP Project. Retrieved October 12, 2004 from http://www.scotese.com/Rodinia3.htm.

Sharma, T. & Clayton, R.N. (1965). Measurement of O-18/O-16 Ratios of Total Oxygen of Carbonates. *Geochimica et Cosmochimica Acta* **29,** 1347 – 1353.

Sharpe, J. (1987). Geochemistry of the Cargill Carbonatite Complex, Kapuskasing, Ontario. *Unpublished M.Sc. Thesis,* Carleton University 73 pages.

Sheppard, S.M.F. & Schwarcz, H.P. (1970). Fractionation of Carbon and Oxygen Isotopes and Magnesium between Coexisting Metamorphic Calcite and Dolomite. *Contributions to Mineralogy and Petrology* **26,** 161 – 198.

Shima, M., Gross, W.H. & Thode, H.G. (1963). Sulphur Isotope Abundances in Basic Sills, Differentiated Granites and Meteorites. *Journal of Geophysical Research* **68,** 2835 – 2847.

Spry, P.G. & Gedlinske, B.L. (1987). Tables for the Determination of Common Opaque Minerals. *The Economic Geology Publishing Company,* 52 pages.

Strauss, H. (1997). The Isotopic Composition of Sedimentary Sulphur through Time. *Palaeogeography, Palaeoclimatology, Palaeoecology* **132,** 97 – 118.

Streckeinsen, A.L. (1980). Classification and Nomenclature of Volcanic Rocks, Lamprophyres, Carbonatites and Melilitic Rocks, IUGS Subcommission on the Systematics of Igneous Rocks, Recommendations and Suggestions. *Geologische Rundschau* **69,** 194 – 207.

Taylor, B.E. (1986). Magmatic Volatiles: Isotopic Variation of C, H and S. *In:* Valley, J.W., Taylor, H.P. and O'Neil, J.R. (Eds.) Stable Isotopes in High Temperature Geological Processes. *Reviews in Mineralogy* **16,** pp. 185 – 225.

Teal, S. (1979). The Geology and Petrology of the Firesand River Carbonatite Complex, North-western Ontario. *Unpublished M.Sc. Thesis,* McMaster University 102 pages.

Thode, H.G., Monster, J. & Dunford, H.B. (1961). Sulphur Isotope Geochemistry. *Geochimica et Cosmochimica Acta* **25,** 159 – 174.

Thurston, P.C., Sage, R.P. & Siragusa, G.M. (1979). Geology of the Winisk Area, District of Kenora, Patricia Portion. *Ontario Geological Survey* Report **193,** 169p.

Timmermans, A.C. (2003). Composition of Apatite from the Oka Carbonatite, Quebec: Implications for Melt Evolution. *Unpublished M.Sc. Thesis,* Carleton University 146 pages.

Treiman, A.H. (1989). Carbonatite Magma: Properties and Processes. *In:* Bell, K. (Ed.) Carbonatites Genesis and Evolution. *Unwin Hyman,* pp. 89 – 104.

Twyman, J.B. (1983). The Generation, Crystallization and Differentiation of Carbonatite Magmas: Evidence from the Argor and Cargill Complexes, Ontario. *Unpublished Ph.D. Thesis,* University of Toronto 248 pages.

Ueda, A. & Sakai, H. (1984). Sulphur Isotope Study of Quaternary Volcanic Rocks from the Japanese Island Arc. *Geochimica et Cosmochimica Acta* **48,** 1837 – 1848.

Zabach, D.A., Pratt, L.M. & Hayes, J.M. (1993). Transport and Reduction of Sulphate and Immobilization of Sulphide in Marine Black Shales. *Geology* **21,** 141 – 144.

Zheng, Y.-F. (1990). Sulphur Isotope Fractionation in Magmatic Systems: Models of Rayleigh Distillation and Selective Flux. *Chinese Journal of Geochemistry* **9,** 27 – 45.

Zheng Y.-F. (1999). Oxygen Isotope Fractionation in Carbonate and Sulphate Minerals. *Geochemical Journal* **33,** 109-126.

Appendix A – Raw Electron Microprobe Data

A.1 Oxides – Magnetite and Ilmenite (Note: all Fe reported as FeO)

Table A-1. Raw and uncorrected electron microprobe analyses of magnetite and ilmenite.

SL3-1 - SL3-5: SR18-5 (Schryburt Lake), magnetite crystal '2'
1=magnetite core, 2=magnetite rim, 3-5=three different ilmenite lamellae in magnetite crystal '2'.
SL3-6 - SL3-10: SR18-5 (Schryburt Lake), magnetite crystal '1'
6=magnetite core, 7=magnetite rim, 8-10=three different ilmenite lamellae in magnetite crystal '1'.
SL3-11 - SL3-15: SR18-5 (Schryburt Lake), magnetite crystal '3'
11=magnetite core, 12=magnetite rim, 13-15=three different ilmenite lamellae in magnetite crystal '3'.

C1-1 - C1-5: CCM 135 IMC 179.3-179.7 (Cargill), magnetite crystal '1'
1=magnetite core, 2=magnetite rim, 3-5=three different ilmenite lamellae in magnetite crystal '1'.
C1-6 - C1-11: CCM 135 IMC 179.3-179.7 (Cargill), magnetite crystal '2'
6=magnetite core, 7=magnetite rim, 8-9= two different ilmenite lamellae in magnetite crystal '2',
10-11=different points along the same ilmenite lamella in magnetite crystal '2'.

C2-1 - C2-6: H24 IMC 28.6-29.0 (Cargill), magnetite crystal '3'
1=magnetite core, 2-3=magnetite rim, 4-6= three different ilmenite lamellae in magnetite crystal '3'.
C2-7 - C2-16: H24 IMC 28.6-29.0 (Cargill), magnetite crystal '4'
7-9=magnetite core, 10-12=magnetite rim, 13-16: four different ilmenite lamellae in magnetite crystal '4'.

	SL3-1	SL3-2	SL3-3	SL3-4	SL3-5	SL3-6	SL3-7	SL3-8	SL3-9	SL3-10
SIO2	0	0	0.01	0.02	0	0	0.01	0.02	0.03	0.03
AL2O3	0.01	0.01	0	0	0	0	0	0	0	0
TIO2	0.5	0.43	51.35	52.28	51.31	0.47	0.54	52.08	51.45	52.73
CR2O3	0.09	0.09	0.03	0.02	0.05	0.08	0.08	0	0.02	0.02
V2O5	1.08	1.13	0.49	0.43	0.49	1.19	1.11	0.5	0.43	0.48
FEO	92.48	92.12	38.92	37.66	37.41	92	92.03	37.7	36.52	37.64
MGO	0.48	0.47	4.64	6.18	6.34	0.54	0.47	5.73	6.09	5.62
MNO	0.13	0.17	3.74	3.89	3.93	0.2	0.27	3.73	4.68	3.62
CAO	0	0.02	0.01	0	0.02	0	0	0.01	0.01	0
TOTAL	94.77	94.44	99.19	100.48	99.55	94.48	94.51	99.77	99.23	100.14

			FORMULA	(BASIS 32	OXYGEN(S))					
SI	0	0	0.003	0.006	0	0	0.004	0.006	0.007	0.007
AL	0.004	0.004	0	0	0	0	0	0	0	0
TI	0.149	0.128	10.233	10.194	10.111	0.139	0.162	10.235	10.168	10.309
CR	0.027	0.027	0.007	0.004	0.01	0.024	0.025	0	0.005	0.003
V	0.283	0.296	0.086	0.073	0.086	0.313	0.291	0.086	0.075	0.083
FE	30.622	30.612	8.625	8.165	8.198	30.519	30.531	8.24	8.026	8.183
MG	0.283	0.28	1.834	2.39	2.476	0.318	0.278	2.231	2.386	2.177
MN	0.044	0.057	0.84	0.855	0.871	0.067	0.092	0.827	1.041	0.798
CA	0	0.007	0.002	0.001	0.005	0	0.001	0.003	0.003	0
	31.412	31.411	21.63	21.688	21.757	31.38	31.384	21.628	21.711	21.56

PAGE 2

	SL3-11	SL3-12	SL3-13	SL3-14	SL3-15	C1-1	C1-2	C1-3	C1-4	C1-5
SIO2	0	0	0	0.04	0.01	0	0	0.05	0.04	0.04
AL2O3	0.01	0	0	0	0	0.27	0.34	0	0.11	0
TIO2	0.47	0.33	52.06	51.18	49.49	0.21	0.26	50.41	49.23	49.3
CR2O3	0.07	0.09	0.03	0	0	0.03	0.04	0.03	0.03	0.03
V2O5	1.17	1.11	0.56	0.48	0.44	0.43	0.72	0.38	0.4	0.53
FEO	91.87	93.51	38.57	37.33	46.34	92.88	92.7	42.05	42.16	42.43
MGO	0.52	0.41	5.77	6.12	0.34	0.03	0.07	0.69	0.86	0.98
MNO	0.2	0.23	3.57	3.95	3.59	0.09	0.36	5.6	5.55	5.66
CAO	0.02	0.02	0.02	0.01	0.03	0.02	0.02	0.02	0.01	0.01
TOTAL	94.33	95.7	100.58	99.11	100.24	93.96	94.51	99.23	98.39	98.98

FORMULA (BASIS 32 OXYGEN(S))

SI	0	0	0	0.01	0.002	0	0.001	0.014	0.01	0.011
AL	0.007	0	0	0	0	0.126	0.158	0	0.034	0
TI	0.14	0.097	10.171	10.133	10.135	0.063	0.077	10.32	10.192	10.15
CR	0.022	0.029	0.007	0	0.001	0.011	0.013	0.006	0.006	0.006
V	0.308	0.288	0.096	0.084	0.08	0.114	0.191	0.069	0.072	0.096
FE	30.525	30.721	8.381	8.219	10.553	31.322	30.942	9.573	9.706	9.715
MG	0.306	0.238	2.235	2.402	0.139	0.019	0.039	0.28	0.352	0.398
MN	0.067	0.077	0.786	0.881	0.827	0.03	0.12	1.292	1.293	1.313
CA	0.008	0.007	0.005	0.003	0.007	0.01	0.008	0.006	0.002	0.002
	31.383	31.457	21.681	21.732	21.744	31.695	31.549	21.56	21.667	21.691

PAGE 3

	C1-6	C1-7	C1-8	C1-9	C1-10	C1-11	C2-1	C2-2	C2-3	C2-4
SIO2	0	0	0.01	0.04	0.04	0	0	0.03	0	0.01
AL2O3	0.42	0.29	0	0	0.91	0	0.01	0.01	0	0
TIO2	0.23	0.14	50.13	50.35	50.12	48.93	0.36	1.13	0.48	53.8
CR2O3	0.05	0.06	0	0	0.03	0.01	0.03	0.02	0.05	0.01
V2O5	0.53	0.78	0.37	0.44	0.35	0.35	0.7	0.59	0.68	0.4
FEO	92.76	93.13	43.18	42.89	42.51	45.12	92.45	92.23	91.96	40.6
MGO	0.02	0	0.74	0.74	0.69	0.53	0.2	0.17	0.14	3.93
MNO	0.14	0.36	4.93	4.95	4.41	3.94	0.06	0.2	0.13	2.13
CAO	0	0	0.01	0.07	0.01	0.01	0	0.01	0.03	0.02
TOTAL	94.15	94.76	99.37	99.48	99.07	98.89	93.81	94.39	93.47	100.9

FORMULA (BASIS 32 OXYGEN(S))

SI	0	0.001	0.003	0.012	0.01	0	0	0.012	0	0.002
AL	0.2	0.134	0	0	0.292	0	0.005	0.003	0.001	0
TI	0.071	0.043	10.273	10.286	10.221	10.146	0.109	0.338	0.146	10.505
CR	0.015	0.019	0	0	0.007	0.003	0.01	0.007	0.014	0.003
V	0.14	0.206	0.066	0.08	0.062	0.064	0.186	0.156	0.181	0.068
FE	31.124	31.043	9.841	9.745	9.641	10.405	31.153	30.718	31.09	8.816
MG	0.013	0	0.3	0.301	0.278	0.216	0.12	0.103	0.084	1.519
MN	0.049	0.123	1.138	1.139	1.014	0.92	0.019	0.068	0.046	0.469

CA	0	0	0.004	0.02	0.002	0.002	0.001	0.005	0.015	0.006
	31.612	31.569	21.625	21.583	21.527	21.756	31.603	31.41	31.577	21.388

	C2-5	C2-6	C2-7	C2-8	C2-9	C2-10	C2-11	C2-12	C2-13	C2-14
SIO2	0	0.02	0.03	0.03	0.03	0.03	0	0.02	0	0
AL2O3	0	0	0.03	0.03	0.01	0.03	0.01	0	0	0
TIO2	53.32	52.94	0.79	1.42	0.78	0.98	1.22	0.7	52.04	52.06
CR2O3	0.01	0.03	0.02	0.03	0.04	0.03	0.02	0.03	0.03	0
V2O5	0.49	0.43	0.72	1.08	1.4	0.97	1.15	1.13	0.72	0.25
FEO	40.85	39.98	92.77	91.29	91.53	91.24	91.5	92.13	42.2	41.31
MGO	4.11	4.49	0.21	0.13	0.26	0.2	0.2	0.16	3.5	3.52
MNO	2.34	2.3	0.38	0.66	0.93	0.33	0.48	0.37	1.82	1.43
CAO	0.02	0.01	0.01	0	0	0	0.01	0.02	0.17	0.25
TOTAL	101.14	100.2	94.96	94.67	94.98	93.81	94.59	94.56	100.48	98.82

FORMULA (BASIS 32 OXYGEN(S))

SI	0	0.006	0.012	0.01	0.012	0.01	0.002	0.007	0	0
AL	0	0	0.012	0.012	0.007	0.012	0.004	0	0	0
TI	10.407	10.4	0.235	0.421	0.232	0.294	0.364	0.209	10.288	10.443
CR	0.002	0.006	0.006	0.009	0.013	0.01	0.006	0.008	0.006	0
V	0.083	0.074	0.188	0.281	0.364	0.256	0.301	0.295	0.125	0.043
FE	8.867	8.735	30.756	30.105	30.111	30.483	30.227	30.588	9.278	9.214
MG	1.589	1.747	0.122	0.079	0.152	0.121	0.116	0.097	1.372	1.399
MN	0.515	0.509	0.129	0.219	0.309	0.112	0.159	0.123	0.405	0.322
CA	0.005	0.002	0.003	0	0	0.002	0.003	0.009	0.049	0.07
	21.468	21.479	31.463	31.136	31.2	31.3	31.182	31.336	21.523	21.491

	C2-15	C2-16
SIO2	0	0
AL2O3	0	0
TIO2	52.45	52.49
CR2O3	0	0
V2O5	0.98	0.84
FEO	41.7	41.5
MGO	3.22	3.37
MNO	2.21	2.07
CAO	0.1	0.26
TOTAL	100.66	100.53

FORMULA (BASIS 32 OXYGEN(S))

SI	0	0
AL	0	0
TI	10.332	10.345
CR	0	0
V	0.17	0.145

FE	9.135	9.097
MG	1.257	1.316
MN	0.491	0.46
CA	0.028	0.074
	21.413	21.437

A.2 Phosphates – Apatite (Note: all Fe reported as FeO)

Table A-2. Raw electron microprobe analyses of apatite.

SR18-7-0 - SR18-7-1: SR18-7 (Schryburt Lake), apatite crystal '1' (Pr2O3 not run)
0=apatite rim, 1=apatite core.
SR18-7-2 - SR18-7-3: SR18-7 (Schryburt Lake), apatite crystal '2' (Pr2O3 not run)
2=apatite core, 3=apatite rim.
SL3-1 - SL3-3: SR18-5 (Schryburt Lake), apatite crystal '1' (Pr2O3 not run)
1=apatite core, 2=apatite intermediate zone, 3=apatite rim.
SL3-4 - SL3-5: SR18-5 (Schryburt Lake), apatite crystal '2' (Pr2O3 not run)
4=apatite core, 5=apatite rim.
SL1-1 - SL1-2: SR18-8 (Schryburt Lake), apatite crystal '1' (Pr2O3 not run)
1=apatite core, 2=apatite rim.
SL1-3 - SL1-4: SR18-8 (Schryburt Lake), apatite crystal '2' (Pr2O3 not run)
3=apatite core, 4=apatite rim.
C4-1 - C4-2: CCM29 136.85-137.2 (Cargill), apatite crystal '1' (Pr2O3 not run)
1=apatite core, 2=apatite rim.
C4-3 - C4-4: CCM29 136.85-137.2 (Cargill), apatite crystal '2' (Pr2O3 not run)
3=apatite core, 4=apatite rim.
C2-1 - C2-2: H24 IMC 28.6-29.0 (Cargill), apatite crystal '1' (Pr2O3 not run)
1=top of crystal, 2=bottom of crystal.
C2-3 - C2-4: H24 IMC 28.6-29.0 (Cargill), apatite crystal '2' (Pr2O3 not run)
3=apatite core, 4=apatite rim.
F2-1 - F2-2: H8 135.65-136.05 (Firesand River), apatite crystal '2' (Pr2O3 not run)
1=apatite core, 2=apatite rim.
F2-3 - F2-4: H8 135.65-136.05 (Firesand River), apatite crystal '1' (Pr2O3 not run)
3=apatite core, 4=apatite rim.
SP1-1 - SP1-2: 107-108 1376.0 (Spanish River), apatite crystal '1'
1=apatite core, 2=apatite rim.
SP1-3 - SP1-4: 107-108 1376.0 (Spanish River), apatite crystal '2'
3=apatite core, 4=apatite rim.
F1-1 - F1-3: ST-34 (Firesand River), apatite crystal '1'
1=apatite core, 2=apatite core, 3=apatite rim.
F1-4 - F1-5: ST-34 (Firesand River), apatite crystal '2'
4=apatite core, 5=apatite rim.
BH4-1 - BH4-2: HED7-36 (Big Beaver House), apatite crystal '1'
1=apatite core, 2=apatite rim.
BH4-3 - BH4-4: HED7-36 (Big Beaver House), apatite crystal '2'
3=apatite core, 4=apatite rim.
C3-1 - C3-2: H35 IMC 128.9-129.3 (Cargill), apatite crystal '1'
1=apatite core, 2=apatite rim.
C3-3 - C3-5: H35 IMC 128.9-129.3 (Cargill), apatite crystal '2'
3=apatite core, 4=apatite intermediate zone, 5=apatite rim.
C3-6 - C3-7: H35 IMC 128.9-129.3 (Cargill), apatite crystal '3'
6=apatite core, 7=apatite rim.
BH2-1 - BH2-2: BB78 (Big Beaver House), apatite crystal '1'
1=apatite core, 2=apatite rim.
BH2-3 - BH2-4: BB78 (Big Beaver House), apatite crystal '2'
3=apatite core, 4=apatite rim.
BH2-5 - BH2-6: BB78 (Big Beaver House), apatite crystal '3'
5=apatite core, 6=apatite rim.
SP1-5 - SP1-6: 107-108 1376.0 (Spanish River), apatite crystal '3'
5=apatite core, 6=apatite rim.
*this data block is rejected due to probe encountering an imperfection on the thin-section.

	*(rejected) SR18-7-1	SR18-7-2	SR18-7-3	SR18-7-1	SR18-7-0	C2-1	C2-2	C2-3	C2-4
P2O5	36.05	41.58	40.49	40.84	40.98	39.84	39.74	42.36	41.18
SIO2	0.04	0.2	0.02	0.04	0.02	0.07	0.08	0.03	0.03
AS2O5	0	0	0	0	0.02	0	0	0	0
SO3	0.05	0.06	0.04	0.04	0.03	0.02	0	0	0
CAO	47.95	53.47	52.69	53.44	52.19	53.8	53.64	54.91	55.02
NA2O	0.11	0.28	0.3	0.22	0.3	0.16	0.16	0.14	0.15
FEO	0.08	0	0	0.04	0.06	0	0.04	0	0.04
MNO	0.03	0.04	0.04	0.03	0.04	0.03	0.01	0.05	0.07
SRO	0.52	0.65	0.82	0.69	0.83	0.35	0.31	0.34	0.36
BAO	0.04	0	0.02	0.01	0	0.03	0	0	0
Y2O3	0	0	0	0	0.01	0	0	0	0
LA2O3	0.1	0.14	0.28	0.13	0.26	0.07	0.05	0.07	0.03
CE2O3	0.24	0.37	0.75	0.46	0.74	0.14	0.21	0.18	0.22
PR2O3	0	0	0	0	0	0	0	0	0
ND2O3	0.23	0.04	0.24	0.08	0.2	0	0	0	0
SM2O3	0	0	0.08	0	0	0	0.03	0	0
F	2.45	2.81	2.85	2.8	2.92	2.06	2.15	2.25	2.19
CL	0	0.03	0	0.02	0.02	0.03	0.02	0.01	0.01
TOTAL	87.89	99.67	98.62	98.84	98.62	96.6	96.44	100.34	99.3
TOT-O	86.86	98.48	97.42	97.66	97.39	95.73	95.53	99.39	98.38
			FORMULA	(BASIS 25	OXYGEN(S)	)			
P	5.929	5.994	5.959	5.964	6.011	5.91	5.911	6.014	5.94
SI	0.008	0.034	0.003	0.008	0.003	0.013	0.014	0.006	0.004
AS	0	0	0	0	0.002	0	0	0	0
S	0.008	0.008	0.005	0.005	0.003	0.003	0	0.001	0
	5.945	6.036	5.967	5.977	6.019	5.926	5.925	6.021	5.944
CA	9.979	9.756	9.813	9.878	9.687	10.101	10.098	9.867	10.043
NA	0.042	0.092	0.1	0.072	0.1	0.054	0.056	0.044	0.05
FE	0.013	0	0	0.006	0.009	0	0.006	0	0.005
MN	0.004	0.005	0.006	0.004	0.006	0.005	0.002	0.008	0.009
SR	0.059	0.064	0.082	0.069	0.084	0.036	0.032	0.033	0.036
BA	0.003	0	0.001	0	0	0.002	0	0	0
Y	0	0	0	0	0.001	0	0	0	0
LA	0.007	0.009	0.018	0.009	0.017	0.004	0.003	0.004	0.002
CE	0.017	0.023	0.048	0.029	0.047	0.009	0.014	0.011	0.014
PR	0	0	0	0	0	0	0	0	0
ND	0.016	0.002	0.015	0.005	0.013	0	0	0	0
SM	0	0	0.004	0	0	0	0.002	0	0
	10.14	9.951	10.087	10.072	9.964	10.211	10.213	9.967	10.159
F	1.508	1.513	1.566	1.527	1.602	1.141	1.194	1.192	1.178
CL	0.001	0.01	0.001	0.007	0.007	0.007	0.005	0.004	0.004
	1.509	1.523	1.567	1.534	1.609	1.148	1.199	1.196	1.182

	C4-2	C4-3	C4-4	F2-1	F2-2	F2-3	F2-4	SL1-1	SL1-2
P2O5	39.7	40.94	40.81	40.8	39.99	40.39	40.69	40.8	40.76
SIO2	0.07	0.17	0.06	0.15	0.18	0.12	0.07	0.09	0.02
AS2O5	0.04	0.03	0.06	0	0	0	0	0	0
SO3	0.06	0.06	0.05	0.03	0	0.01	0	0.03	0.05
CAO	54.76	54.43	54.76	54.36	54.88	54.69	54.05	53.76	52.32
NA2O	0.21	0.27	0.21	0.08	0.13	0.1	0.13	0.27	0.37
FEO	0.04	0.02	0.05	0	0.12	0	0	0	0
MNO	0.09	0.09	0.09	0.02	0.05	0	0.03	0.03	0.06
SRO	0.4	0.32	0.44	1.06	0.97	1.01	1.19	0.8	1.02
BAO	0.03	0.07	0.04	0.04	0.04	0.02	0.02	0	0.01
Y2O3	0.03	0.02	0.01	0	0	0	0	0	0.03
LA2O3	0.12	0.21	0.11	0.18	0.05	0.08	0.22	0.27	0.37
CE2O3	0.29	0.49	0.29	0.28	0.13	0.17	0.43	0.55	0.9
PR2O3	0	0	0	0	0	0	0	0	0
ND2O3	0	0.13	0	0	0	0	0	0.26	0.51
SM2O3	0	0.08	0.02	0	0	0	0	0.07	0.19
F	2.35	2.1	2.3	2.54	2.45	2.59	2.67	2.79	3.12
CL	0.03	0.02	0.04	0.01	0.02	0.01	0.03	0.01	0.01
TOTAL	98.22	99.45	99.34	99.55	99.01	99.19	99.53	99.73	99.74
TOT-O	97.22	98.56	98.36	98.48	97.97	98.1	98.4	98.55	98.42
			FORMULA	(BASIS 25	OXYGEN(S)	)			
P	5.842	5.913	5.909	5.917	5.847	5.888	5.923	5.932	5.967
SI	0.012	0.03	0.01	0.026	0.031	0.021	0.011	0.015	0.003
AS	0.004	0.002	0.006	0	0	0	0	0	0
S	0.008	0.007	0.006	0.004	0	0.002	0.001	0.003	0.007
	5.866	5.952	5.931	5.947	5.878	5.911	5.935	5.95	5.977
CA	10.198	9.948	10.035	9.977	10.154	10.09	9.959	9.893	9.693
NA	0.069	0.088	0.069	0.025	0.043	0.034	0.044	0.09	0.122
FE	0.005	0.003	0.007	0	0.018	0	0	0	0
MN	0.013	0.013	0.013	0.003	0.008	0	0.005	0.004	0.009
SR	0.04	0.031	0.044	0.105	0.097	0.101	0.119	0.08	0.103
BA	0.002	0.004	0.003	0.003	0.003	0.001	0.001	0	0.001
Y	0.003	0.002	0.001	0	0	0	0	0	0.003
LA	0.008	0.013	0.007	0.011	0.003	0.005	0.014	0.017	0.024
CE	0.019	0.031	0.018	0.018	0.008	0.011	0.027	0.034	0.057
PR	0	0	0	0	0	0	0	0	0
ND	0	0.008	0	0	0	0	0	0.016	0.031
SM	0	0.005	0.001	0	0	0	0	0.004	0.011
	10.357	10.146	10.198	10.142	10.334	10.242	10.169	10.138	10.054
F	1.29	1.134	1.245	1.378	1.337	1.411	1.452	1.517	1.708
CL	0.008	0.006	0.012	0.002	0.005	0.003	0.008	0.002	0.004
	1.298	1.14	1.257	1.38	1.342	1.414	1.46	1.519	1.712

	SL1-4	SL3-1	SL3-2	SL3-3	SL3-4	SL3-5	SP1-1	SP1-2	SP1-3
P2O5	40.82	40.64	40.99	42.06	40.22	41.28	41.66	41.53	41.91
SIO2	0.04	0.1	0.06	0.03	0.04	0.06	0.05	0.11	0.1
AS2O5	0	0	0	0	0	0	0.01	0	0
SO3	0	0.03	0	0	0.03	0.06	0	0	0
CAO	52.5	53.5	52.04	53.57	54.16	53.39	54.57	54.34	54.75
NA2O	0.36	0.27	0.56	0.25	0.19	0.34	0.12	0.09	0.12
FEO	0.03	0.04	0.04	0.02	0	0	0.05	0.09	0
MNO	0.03	0.05	0.02	0	0.07	0.01	0.07	0.01	0
SRO	1	0.77	1.04	0.95	0.72	1.06	0.34	0.38	0.35
BAO	0.05	0.05	0.01	0	0.02	0	0	0.07	0.14
Y2O3	0.01	0	0.03	0.05	0	0	0	0	0
LA2O3	0.37	0.22	0.59	0.29	0.22	0.41	0.05	0.05	0.14
CE2O3	1.01	0.47	1.38	0.75	0.45	1.04	0.14	0.16	0.21
PR2O3	0	0	0	0	0	0	0	0.02	0.09
ND2O3	0.49	0.23	0.63	0.29	0.24	0.51	0	0.06	0.08
SM2O3	0.13	0.08	0.11	0.11	0.1	0.13	0.06	0	0
F	2.92	2.58	2.45	2.5	2.73	2.72	2.43	2.5	2.47
CL	0.01	0.01	0.02	0	0.02	0	0	0	0.01
TOTAL	99.77	99.04	99.97	100.87	99.21	101.01	99.55	99.41	100.37
TOT-O	98.54	97.95	98.93	99.82	98.06	99.86	98.53	98.36	99.33
			FORMULA	(BASIS 25	OXYGEN(S)	)			
P	5.966	5.935	5.97	6.01	5.889	5.947	5.985	5.983	5.985
SI	0.006	0.017	0.01	0.005	0.008	0.01	0.009	0.019	0.016
AS	0	0	0	0	0	0	0.001	0	0
S	0	0.003	0	0	0.004	0.008	0.001	0	0
	5.972	5.955	5.98	6.015	5.901	5.965	5.996	6.002	6.001
CA	9.71	9.888	9.591	9.687	10.038	9.734	9.922	9.906	9.894
NA	0.12	0.089	0.186	0.082	0.064	0.113	0.038	0.03	0.039
FE	0.005	0.005	0.006	0.003	0.001	0	0.008	0.013	0
MN	0.004	0.007	0.003	0	0.01	0.001	0.01	0.002	0
SR	0.1	0.077	0.104	0.093	0.072	0.104	0.033	0.037	0.034
BA	0.003	0.003	0	0	0.001	0	0	0.005	0.009
Y	0.001	0	0.003	0.005	0	0	0	0	0
LA	0.024	0.014	0.038	0.018	0.014	0.026	0.003	0.003	0.009
CE	0.064	0.029	0.087	0.046	0.029	0.065	0.009	0.01	0.013
PR	0	0	0	0	0	0	0	0.001	0.006
ND	0.03	0.014	0.039	0.017	0.015	0.031	0	0.004	0.005
SM	0.008	0.004	0.006	0.007	0.006	0.008	0.004	0	0
	10.069	10.13	10.063	9.958	10.25	10.082	10.027	10.011	10.009
F	1.593	1.409	1.334	1.334	1.493	1.464	1.303	1.345	1.315
CL	0.003	0.002	0.007	0	0.005	0	0	0	0.003
	1.596	1.411	1.341	1.334	1.498	1.464	1.303	1.345	1.318

	SP1-4	F1-1	F1-2	F1-3	F1-4	F1-5	BH4-1	BH4-2	BH4-3
P2O5	42.1	40.97	42.47	41.44	42.01	41.12	40.65	41.1	41.04
SIO2	0.09	0.42	0.02	0.07	0.06	0.31	0.47	0.22	0.34
AS2O5	0	0.03	0.04	0	0	0.03	0	0.03	0
SO3	0	0.03	0	0	0	0.02	0.02	0.04	0
CAO	53.68	53.33	53.62	51.91	53.09	52.27	52.47	52.17	54.79
NA2O	0.1	0.17	0.15	0.34	0.1	0.1	0.08	0.1	0.06
FEO	0.06	0.13	0.05	0.04	0.07	0.11	0.01	0.08	0.04
MNO	0.04	0.03	0.07	0.01	0	0	0.04	0.05	0
SRO	0.37	0.5	1.46	0.5	1.14	0.56	0.6	0.67	0.65
BAO	0	0.07	0	0.01	0	0.23	0.21	0	0
Y2O3	0.01	0.28	0.01	0.25	0	0.17	0.02	0.04	0.02
LA2O3	0.16	0.14	0.16	0.27	0.05	0.2	0.05	0.19	0.05
CE2O3	0.27	0.34	0.2	0.6	0.22	0.32	0.12	0.16	0.14
PR2O3	0.04	0	0	0	0	0.02	0	0.03	0
ND2O3	0.05	0.17	0.13	0.23	0.04	0.19	0.01	0.04	0.1
SM2O3	0	0.1	0.04	0.07	0	0.09	0.08	0.09	0
F	2.19	2.38	2.39	2.47	2.68	2.44	2.37	2.27	2.55
CL	0	0	0.02	0	0	0.01	0.02	0	0
TOTAL	99.16	99.09	100.83	98.21	99.46	98.19	97.22	97.28	99.78
TOT-O	98.24	98.09	99.82	97.17	98.33	97.16	96.22	96.32	98.71

			FORMULA	(BASIS 25	OXYGEN(S)				
P	6.041	5.937	6.04	6.05	6.052	6.005	5.977	6.026	5.913
SI	0.016	0.072	0.004	0.012	0.01	0.054	0.082	0.038	0.059
AS	0	0.003	0.004	0	0	0.003	0	0.003	0
S	0	0.003	0	0	0.001	0.003	0.003	0.005	0
	6.057	6.015	6.048	6.062	6.063	6.065	6.062	6.072	5.972
CA	9.748	9.782	9.652	9.591	9.681	9.659	9.763	9.68	9.99
NA	0.033	0.057	0.048	0.115	0.032	0.034	0.026	0.033	0.019
FE	0.008	0.019	0.006	0.006	0.009	0.016	0.002	0.012	0.005
MN	0.006	0.005	0.01	0.001	0.001	0	0.005	0.008	0
SR	0.036	0.05	0.142	0.05	0.113	0.056	0.061	0.068	0.064
BA	0	0.004	0	0.001	0	0.016	0.014	0	0
Y	0.001	0.026	0.001	0.023	0	0.015	0.002	0.003	0.002
LA	0.01	0.009	0.01	0.017	0.003	0.013	0.003	0.012	0.003
CE	0.017	0.021	0.012	0.038	0.014	0.02	0.008	0.01	0.009
PR	0.003	0	0	0	0	0.001	0	0.002	0
ND	0.003	0.01	0.008	0.014	0.003	0.012	0.001	0.002	0.006
SM	0	0.006	0.002	0.004	0	0.005	0.005	0.006	0
	9.865	9.989	9.891	9.86	9.856	9.847	9.89	9.836	10.098
F	1.176	1.289	1.268	1.345	1.44	1.334	1.3	1.243	1.37
CL	0	0.001	0.005	0	0.001	0.003	0.006	0	0
	1.176	1.29	1.273	1.345	1.441	1.337	1.306	1.243	1.37

	BH4-4	C3-1	C3-2	C3-3	C3-4	C3-5	C3-6	C3-7	BH2-1
P2O5	40.94	40.98	40.97	41.05	41.09	41.09	41.07	40.79	39.42
SIO2	0.17	0.11	0.03	0.04	0.03	0.08	0.08	0.03	0.5
AS2O5	0.08	0	0	0	0	0	0	0.03	0.01
SO3	0.03	0.08	0	0.07	0	0	0.06	0.02	0.05
CAO	53.68	54.02	53.71	54.32	53.71	53.93	54.76	54.12	54.29
NA2O	0.09	0.2	0.23	0.19	0.22	0.16	0.16	0.34	0.08
FEO	0.04	0.01	0	0.05	0.05	0.11	0.05	0.02	0.05
MNO	0.03	0	0.01	0.01	0	0	0.03	0	0.01
SRO	0.67	0.4	0.37	0.4	0.4	0.4	0.44	0.37	0.63
BAO	0.07	0	0.08	0	0.05	0.08	0	0	0.11
Y2O3	0.04	0.04	0	0	0.06	0.06	0.02	0.04	0
LA2O3	0.19	0.15	0.23	0.08	0.62	0.09	0.14	0.19	0.13
CE2O3	0.27	0.22	0.63	0.27	0.68	0.02	0.19	0.69	0.18
PR2O3	0.01	0.08	0.03	0	0.12	0	0	0.09	0.01
ND2O3	0.01	0.1	0.43	0.11	0.39	0.36	0.17	0.4	0.14
SM2O3	0	0.12	0.17	0	0.02	0.04	0.02	0.11	0
F	2.64	2.36	2.57	2.2	2.12	2.48	2.27	2.48	2.11
CL	0.01	0.01	0	0.03	0	0	0	0.01	0
TOTAL	98.97	98.88	99.46	98.82	99.56	98.9	99.46	99.73	97.72
TOT-O	97.86	97.88	98.38	97.89	98.67	97.86	98.5	98.68	96.83

			FORMULA	(BASIS 25	OXYGEN(S)				
P	5.953	5.947	5.955	5.949	5.951	5.967	5.926	5.918	5.813
SI	0.03	0.018	0.005	0.007	0.005	0.013	0.014	0.006	0.086
AS	0.008	0	0	0	0	0	0	0.003	0.001
S	0.004	0.011	0	0.009	0	0	0.008	0.002	0.007
	5.995	5.976	5.96	5.965	5.956	5.98	5.948	5.929	5.907
CA	9.878	9.921	9.881	9.961	9.846	9.912	10.001	9.939	10.133
NA	0.031	0.068	0.076	0.063	0.073	0.053	0.052	0.113	0.027
FE	0.006	0.002	0.001	0.007	0.008	0.016	0.007	0.003	0.007
MN	0.004	0.001	0.001	0.002	0	0	0.004	0	0.002
SR	0.067	0.039	0.037	0.04	0.04	0.039	0.043	0.037	0.063
BA	0.005	0	0.005	0	0.003	0.006	0	0	0.008
Y	0.004	0.004	0	0	0.005	0.006	0.002	0.004	0
LA	0.012	0.009	0.015	0.005	0.039	0.006	0.009	0.012	0.008
CE	0.017	0.014	0.04	0.017	0.042	0.001	0.012	0.043	0.011
PR	0.001	0.005	0.002	0	0.007	0	0	0.005	0.001
ND	0	0.006	0.026	0.007	0.024	0.022	0.01	0.025	0.008
SM	0	0.007	0.01	0	0.001	0.002	0.001	0.006	0
	10.025	10.076	10.094	10.102	10.088	10.063	10.141	10.187	10.268
F	1.435	1.282	1.395	1.191	1.145	1.345	1.226	1.343	1.162
CL	0.003	0.004	0	0.009	0	0	0.001	0.003	0
	1.438	1.286	1.395	1.2	1.145	1.345	1.227	1.346	1.162

	BH2-2	BH2-3	BH2-4	BH2-5	BH2-6	SP1-5	SP1-6
P2O5	41.38	40.6	40.06	40.97	40.58	40.75	40.33
SIO2	0.01	0.27	0.36	0.07	0.07	0.11	0.19
AS2O5	0	0	0	0.04	0	0	0.01
SO3	0.02	0.05	0.01	0.01	0.02	0	0.03
CAO	54.32	55.08	55.17	55.54	54.45	54.93	55.36
NA2O	0.14	0.02	0.12	0.09	0.15	0.09	0.12
FEO	0.07	0.05	0.07	0.11	0.04	0.11	0.16
MNO	0.03	0.04	0.01	0.02	0	0.01	0.01
SRO	0.27	0.58	0.64	0.58	0.51	0.43	0.36
BAO	0	0.14	0.03	0	0	0.1	0
Y2O3	0.03	0.07	0.07	0	0.03	0.03	0.02
LA2O3	0.11	0.08	0.1	0.05	0.17	0.11	0.12
CE2O3	0.19	0.2	0.26	0.2	0.42	0.29	0.19
PR2O3	0.04	0.05	0.14	0.06	0.05	0.05	0
ND2O3	0.12	0.07	0.09	0.09	0.2	0.07	0.11
SM2O3	0	0.03	0.03	0.1	0	0	0
F	2.47	2.3	2.4	2.35	2.44	2.63	2.63
CL	0.01	0	0.01	0	0	0	0
TOTAL	99.21	99.63	99.57	100.28	99.13	99.71	99.64
TOT-O	98.17	98.66	98.56	99.29	98.1	98.6	98.53

			FORMULA	(BASIS 25	OXYGEN(S)		
P	5.979	5.871	5.824	5.89	5.908	5.903	5.853
SI	0.002	0.046	0.061	0.011	0.012	0.019	0.033
AS	0	0	0	0.004	0	0	0.001
S	0.003	0.006	0.001	0.001	0.003	0	0.003
	5.984	5.923	5.886	5.906	5.923	5.922	5.89
CA	9.932	10.081	10.151	10.104	10.033	10.069	10.167
NA	0.048	0.006	0.038	0.031	0.051	0.03	0.04
FE	0.01	0.007	0.01	0.016	0.006	0.016	0.023
MN	0.004	0.005	0.001	0.003	0	0.001	0.002
SR	0.026	0.057	0.063	0.057	0.051	0.043	0.035
BA	0	0.009	0.002	0	0	0.006	0
Y	0.002	0.007	0.007	0	0.003	0.002	0.002
LA	0.007	0.005	0.006	0.003	0.011	0.007	0.008
CE	0.012	0.012	0.016	0.013	0.026	0.018	0.012
PR	0.002	0.003	0.009	0.004	0.003	0.003	0
ND	0.007	0.004	0.005	0.006	0.012	0.004	0.007
SM	0	0.002	0.002	0.006	0	0	0
	10.05	10.198	10.31	10.243	10.196	10.199	10.296
F	1.331	1.243	1.305	1.26	1.325	1.422	1.427
CL	0.004	0	0.002	0	0	0	0
	1.335	1.243	1.307	1.26	1.325	1.422	1.427

A.3 Sulphides – Pyrrhotite, Pyrite and Chalcopyrite

Table A-3. Raw electron microprobe analyses of pyrrhotite, pyrite and chalcopyrite.

'TROI', 'TROIL', ' FNS4', 'X'= Electron Microprobe Standards.
1-1-1 - 1-1-3: SR18-5 (Schryburt Lake), pyrrhotite crystal '1'
1=pyrrhotite core, 2-3=pyrrhotite rim.
1-2-1 - 1-2-3: SR18-5 (Schryburt Lake), pyrrhotite crystal '2'
1=pyrrhotite core, 2-3=pyrrhotite rim.
1-3-1 - 1-3-3: SR18-5 (Schryburt Lake), pyrrhotite crystal '3'
1=pyrrhotite core, 2-3=pyrrhotite rim.
2-1-1 - 2-1-3: 107-108 1201.0 (Spanish River), pyrrhotite crystal '1'
1=pyrrhotite core, 2-3=pyrrhotite rim.
2-2-1 - 2-2-3: 107-108 1201.0 (Spanish River), pyrrhotite crystal '2'
1=pyrrhotite core, 2-3=pyrrhotite rim.
2-3-1 - 2-3-3: 107-108 1201.0 (Spanish River), pyrrhotite crystal '3'
1=pyrrhotite core, 2-3=pyrrhotite rim.
3-1-1 - 3-1-3: 3-439-454B ("Carb" Lake), pyrrhotite crystal '1'
1=pyrrhotite core, 2-3=pyrrhotite rim.
3-2-1 - 3-2-3: 3-439-454B ("Carb" Lake), pyrrhotite + chalcopyrite crystal '2'
1-2=pyrrhotite core, 3=chalcopyrite core.
3-3-1 - 3-3-3: 3-439-454B ("Carb" Lake), pyrrhotite crystal '3'
1=pyrrhotite core, 2-3=pyrrhotite rim.
4-1-1 - 4-1-3: H8 285.4-285.8 (Firesand River), pyrrhotite crystal '1'
1=pyrrhotite core, 2-3=pyrrhotite rim.
4-2-1 - 4-2-3: H8 285.4-285.8 (Firesand River), pyrrhotite crystal '2'
1=pyrrhotite core, 2-3=pyrrhotite rim.
5-1-1: 107-108 1376.0 (Spanish River), pyrrhotite crystal '1'
1=pyrrhotite core.
5-1-2: 107-108 1376.0 (Spanish River), pyrrhotite crystal '2'
2=pyrrhotite core.
5-3-1: 107-108 1376.0 (Spanish River), pyrrhotite crystal '3'
1=pyrrhotite core.
6-1-1: ST-34 (Firesand River), pyrite crystal '1'.
6-2-1: ST-34 (Firesand River), pyrite crystal '2'.
6-3-1: ST-34 (Firesand River), chalcopyrite crystal '3'.

	TROI	#1-1-1	#1-1-2	#1-1-2	#1-1-1	#1-1-3	#1-2-1	#1-2-2	#1-2-3	#1-3-1
FE	63.40	61.12	61.15	61.59	61.27	61.40	61.06	61.04	60.39	61.08
CO	.01	.08	.06	.08	.09	.08	.07	.07	.09	.09
NI	.01	.04	.02	.03	.04	.04	.00	.02	.02	.03
CU	.00	.00	.00	.00	.02	.01	.01	.00	.01	.01
AG	.00	.00	.00	.00	.00	.00	.00	.00	.00	.00
S	37.02	38.85	39.08	38.64	38.61	38.76	38.99	38.81	39.18	38.76
TOTAL	100.44	100.09	100.31	100.34	100.03	100.29	100.13	99.94	99.69	99.97

(BASIS 1 ATOM(S))

FE	.496	.474	.473	.477	.476	.476	.473	.474	.469	.475
CO	.000	.001	.000	.001	.001	.001	.000	.001	.001	.001
NI	.000	.000	.000	.000	.000	.000	.000	.000	.000	.000
CU	.000	.000	.000	.000	.000	.000	.000	.000	.000	.000
AG	.000	.000	.000	.000	.000	.000	.000	.000	.000	.000
S	.504	.525	.526	.522	.523	.523	.526	.525	.530	.525
	1.000	1.000	.999	1.000	1.000	1.000	.999	1.000	1.000	1.001

PAGE 2

	#1-3-2	#1-3-3	2-1-1	2-1-2	FNS4	2-1-3	2-2-1	2-2-2	2-2-3	2-3-1
FE	60.69	60.97	61.63	61.51	57.12	61.55	61.37	61.22	61.28	61.53
CO	.11	.07	.07	.04	1.40	.07	.06	.06	.05	.06
NI	.01	.01	.00	.01	1.28	.03	.01	.02	.01	.00
CU	.00	.01	.00	.00	1.29	.02	.00	.00	.00	.00
AG	.00	.00	.00	.00	.00	.00	.00	.00	.00	.00
S	39.32	38.89	38.17	38.23	38.42	38.58	38.50	38.24	38.81	38.71
TOTAL	100.13	99.95	99.87	99.79	99.51	100.25	99.94	99.54	100.15	100.30

(BASIS 1 ATOM(S))

FE	.469	.473	.481	.480	.447	.478	.478	.479	.475	.477
CO	.001	.001	.001	.000	.010	.001	.000	.000	.000	.000
NI	.000	.000	.000	.000	.010	.000	.000	.000	.000	.000
CU	.000	.000	.000	.000	.009	.000	.000	.000	.000	.000
AG	.000	.000	.000	.000	.000	.000	.000	.000	.000	.000
S	.530	.526	.519	.520	.524	.521	.522	.521	.524	.523
	1.000	1.000	1.001	1.000	1.000	1.000	1.000	1.000	.999	1.000

PAGE 3

	2-3-2	2-3-3	3-1-1	3-1-2	3-1-3	FNS4	X	3-2-1	3-2-2	3-2-3
FE	61.21	61.64	60.27	59.95	59.69	57.31	61.00	59.25	59.48	30.96
CO	.04	.08	.01	.03	.01	1.40	.09	.02	.02	.01
NI	.01	.00	.51	.49	.48	1.28	.03	.47	.54	.01
CU	.00	.00	.01	.00	.01	1.38	.02	.01	.00	34.24
AG	.00	.00	.00	.00	.00	.00	.00	.00	.00	.02
S	38.46	38.21	39.56	38.96	39.03	38.38	38.36	39.83	39.44	33.94
TOTAL	99.72	99.93	100.36	99.43	99.22	99.75	99.50	99.58	99.48	99.18

(BASIS 1 ATOM(S))

FE	.477	.481	.465	.467	.466	.448	.477	.459	.462	.258
CO	.000	.001	.000	.000	.000	.010	.001	.000	.000	.000
NI	.000	.000	.004	.004	.004	.010	.000	.003	.004	.000
CU	.000	.000	.000	.000	.000	.009	.000	.000	.000	.250
AG	.000	.000	.000	.000	.000	.000	.000	.000	.000	.000
S	.522	.519	.531	.529	.530	.523	.522	.537	.534	.492
	.999	1.001	1.000	1.000	1.000	1.000	1.000	.999	1.000	1.000

PAGE 4

	3-3-1	3-3-2	3-3-3	4-1-1	4-1-2	4-1-3	4-2-1	4-2-2	4-2-3	5-1-1
FE	60.09	60.44	59.90	61.27	61.51	61.31	62.23	60.97	61.39	61.08
CO	.02	.00	.03	.09	.07	.10	.07	.10	.08	.06
NI	.45	.48	.50	.00	.01	.00	.00	.01	.01	.00
CU	.00	.01	.00	.00	.00	.03	.01	.00	.01	.00

AG	.01	.01	.00	.00	.00	.00	.00	.00	.00	.00
S	39.66	40.18	40.12	38.85	38.17	38.16	37.54	38.50	38.39	38.60
TOTAL	100.23	101.12	100.55	100.21	99.76	99.60	99.85	99.58	99.88	99.74

(BASIS 1 ATOM(S))

FE	.464	.462	.460	.475	.480	.479	.487	.476	.478	.476
CO	.000	.000	.000	.001	.001	.001	.001	.001	.001	.000
NI	.003	.003	.004	.000	.000	.000	.000	.000	.000	.000
CU	.000	.000	.000	.000	.000	.000	.000	.000	.000	.000
AG	.000	.000	.000	.000	.000	.000	.000	.000	.000	.000
S	.533	.535	.536	.524	.519	.520	.512	.523	.521	.524
	1.000	1.000	1.000	1.000	1.000	1.000	1.000	1.000	1.000	1.000

	5-1-2	5-3-1	6-1-1	6-2-1	6-3-1	TROIL
FE	61.50	61.12	47.39	47.74	30.86	63.28
CO	.05	.06	.11	.09	.00	.01
NI	.00	.01	.00	.02	.01	.00
CU	.00	.01	.00	.00	34.00	.01
AG	.00	.00	.00	.00	.00	.01
S	38.66	38.78	51.66	52.79	34.32	36.52
TOTAL	100.21	99.98	99.16	100.64	99.19	99.83

(BASIS 1 ATOM(S))

FE	.477	.475	.345	.341	.256	.499
CO	.000	.000	.001	.001	.000	.000
NI	.000	.000	.000	.000	.000	.000
CU	.000	.000	.000	.000	.248	.000
AG	.000	.000	.000	.000	.000	.000
S	.522	.525	.655	.658	.496	.501
	.999	1.000	1.001	1.000	1.000	1.000

Appendix B – Analytical Methodology

B.1 Stable Isotope Geochemistry

B.1.1 Sample Selection

During the late 1980s, the Ontario Geological Survey undertook an examination of carbonatite-alkalic rock complexes in Ontario with the goal of evaluating their mineral deposit potential. Dr. Ron Sage completed many detailed reports on these complexes, including detailed petrographic, petrological and geochemical descriptions. After these studies were completed, the remaining hand specimens, drill-cores and thin-sections were donated to the Earth Sciences Section at the Royal Ontario Museum (ROM). The OGS reports were used to assess the whole-rock S-concentrations as a discriminator for sulphide and sulphate minerals. Samples whose S-concentrations equalled or exceeded 0.40 wt.% S were selected for this study. In addition, those samples for which sulphides could be identified in hand specimen or drill-core were also selected whether or not their whole-rock sulphur concentrations were greater than 0.40 wt.%. Selected samples were either split (drill-cores) or broken into variously sized pieces (hand specimens).

B.1.2 Sample Preparation

Samples were first (if necessary) split into walnut-sized portions using an anvil-press and weathered portions discarded. Samples were then again reduced in size to pea-sized portions using a chipmunk crusher®. This was followed by crushing using a BICO Pulverizer® disk-mill. Sieving removed the >20 mesh sized portions, while the <20

mesh portions were re-crushed in the disk-mill to reduce the fraction to at least >20 mesh. This fraction was then sieved and the 20-80 mesh size collected. This final sieving procedure was repeated twice in order to remove as much dust as possible from the 20-80 mesh sized aliquot.

The second stage of the sample preparation involved heavy liquid separation. Samples were first cleaned with water and acetone in order to remove any remaining dust on the mineral grains. Samples were then placed in a 500 ml separating funnel using methylene iodide (CH_2I_2) with a density of about 3.30 g/cm^3. The heavy fraction was collected, cleaned with acetone and then dried. The light fraction was also collected for later separation using bromoform ($CHBr_3$) with a density of about 2.90 g/cm^3. Heavy liquid separation was followed by magnetic separation using a hand-held magnet to separate out magnetite and pyrrhotite from other sulphides and minerals in the heavy methylene iodide fraction. The final step involved hand picking under a binocular microscope. Care was taken in order to maximize sample purity; in most cases this final step was effective in removing both weathered and different sulphide grains. In some cases, however, it was not possible to achieve optimal sample purity i.e. >99%, due to an inadequately sized aliquot and/or inclusions and/or composite grains. Although most of the sulphides were found to be pyrrhotite, in some cases rims of pyrite were found in back-scattered electron images and in thin section. After the sulphides were picked, they were then crushed into silt-sized powder using an agate mortar and pestle. After each sample was crushed, the mortar and pestle were with a small amount of silica sand which was crushed in the mortar. The mortar and pestle were then cleaned once again using kimwipes®. The powdered samples were then placed in screw top glass vials.

B.1.3 Isotopic Sample Analysis (Sulphides)

Depending on the type of sulphide, between 0.09 and 0.15 mg were placed in a tin capsule, approximately 1 mg of V_2O_5 was added and the capsule was sealed. The sealed capsules were then placed into an elemental analyser (EA) where they were flash combusted at 1800°C which allowed the V_2O_5 to react with the sulphide and convert it to gaseous SO_2. He gas was then injected in order to carry the SO_2, which was then purified in an SO_2 gas chromatographic column and carried into a Thermo Finnigan MAT Delta^{advantage} mass spectrometer for isotopic analysis (N.B. the reference gas was injected from the bellows of the dual inlet). The results were reported using the conventional δ-notation with a precision of ± 0.2‰ at the 2σ level. Various standards were used for mass spectrometer calibration and to monitor precision.

B.1.4 Isotopic Sample Analysis (Carbonates)

After the carbonates were separated and/or purified by heavy liquid separation (bromoform), they were also hand-picked under the binocular microscope. Care was also taken to insure optimal sample purity with the removal of both weathered/altered crystals and crystals containing inclusions. After hand picking, the carbonates (calcite and dolomite) were stored in screw top glass vials.

Approximately 10 mg of calcite (≈ 15 mg for dolomite), were placed in the main tube of a two-fingered Pyrex vessel and 1 ml of 100% H_3PO_4 was then added into the vessel side arm. The vessels were then pumped down on a Pyrex 10-port vacuum line for about one hour, and the acid heated by a heat gun periodically to help promote degassing.

The vessels were then removed from the line and placed in temperature-controlled bath at 25°C and allowed to equilibrate for 15 minutes. The acid was then tipped from the vessel side-arm into the main tube and the samples were reacted under vacuum, at 25°C in a carbonate bath for approximately 24 hours to produce CO_2 and H_2O (McCrea, 1950). Samples were placed into the carbonate extraction line where the CO_2 was purified. During purification, the gases were transferred into the extraction line and frozen with liquid nitrogen ($T \approx -190°C$). The main pump valve was then opened to release any incondensables. After closing this valve, the liquid nitrogen was substituted for by ethanol ($T \approx -80°C$), which allowed for the cryogenic collection of the CO_2 into a Pyrex breakseal while leaving the H_2O frozen in the extraction line. The CO_2 was then fed directly into the stable isotope mass spectrometer for analysis. For two of the samples the CO_2 was transferred to exetainers® using He as the carrier gas before isotopic analysis. Oxygen isotopic fractionation was corrected for by using an α-value of 1.01025 at 25°C derived for calcite (Friedman and O'Neil, 1977 and Sharma and Clayton, 1965). A similar procedure was followed for the CO_2 extraction of dolomites. After 24 hours of reaction with 100% H_3PO_4, the dolomites were placed in the carbonate extraction line and any CO_2 produced by H_3PO_4 reaction with calcite impurities was removed. The dolomite was then returned to the carbonate bath at 50°C for another 24 hours to allow the H_3PO_4 to react with the dolomite. Dolomite was then placed back on the carbonate extraction line and the CO_2 was extracted in the same manner as for the calcites (this procedure is known as "selective-acid extraction" and the reader is referred to Al-Aasm et al. (1990) for details on the analytical procedures). Oxygen isotopic fractionation was

corrected using an α-value of 1.01065 at 50°C derived for dolomite (Rosenbaum and Sheppard, 1986).

The CO_2 was analysed using a Thermo Finnigan MAT Delta^{plus}xl isotope ratio mass spectrometer (the two samples that were transferred to exetainers® were analysed using a Thermo Finnigan MAT Delta^{plus}xp isotope ratio mass spectrometer). Results are reported using the conventional δ-notation, with a routine precision of ± 0.1‰ at the 2σ level for both of the mass spectrometers. Oxygen isotope analyses were initially quoted relative to V-PDB and were converted to V-SMOW using the following equation for carbonates: $1.03037\delta^{18}O_{PDB} + 30.37 = \delta^{18}O_{SMOW}$ (Craig, 1965; Clayton et al., 1968).

B.2 Electron Microscopy

B.2.1 Electron Microprobe

Mineral analyses (apatite, magnetite and ilmenite) were performed on selected thin-sections using a Camebax MBX Electron Microprobe equipped with four WDX X-ray spectrometers in the Department of Earth Sciences at Carleton University. Polished thin-sections (~ 30 μm thick) were first coated with a conductive film of carbon (~ 200 Å thick) before being analysed by WDX. A 15 kV accelerating voltage and 20 nA electron beam current were used for a raster area of 5x5 to 10x10 μm^2 (5x5 μm^2 for apatite). A variety of natural and synthetic standards were used. Mineral analyses of the sulphides (pyrrhotite, pyrite and chalcopyrite) were performed on selected grain mounts (also coated with ~ 200 Å of carbon) as opposed to thin sections. The electron microprobe was operated at a 20 kV accelerating voltage, an electron beam current of 35

nA and a beam diameter of 1 – 2 μm. Peak counting times for the various phosphate, oxide and sulphide minerals were element dependent and ranged from 10 to 40 seconds or 40 000 accumulated counts. A variety of natural and synthetic standards were used. The raw X-ray data was converted to elemental wt.% using the Cameca PAP matrix correction program. The quoted values for the major elements are accurate to 1-2% while the quoted values for the minor elements are accurate to 3-10%. Tables B-1, B-2 and B-3 list the detection limits during analyses of apatite, magnetite and ilmenite, and the sulphides (pyrrhotite, pyrite and chalcopyrite) respectively, using the Electron Microprobe.

Table B-1. Detection limit (in wt.%) of the Camebax MBX Electron Microprobe during analyses of apatite by WDX (D. Hogarth and P. Jones, pers. comm., 2005).

Element (as oxide)	Detection limit (in wt.%)
P_2O_5	0.03
SiO_2	0.077
As_2O_5	0.10
SO_3	0.137
CaO	0.03
Na_2O	0.048
FeO_{Total}	0.064
MnO	0.062
SrO	0.048
BaO	0.061
Y_2O_3	0.063
La_2O_3	0.083
Ce_2O_3	0.076
Pr_2O_3	~ 0.1
Nd_2O_3	0.100
Sm_2O_3	~ 0.1
F	0.04
Cl	0.012

Table B-2. Detection limit (in wt.%) of the Camebax MBX Electron Microprobe during analyses of magnetite and ilmenite by WDX (P. Jones, pers. comm., 2005).

Element (as oxide)	Detection limit (in wt.%)
SiO_2	0.03
Al_2O_3	0.02
TiO_2	0.02
Cr_2O_3	0.03
V_2O_5	0.06
FeO_{Total}	0.05
MgO	0.03
MnO	0.04
CaO	0.02

Table B-3. Detection limit (in wt.%) of the Camebax MBX Electron Microprobe during analyses of pyrrhotite, pyrite, and chalcopyrite by WDX (P. Jones, pers. comm., 2005).

Element	Detection limit (in wt.%)
Fe	0.02
Co	0.02
Ni	0.02
Cu	0.02
Ag	0.03
S	0.02

B.2.2 Scanning Electron Microscope (SEM)

A JEOL 6400 scanning electron-microscope located within the Department of Earth Sciences at Carleton University was used to obtain back-scattered electron (BSE) images of various sulphides, sulphates, silicates and oxides from selected thin-sections (also coated with ~ 200 Å of carbon). In addition, the SEM was used to obtain qualitative data on the chemical composition of these various minerals using an energy-dispersive X-ray system (EDS). The EDS detection for the SEM operated at a 20 kV accelerating voltage, an electron beam current of 1.0 nA and a beam diameter of ~ 2 – 5 μm. The preset count time for all of the analyses was 40 seconds.

Appendix C – Plates

C.1 – General Plates (Note: F.O.V. = Field Of View)

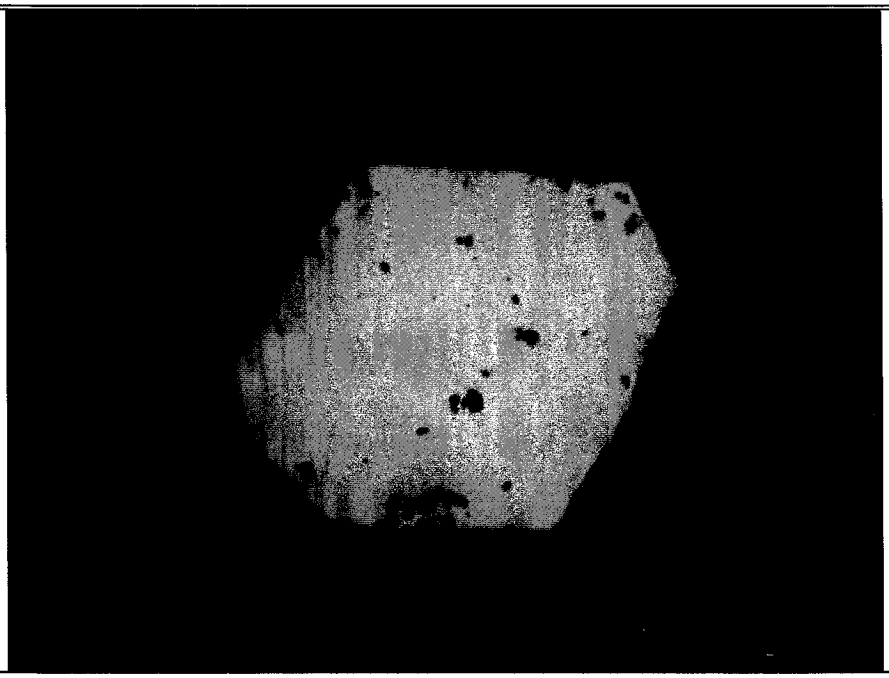

Plate 1.1. Reflective light photomicrograph of a euhedral crystal of pyrrhotite in a sövite from the Schryburt Lake complex. Sample ID: SR18-8; F.O.V. ≈ 1.0 mm.

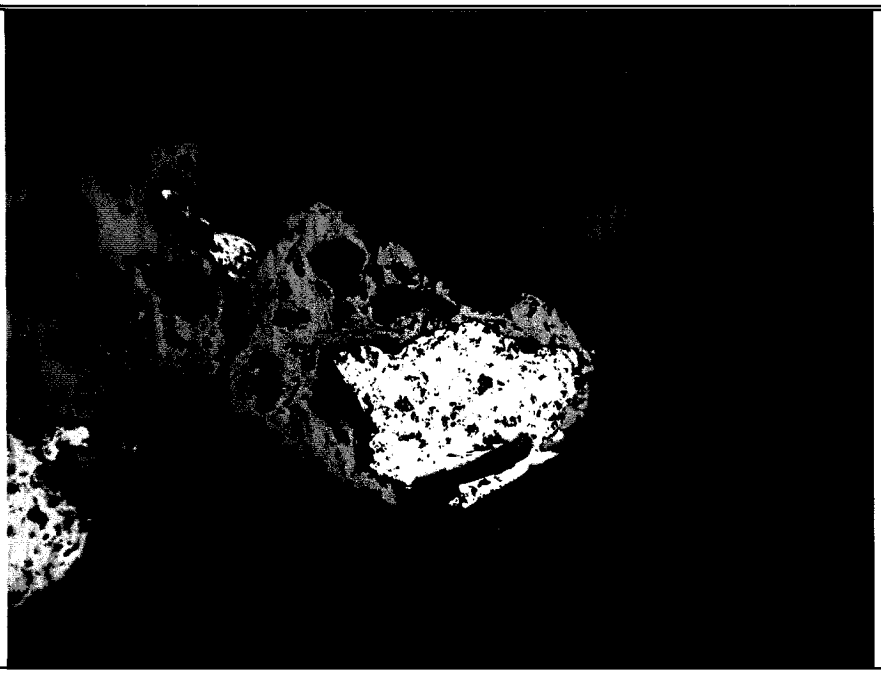

Plate 1.2. Reflective light photomicrograph of coexisting magnetite (grey) and pyrrhotite (faint yellow) in a sövite from the Schryburt Lake complex. Sample ID: SR18-8; F.O.V. ≈ 1.5 mm.

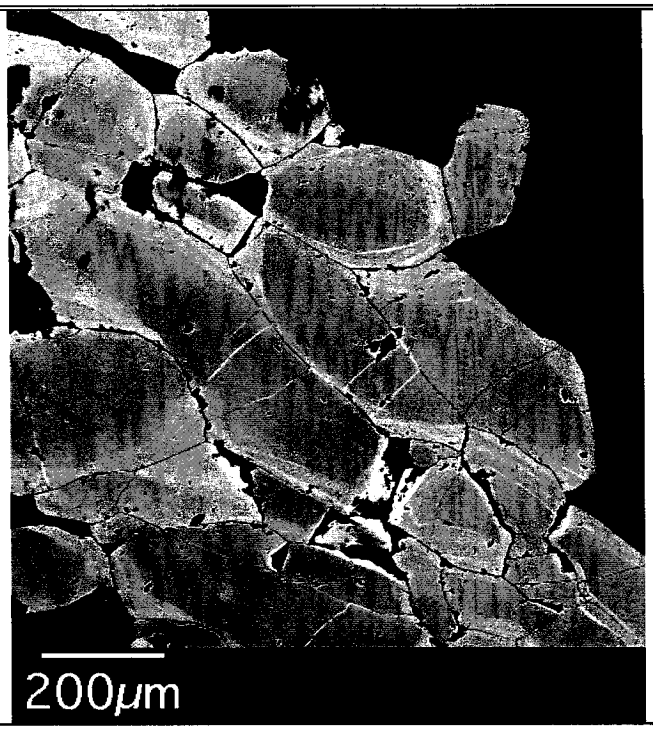

Plate 1.3. BSE image of an aggregate of compositionally zoned apatite crystals in a sövite from the Schryburt Lake complex. The lighter areas are LREE enriched when compared to the darker areas. Sample ID: SR18-7; Scale: as shown.

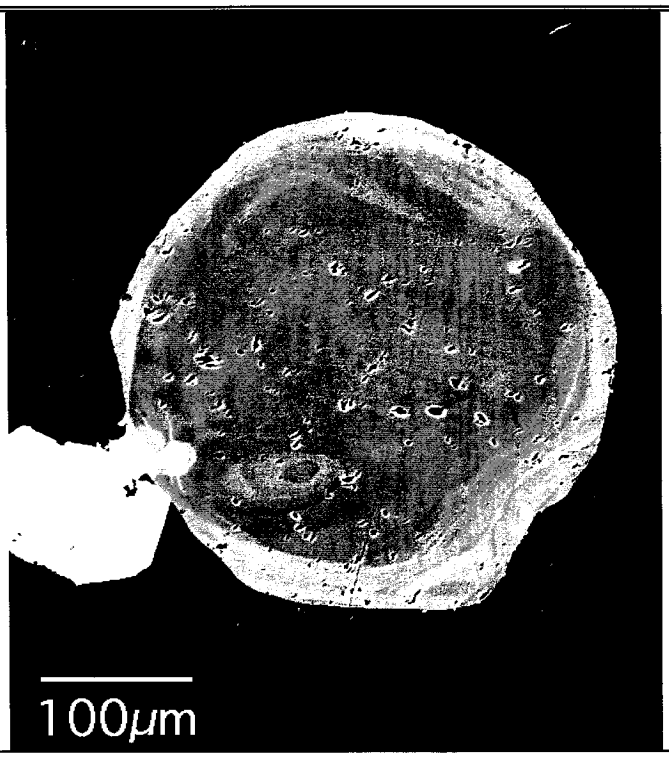

Plate 1.4. BSE image of a compositionally zoned apatite crystal (centre) whose rim has been partially penetrated by a crystal of pyrrhotite (lower left) in a sövite from the Schryburt Lake complex. Sample ID: SR18-8; Scale: as shown.

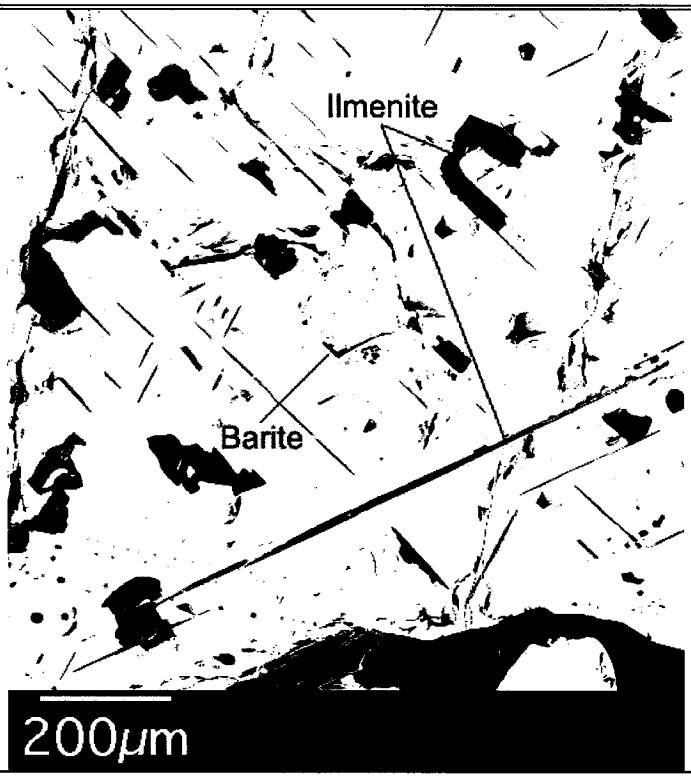

Plate 1.5. BSE image of a magnetite crystal poikilitically enclosing a euhedral crystal of barite. Also note the abundant exsolution lamellae of ilmenite within the magnetite. Sample ID: SR18-5 (sövite); Scale: as shown.

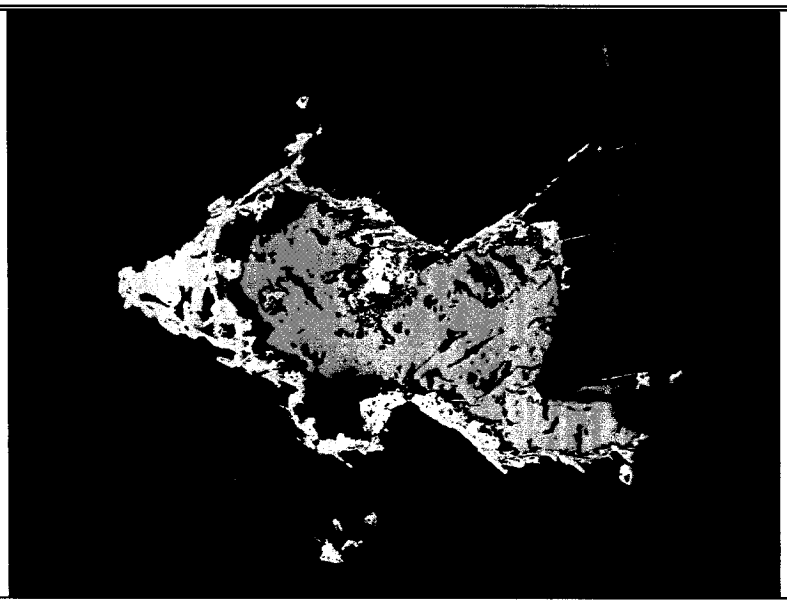

Plate 2.1. Reflective light photomicrograph of an anhedral crystal of pyrrhotite (pinkish-yellow), possessing a discontinuous rim of pyrite (yellow). Sample ID: BB78 (ijolite); F.O.V. ≈ 1.0 mm.

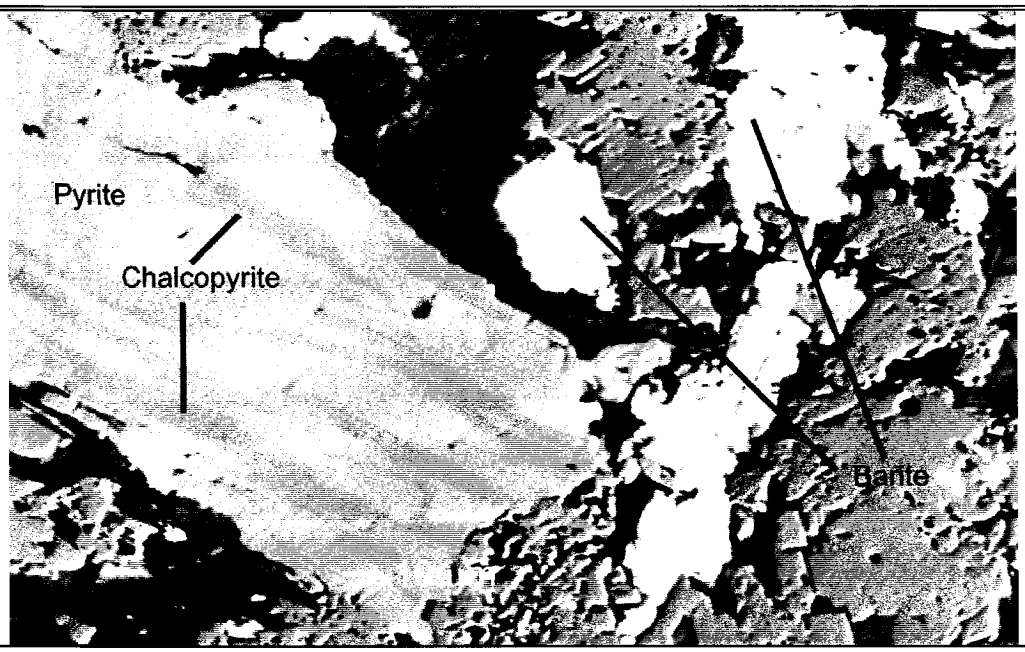

Plate 2.2. BSE image of a crystal of pyrite containing wispy inclusions of chalcopyrite. Also note the presence of proximal barite. Sample ID: HED7-36 (pyroxenite); Scale: as shown.

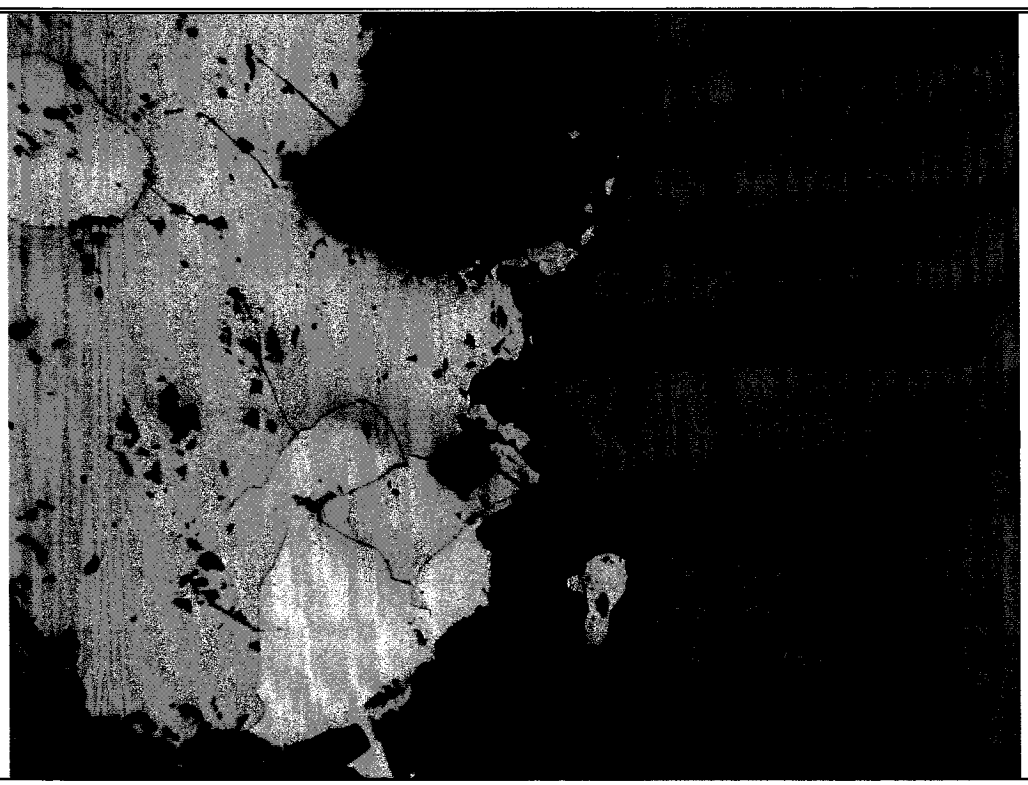

Plate 3.1. Reflective light photomicrograph of a chalcopyrite-rich pyrrhotite crystal (left) that is both mantling and penetrating a crystal of magnetite (right). Sample ID: CMM 135 IMC 179.3 – 179.7 (hornblendite); F.O.V. ≈ 1.0 mm.

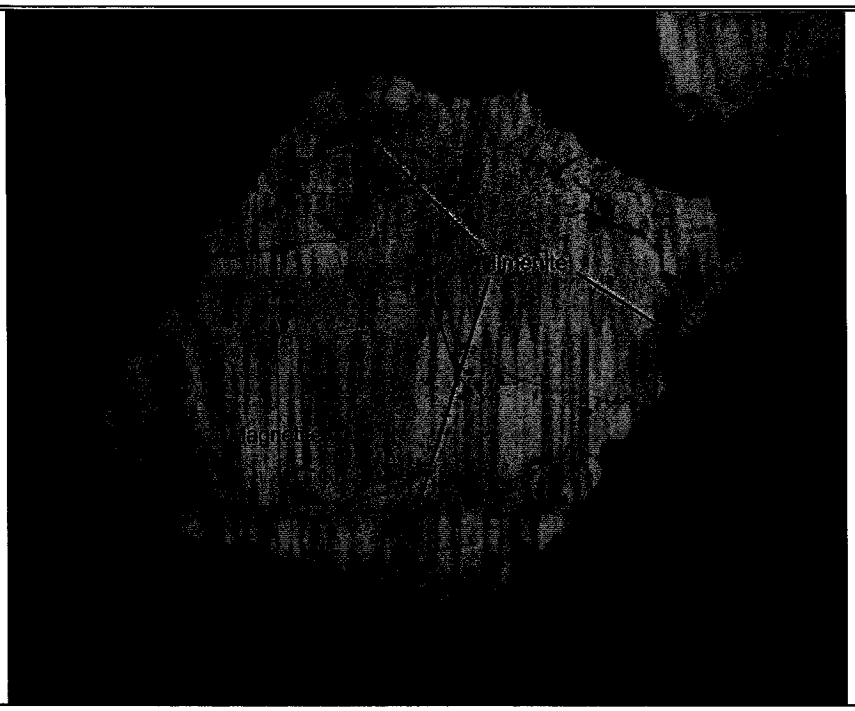

Plate 3.2. Reflective light photomicrograph of a magnetite crystal with exsolved ilmenite and possessing a reaction rim of titanite. Sample ID: CMM 135 IMC 179.3 – 179.7 (hornblendite); F.O.V. ≈ 1.5 mm.

Plate 3.3. Reflective light photomicrograph of a blebby crystal of pyrrhotite (yellow) adjacent to a crystal of magnetite (grey) both in an oikocryst of phlogopite. Note also the presence of ilmenite lamellae within the magnetite. Sample ID: CMM 135 IMC 179.3 – 179.7 (hornblendite); F.O.V. ≈ 0.9 mm.

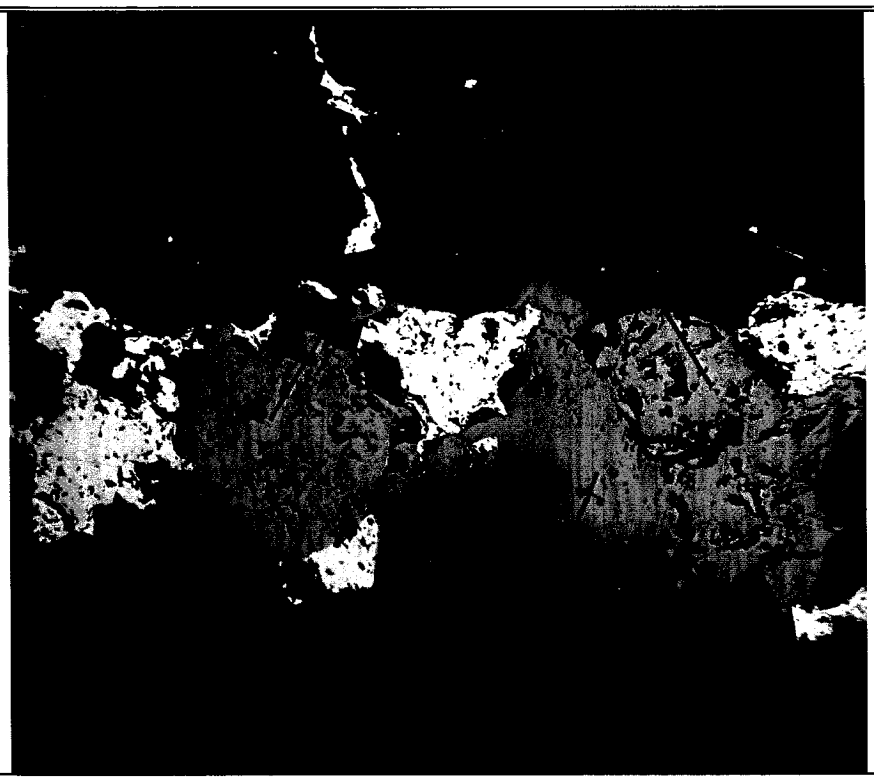

Plate 3.4. Reflective light photomicrograph of pyrrhotite (pinkish-yellow) and chalcopyrite (golden-yellow) in association with magnetite and ilmenite. Sample ID: CMM29 136.85 – 137.2 (hornblendite); F.O.V. ≈ 1.5 mm.

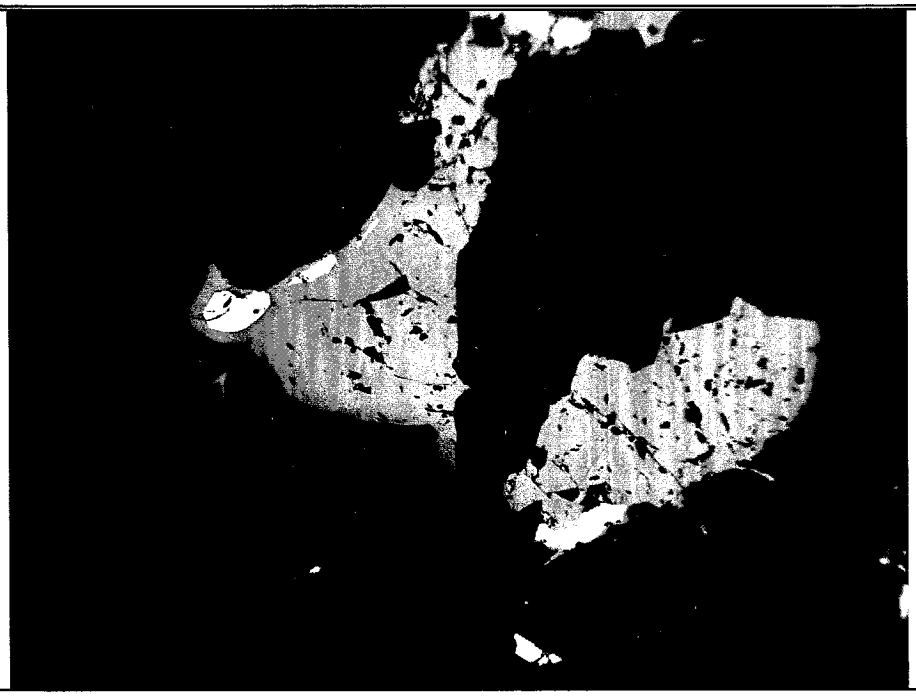

Plate 3.5. Reflective light photomicrograph of two anhedral crystals of magnetite (grey) with inclusions of pyrrhotite (pale yellow) and chalcopyrite (golden-yellow). Sample ID: CMM29 136.85 – 137.2 (hornblendite); F.O.V. ≈ 1.3 mm.

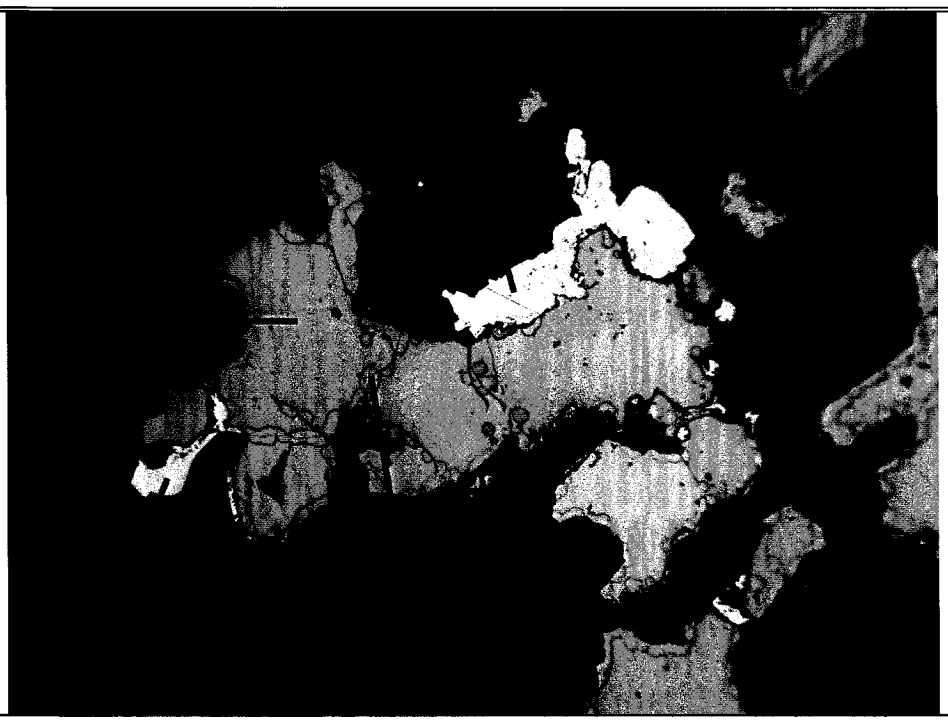

Plate 4.1. Reflective light photomicrograph of large crystals of pyrrhotite mantled by pyrite and possibly marcasite. Sample ID: ST-62 (ijolite); F.O.V. ≈ 1.3 mm.

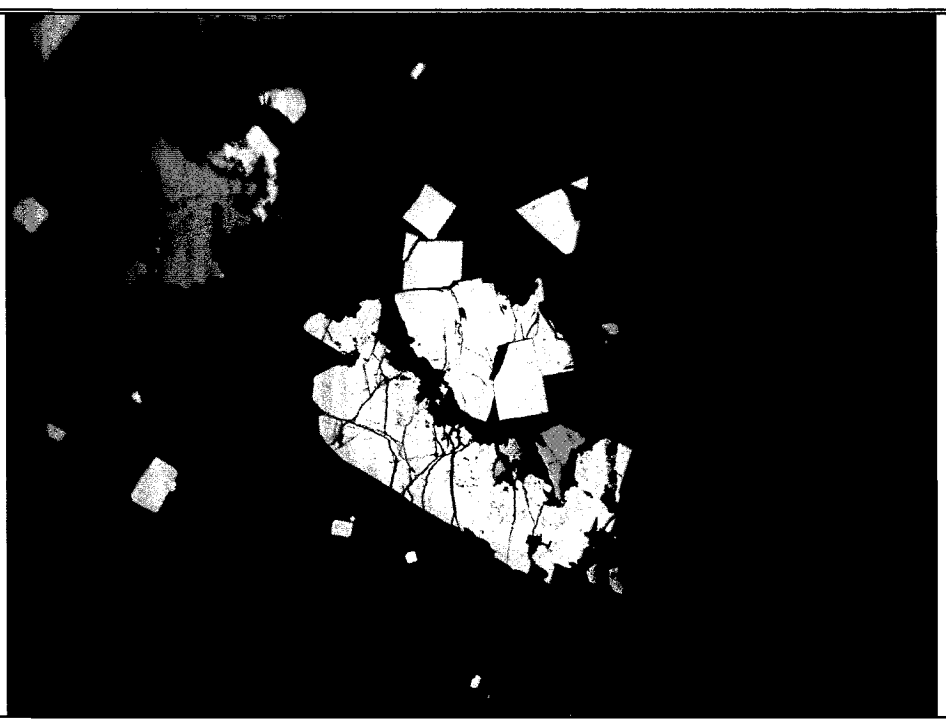

Plate 4.2. Reflective light photomicrograph of euhedral and anhedral crystals of pyrite (yellow) with minor pyrrhotite (pinkish-yellow) and chalcopyrite (golden-yellow). Sample ID: ST-62 (ijolite); F.O.V. ≈ 1.3 mm.

Plate 4.3. Reflective light photomicrograph of a crystal of pyrite (yellow) surrounded by pyrrhotite (pinkish-yellow). Sample ID: ST-62 (ijolite); F.O.V. ≈ 1.0 mm.

C.2 – BSE Images of Apatite Analyzed by the Electron Microprobe
(All scales are as shown)

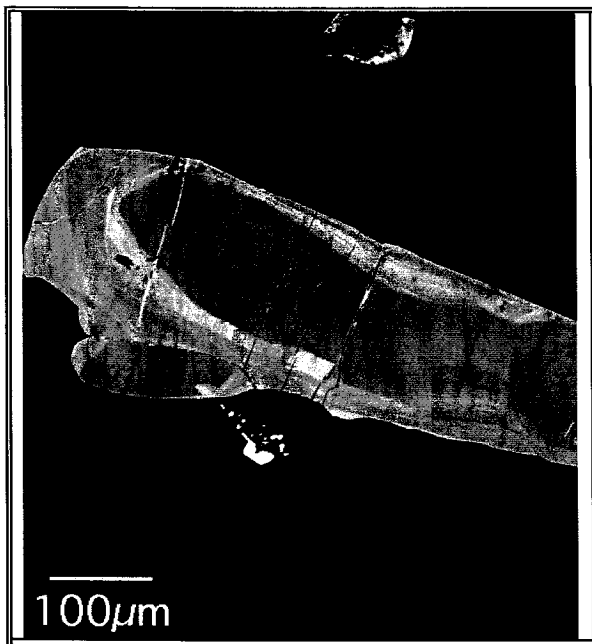

Plate AP1, Schryburt Lake complex. Sample ID: SR18-5 (sövite)

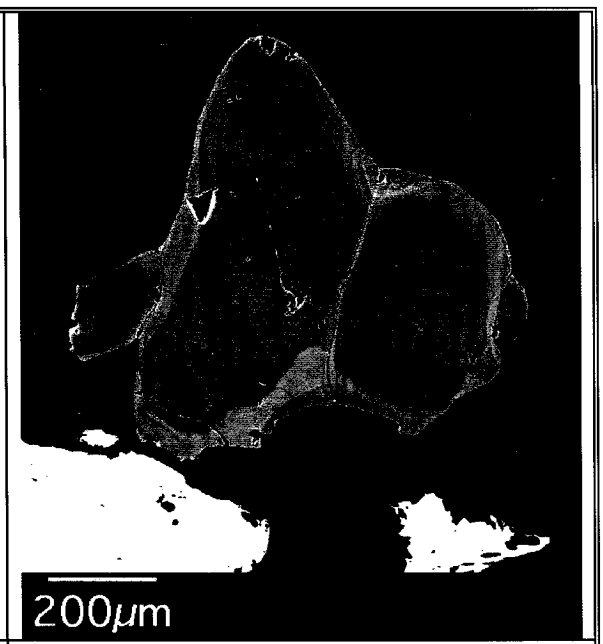

Plate AP2 (greyish crystal), Schryburt Lake complex. Sample ID: SR18-5 (sövite)

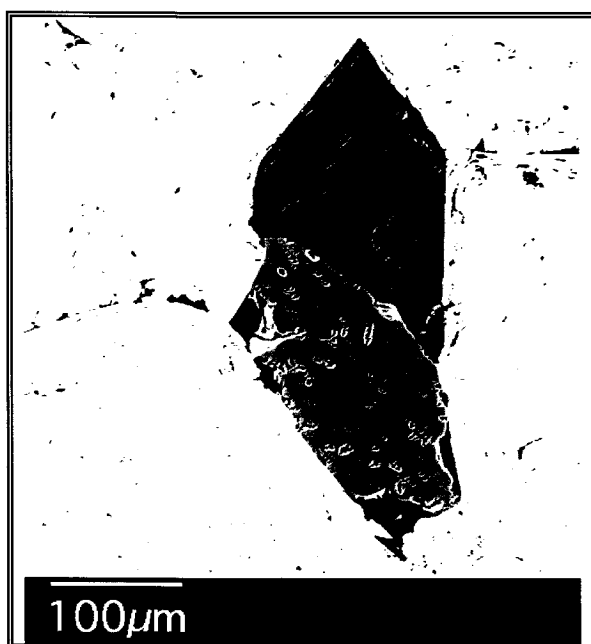

Plate AP3 (greyish crystal), Schryburt Lake complex. Sample ID: SR18-7 (sövite)

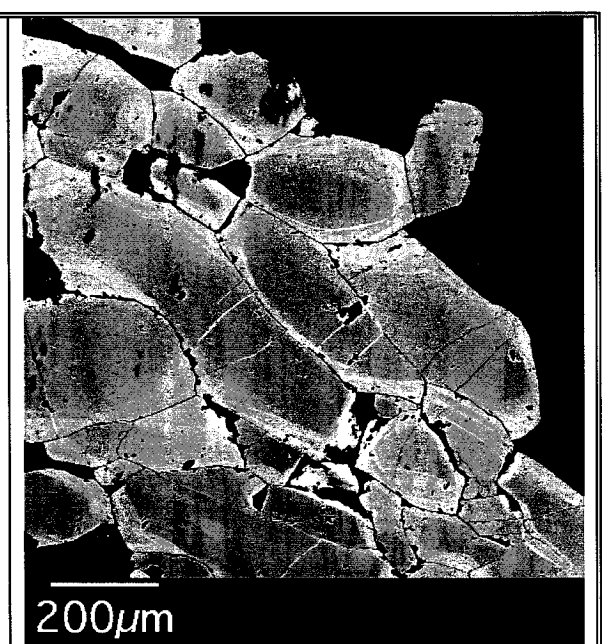

Plate AP4, Schryburt Lake complex. Sample ID: SR18-7 (sövite)

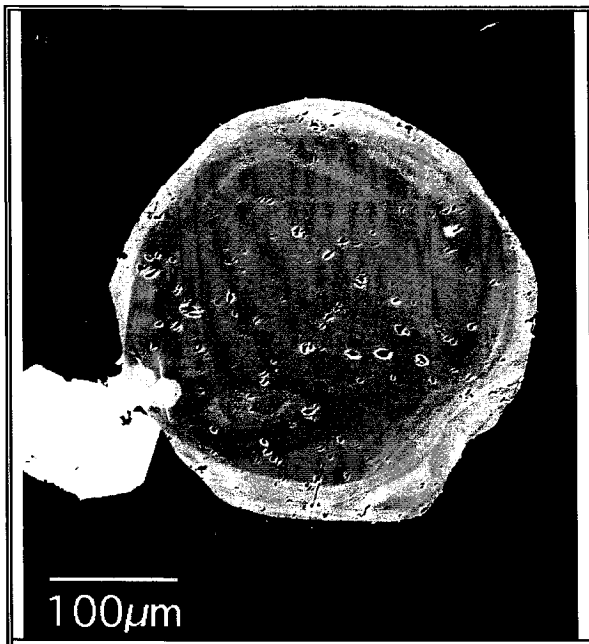

Plate AP5 (greyish crystal), Schryburt Lake complex. Sample ID: SR18-8 (sövite)

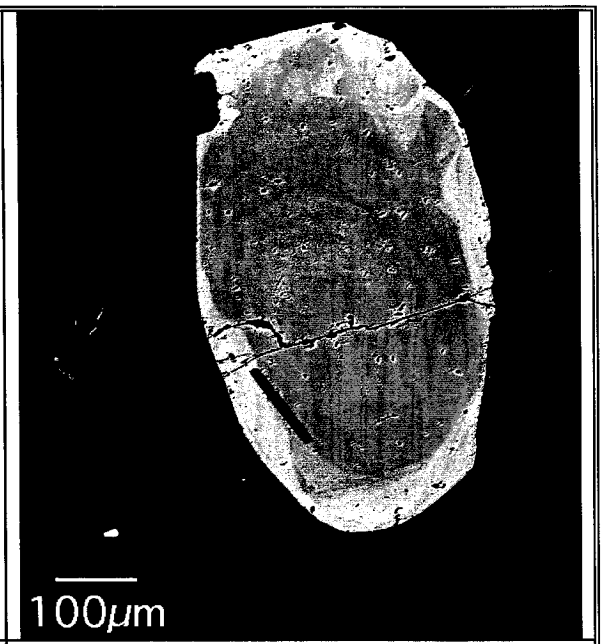

Plate AP6, Schryburt Lake complex. Sample ID: SR18-8 (sövite)

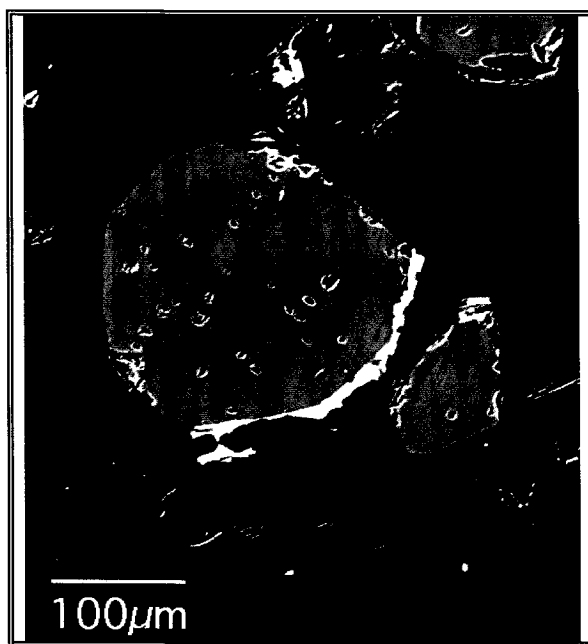

Plate AP7, Firesand River complex. Sample ID: H8 135.65 – 136.05 (sövite)

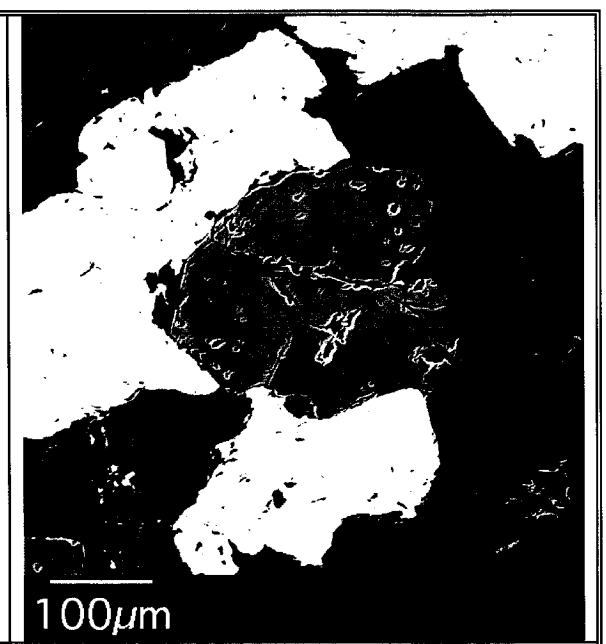

Plate AP8 (greyish crystal), Firesand River complex. Sample ID: H8 135.65 – 136.05 (sövite)

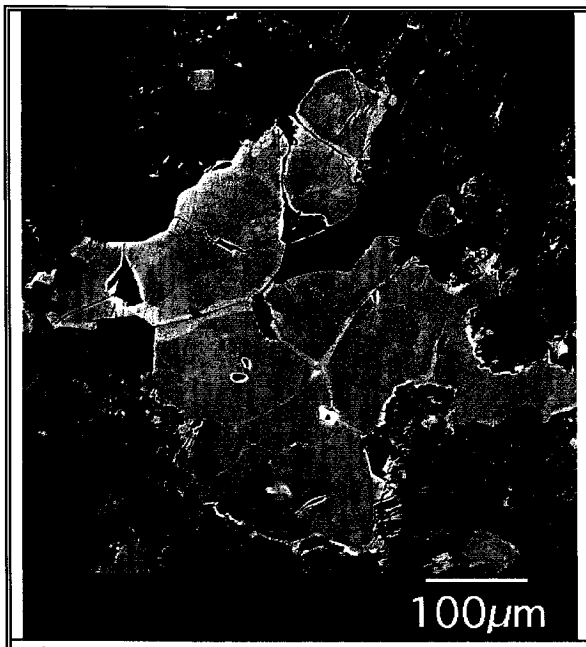

Plate AP9, Firesand River complex. Sample ID: ST-34 (silicocarbonatite)

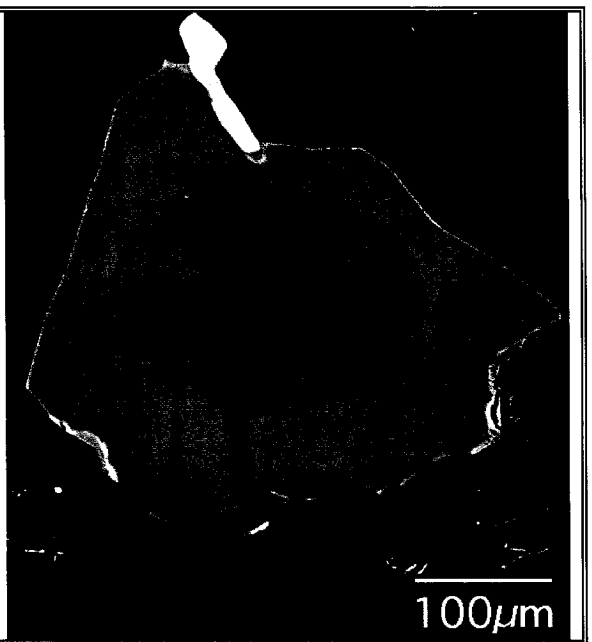

Plate AP10, Firesand River complex. Sample ID: ST-34 (silicocarbonatite)

Plate AP11 (greyish crystal), Spanish River complex. Sample ID: 107-108 1376.0 (pyroxenite)

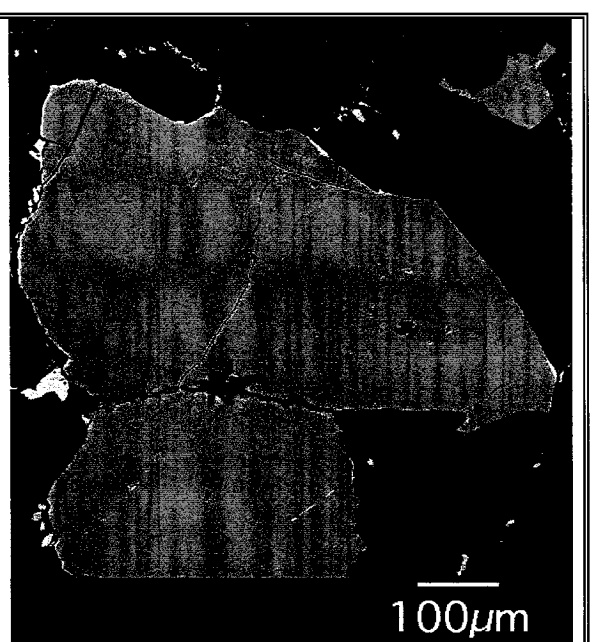

Plate AP12, Spanish River complex. Sample ID: 107-108 1376.0 (pyroxenite)

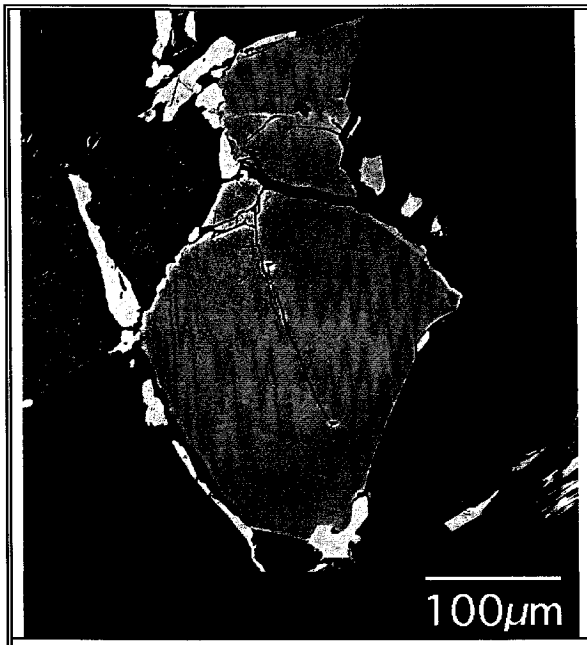

Plate AP13, Spanish River complex. Sample ID: 107-108 1376.0 (pyroxenite)

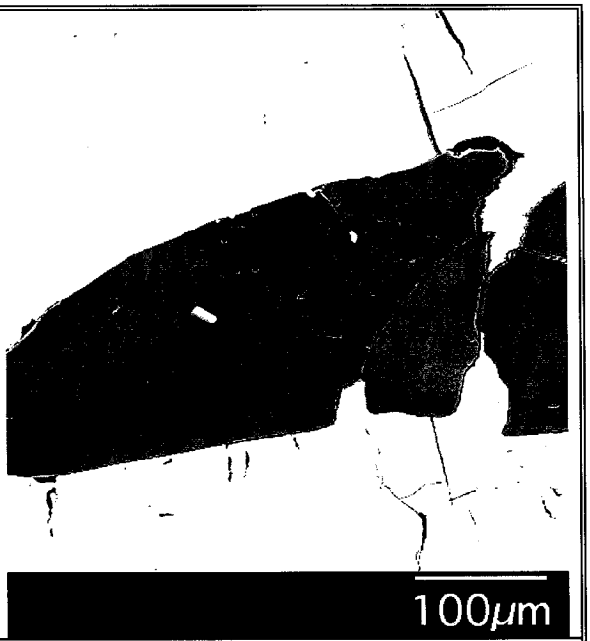

Plate AP14 (greyish crystals), Big Beaver House complex. Sample ID: BB78 (ijolite)

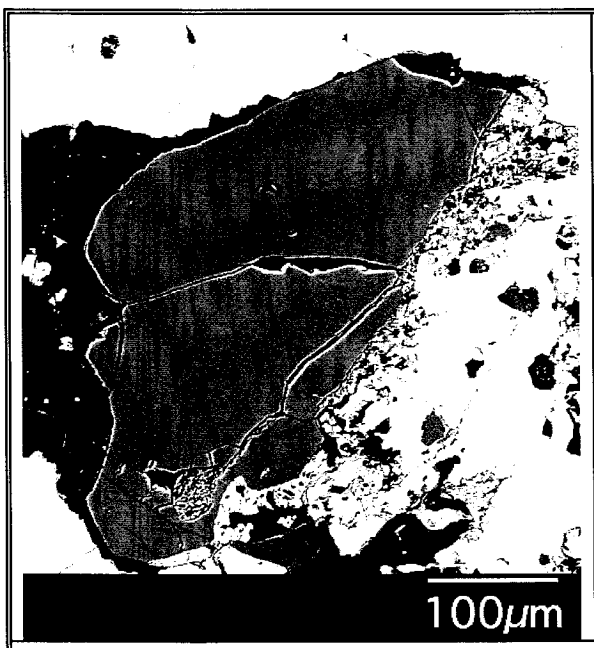

Plate AP15 (greyish crystal), Big Beaver House complex. Sample ID: BB78 (ijolite)

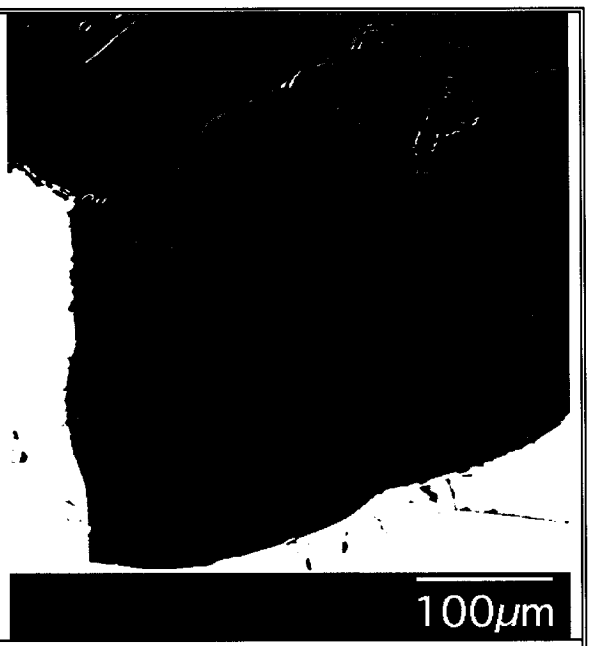

Plate AP16 (greyish crystal), Big Beaver House complex. Sample ID: BB78 (ijolite)

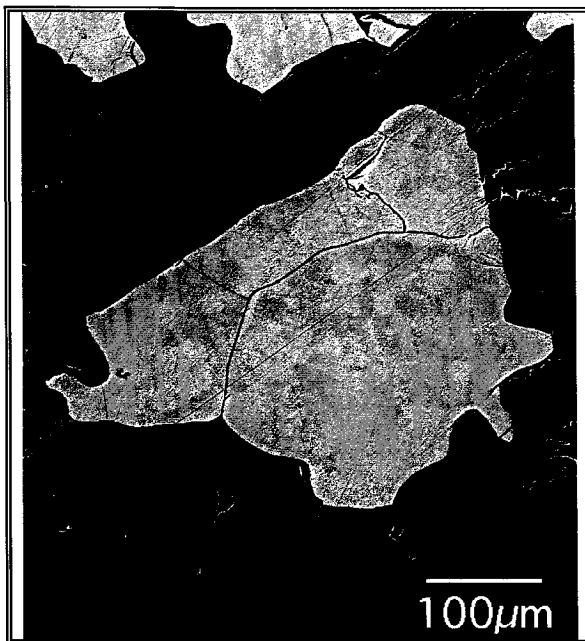

Plate AP17, Big Beaver House complex.
Sample ID: HED7-36 (pyroxenite)

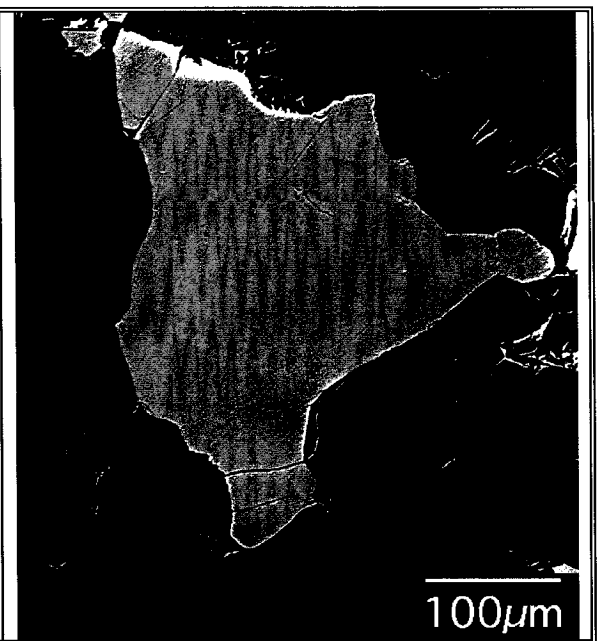

Plate AP18, Big Beaver House complex.
Sample ID: HED7-36 (pyroxenite)

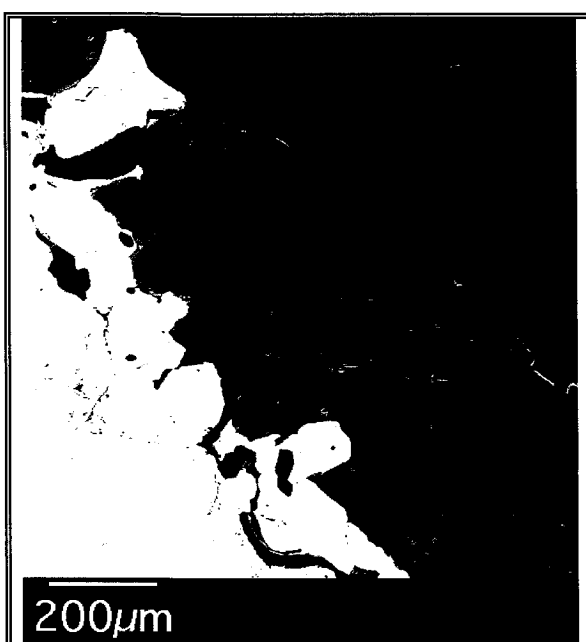

Plate AP19 (greyish crystal), Cargill complex.
Sample ID: H24 IMC 28.6 – 29.0 (sövite)

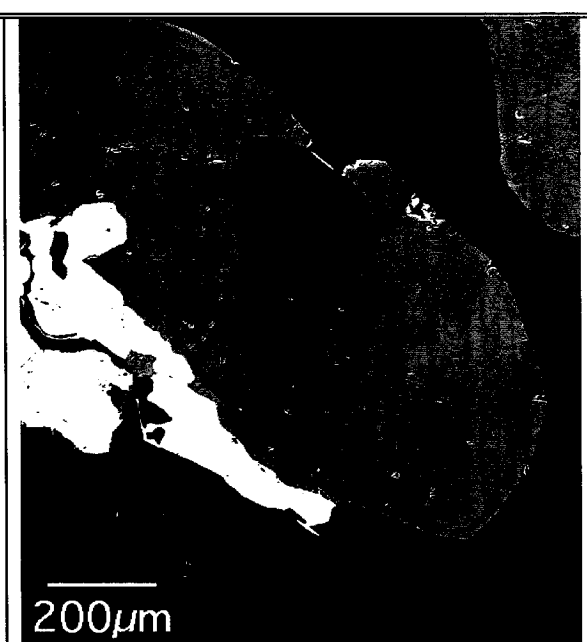

Plate AP20 (greyish crystal), Cargill complex.
Sample ID: H24 IMC 28.6 – 29.0 (sövite),
(bottom of crystal from AP19)

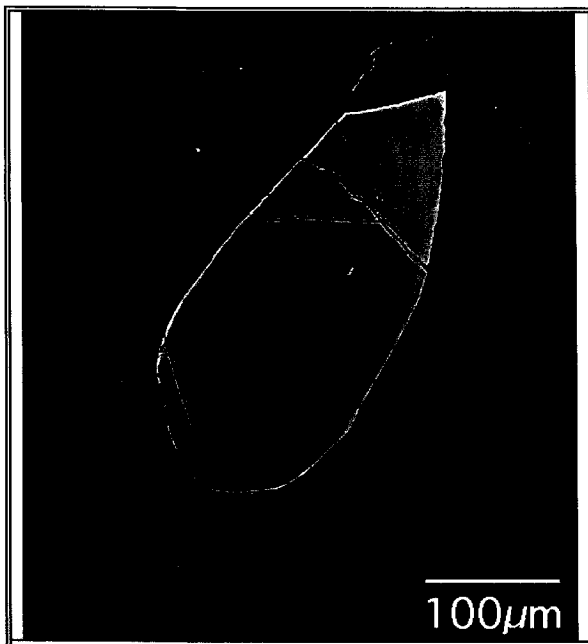

Plate AP21, Cargill complex. Sample ID: H35 IMC 128.9 – 129.3 (silicocarbonatite)

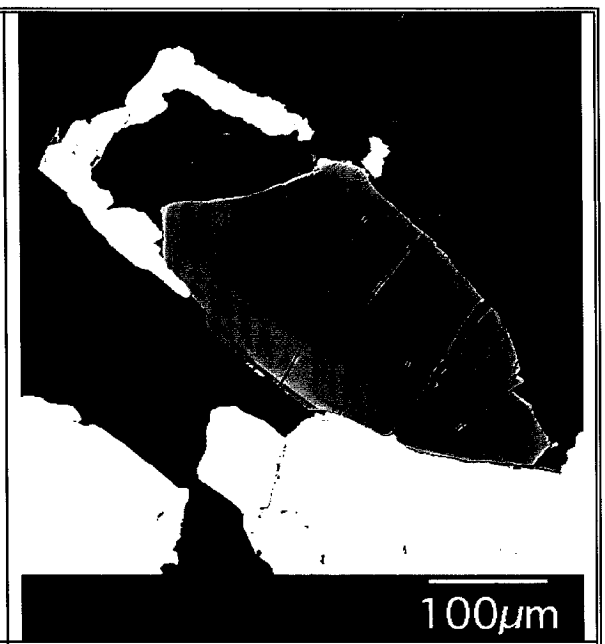

Plate AP22 (greyish crystal), Cargill complex. Sample ID: H35 IMC 128.9 – 129.3 (silicocarbonatite)

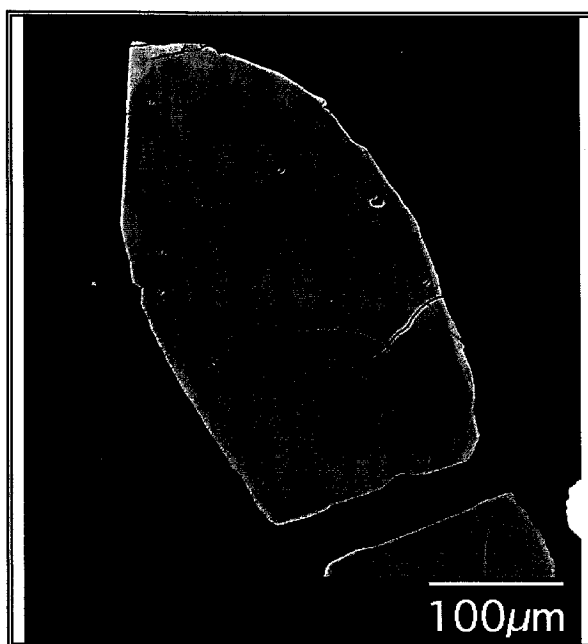

Plate AP23, Cargill complex. Sample ID: H35 IMC 128.9 – 129.3 (silicocarbonatite)

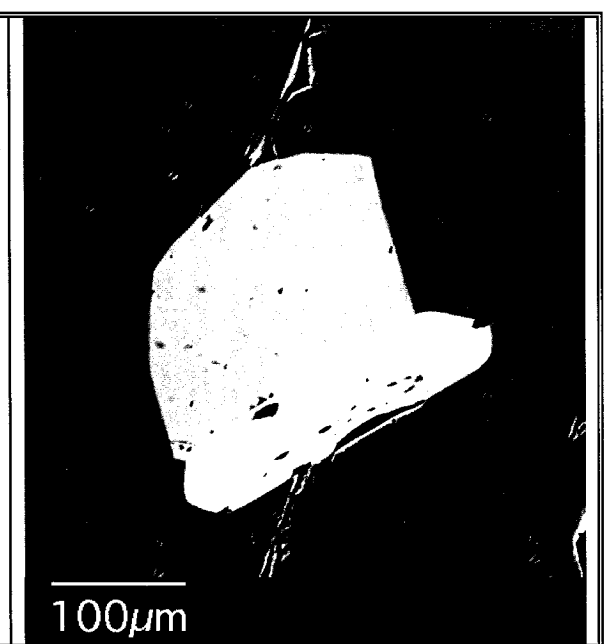

Plate AP24 (greyish crystal), Cargill complex. Sample ID: CCM29 136.85 – 137.2 (hornblendite)

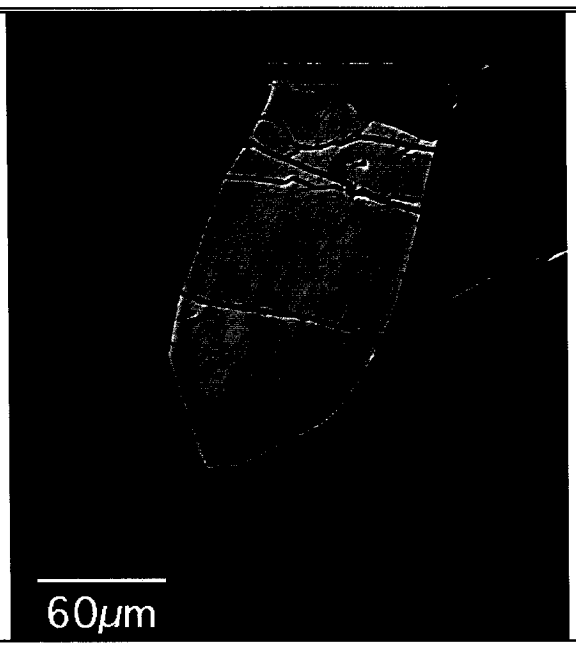

Plate AP25, Cargill complex. Sample ID: CCM29 136.85 – 137.2 (hornblendite)

Appendix D – Reflective Light Petrography

D.1 Methodology

Polished thin-sections (~ 30 μm thick) and grain mounts were prepared for reflective light petrography for some of the samples. A Nikon OPTIPHOT – POL petrographic microscope in reflective-light mode, located in the Department of Earth Sciences at Carleton University was used for petrographic analyses. Transmitted-light mode was also used to evaluate the sulphide/oxide relationship with the surrounding silicate, phosphate and/or carbonate minerals. In addition, a Nikon digital camera was mounted on the microscope to obtain various images of the sulphides and oxides (these can be found in Appendix C). The prepared grain mounts were used for both petrographic identification of sulphide mineralogy and elemental analyses on the electron microprobe. The petrographic observations are given in Section D.2 below (see Table. Petrographic descriptions using transmitted light for the majority of these samples and the other isotopically analyzed samples can be found in the respective OGS studies produced by R.P. Sage.

D.2 Sample Descriptions

Table D-1. Reflective-light petrographic analyses of selected samples from the Schryburt Lake, Big Beaver House, Cargill, Firesand River and Spanish River carbonatite-alkalic rock complexes.

Complex; plate(s) in appendix D	Sample ID	Major Oxides and Sulphides (%)	Minor/Trace Oxides and Sulphides	Mineral sizes and crystallinities	Notes
Schryburt Lake Plate: 1.5	SR18-5	mgt (75); *ilm (25) *=crystalline ilm	po	mgt: ~0.6 mm - >3mm (subhedral); ilm: ~0.2 mm – 0.4 mm (tabular habit). The magnetite contain abundant exsolution lamellae and patches of ilmenite	The magnetite is generally interspersed throughout the thin-section, though they are concentrated in three weakly defined bands. Some of the larger magnetite appears to contain silicate/carbonate inclusions. The magnetite appears to have been only moderately broken up by the carbonatitic magma. Po was seen as both independent crystals and as small inclusions in the mgt.
Schryburt Lake Plate: 1.3	SR18-7	po (90); mgt (~10)	ccp	po: ~0.2 mm - ~2 mm (subhedral – euhedral); mgt: up to ~0.4 mm	The sulphides (principally po) occur in one distinct band within the host sövite. The only observed inclusions in the po are a few crystals of apatite. The only mgt in this specimen is found associated with a crystal of po.
Schryburt Lake Plates: 1.1, 1.2, 1.4	SR18-8	mgt (60); po (40)	ilm, ccp	mgt: ~0.05 mm – 2 mm (anhedral – subhedral); po: ~0.1 mm – 4 mm (subhedral – euhedral)	Both sulphides and oxides tend to occur as distinct bands/layers and occur both together and as distinctive crystals. Ilmenite is present as discreet, tabular crystals, zones within the magnetite and more rarely as exsolution lamellae within the magnetite. It would appear that the sulphides and the oxides crystallized concomitantly.
Big Beaver House	BB9	mgt + hem (65); po (35)	ccp, pn	mgt+hem: ~0.1 mm – ~2.6 mm (anhedral – subhedral); po: ~0.04 mm – ~0.7 mm (anhedral – subhedral & blebby)	Abundant opaques in this sample commonly form an interlocking network around silicate minerals. The mgt is commonly altered to haematite. The po is usually associated with the mgt. The mgt seem to be concomitant with the pyrrhotites; both are seen to poikilitically enclose one another.

Big Beaver House Plate: 2.1	BB78	po (45); mgt (40); py (15)	ccp	po: 0.3 mm – ~4.5 mm (generally anhedral – subhedral & blebby); mgt: 0.1 mm – 0.4 mm (subhedral – euhedral); py: 0.1 mm – ~1.4 mm (anhedral)	Dominant sulphide is po; py is also present and is usually found to rim po. Py is also seen as isolated crystals. The magnetite generally occurs as isolated crystals not in contact with the sulphides. When the sulphides are seen in contact with mgt they are rimming and/or replacing the magnetite.
Big Beaver House Plate: 2.2	HED7-36	*po (85); ccp (15) *it was difficult to determine whether this was po and/or py	mgt	po: ~0.05 mm – ~1.2 mm (euhedral – anhedral); ccp (occurs as blebs & streaks within or beside crystals of po. Rarely found associated with mgt.	Po occurs as well developed crystals that have been broken apart by the surrounding pyroxenitic magma. In addition, much of the po occurs between silicate mineral grain boundaries as veins. Therefore, it would appear that the sulphides and silicates could have been cogenetic. Some of the large broken-up po have a core of ccp.
Cargill Plates: 3.1, 3.2, 3.3	CCM 135 IMC 179.3 – 179.7	mgt (60); po (35); ccp (~5)		mgt: ~0.2 mm – 4 mm (generally subhedral); po: ~0.2 mm – ~3 mm (blebby with a few anhedral crystals)	Po is commonly found associated with mgt. Po usually mantles and/or partially penetrates the mgt. Some of the mgt have been fractured into which po appears to have invaded. Po also occurs as blebs within large silicate minerals. The ccp is either found as blebs on the rims of the po or as inclusions in the po.
Cargill Plate: 3.4	CCM29 136.85 – 137.2	mgt + ilm (55); po (35); ccp (10)		mgt: 0.1 mm – ~1 mm (anhedral and generally interstitial to the silicates); po: 0.1 mm – ~0.6 mm (blebby and anhedral); ccp: 0.1 mm – ~0.2 mm (blebby and anhedral)	Mgt and po appear to be an intersilicate crystalline phase. The mgt and po occur with one another and as distinct phases. Some po is also poikilitically enclosed in mgt, but not vice-versa.
Cargill	H35 IMC 128.9 – 129.3	mgt (70); po (30)	ccp	mgt: up to 7 mm but generally ~0.2 mm (anhedral – subhedral), some of the larger mgt crystals appear to have cores of ilm; po: ~0.1 mm – ~3.2 mm (generally anhedral & blebby).	Many of the larger mgt crystals appear to have been largely resorbed into the melt. Most of the po is associated mgt and/or carbonate. The magnetite appears to have formed before the po (e.g. there is some po found in some of the broken apart portions of the mgt; po is also seen rimming some of the mgt).
Firesand River	H8 135.65 – 136.05	po (95); ccp (~5)		po: 0.1 mm – 0.3 mm (anhedral, slightly elongate crystals)	Po generally occurs interstitial to, and as inclusions in cc crystals. Most of the po is found in a single, discontinuous layer where there is also the highest concentration of px and/or amp. One of the largest po crystals poikilitically encloses a crystal of px and/or amp.

Firesand River	ST-34	py (100)	ccp, mgt	py: ~0.04 mm – ~0.3 mm (anhedral – euhedral)	Py occurs as euhedral cubes as well as elongated inclusions along phlogopite cleavage planes (py was commonly seen associated with phlogopite). Some py appears to have been broken up. In addition, some of the py may have reacted with the surrounding melt/fluids as it is often seen partially enclosing an unidentified green alteration mineral.
Firesand River Plates: 4.1, 4.2, 4.3	ST-62	pot (~70); **py (~30) **Including the py seen rimming the po	ccp	po: up to 1.2 mm but generally ~0.2 mm (mostly anhedral); py: up to 0.5 mm but generally less then 0.1 mm (anhedral – subhedral with a few well defined euhedral cubic crystals)	Most of the po possesses a thin rim of py and in some cases the po appears to have been invaded by py. Most py is seen mantling po. A few well defined cubic crystals of py were also observed in addition to some py crystals in contact with po. Also there was at least one crystal of py poikilitically enclosed in an oikocryst of po.
Firesand River	F 384-A	py (70); mgt (30)		py: ~0.2 mm – 2 mm (subhedral); mgt: up to ~2 mm but mostly ~0.2 mm (anhedral)	This sample is made up of two distinct zones: (1) carbonate matrix with one large, broken mgt crystal attached to a small, also broken py crystal; (2) large subhedral py crystals scattered throughout a matrix of fine grained of what appears to be partially oxidized carbonate and some mgt. Two of the large py crystals in this zone contain inclusions of mgt. and appear to be also partially penetrated by mgt.
Spanish River	107-108 1376.0	po (60); mgt (40)	ccp	po: ~0.08 mm – ~0.6 mm (anhedral – subhedral & blebby); mgt: ~0.1 mm – ~1.4 mm (anhedral – subhedral)	Both mgt and po occur together and separately. When they occur together it would appear that the po is invading the magnetite. In general, it would seem that the po formed mostly after the crystallization of the silicates.

Note: Modal abundances for oxides + sulphides only; ilm=ilmenite, mgt=magnetite, po=pyrrhotite, py=pyrite, ccp=chalcopyrite, pn=pentlandite, hem=haematite, amp=amphibole, px=pyroxene, cc=calcite.